INFORMATION TO USERS

This manuscript has been reproduced from the microfilm master. UMI films the text directly from the original or copy submitted. Thus, some thesis and dissertation copies are in typewriter face, while others may be from any type of computer printer.

The quality of this reproduction is dependent upon the quality of the copy submitted. Broken or indistinct print, colored or poor quality illustrations and photographs, print bleedthrough, substandard margins, and improper alignment can adversely affect reproduction.

In the unlikely event that the author did not send UMI a complete manuscript and there are missing pages, these will be noted. Also, if unauthorized copyright material had to be removed, a note will indicate the deletion.

Oversize materials (e.g., maps, drawings, charts) are reproduced by sectioning the original, beginning at the upper left-hand corner and continuing from left to right in equal sections with small overlaps.

Photographs included in the original manuscript have been reproduced xerographically in this copy. Higher quality 6" x 9" black and white photographic prints are available for any photographs or illustrations appearing in this copy for an additional charge. Contact UMI directly to order.

Bell & Howell Information and Learning
300 North Zeeb Road, Ann Arbor, MI 48106-1346 USA
800-521-0600

UMI®

Experimental Electrochemical Investigation of Si/Al in Tetra-Methyl Ammonium Hydroxide (TMAH)

ABDULLAH TASHTOUSH

A Thesis

in

The Department

of

ELECTRICAL & COMPUTER ENGINEERING

Presented in Partial Fulfillment of the Requirements
For the Degree of Master of Applied Science at
Concordia University
Montreal, Quebec, Canada

April 2000

© Tashtoush Abdullah, 2000

National Library of Canada

Acquisitions and Bibliographic Services

395 Wellington Street
Ottawa ON K1A 0N4
Canada

Bibliothèque nationale du Canada

Acquisitions et services bibliographiques

395, rue Wellington
Ottawa ON K1A 0N4
Canada

Your file Votre référence

Our file Notre référence

The author has granted a non-exclusive licence allowing the National Library of Canada to reproduce, loan, distribute or sell copies of this thesis in microform, paper or electronic formats.

The author retains ownership of the copyright in this thesis. Neither the thesis nor substantial extracts from it may be printed or otherwise reproduced without the author's permission.

L'auteur a accordé une licence non exclusive permettant à la Bibliothèque nationale du Canada de reproduire, prêter, distribuer ou vendre des copies de cette thèse sous la forme de microfiche/film, de reproduction sur papier ou sur format électronique.

L'auteur conserve la propriété du droit d'auteur qui protège cette thèse. Ni la thèse ni des extraits substantiels de celle-ci ne doivent être imprimés ou autrement reproduits sans son autorisation.

0-612-47833-5

Canada

ABSTRACT

Experimental Electrochemical Investigation of Si/Al in Tetra-Methyl Ammonium Hydroxide (TMAH)

Abdullah Tashtoush

This thesis considers the micromachining of silicon for the fabrication of micro-sensors, microactuators, and microsystems. At present it is problematic to anisotropically etch silicon, in wet etchants such as TMAH, while protecting deposited aluminum layers. This is especially a problem in CMOS-compatible micromachining, where the etch occurs as a post-process step after the creation of the microelectronic circuitry. It is suspected that this difficulty is related to electrochemical phenomena, and this work explores the electrochemistry of Si/TMAH and Al/Si/TMAH by measurements of open-circuit potentials (OCP) of a galvanic cell. It is found that the presence of Al in the etchant, electrically connected to the silicon, dominates the electrochemical reactions, and shifts the overall cell potential to a potential substantially more negative than the OCP of Si only. This change in potential reduces the Si etch reaction, as manifested in the relative rate of bubbling at the Si electrode, especially for n-type silicon, consistent with literature results from linear-sweep voltammetry. These results are compared with the result of Ashruf *et al*, and found to form a consistent electrochemical understanding. The variation of the cell behaviour with solution temperature and pH are analyzed, and found to be inconsistent with the Nernst equation, confirming the non-equilibrium nature (irreversibility) of the silicon anisotropic etch reaction.

ACKNOWLEDGMENTS

I would like to express my sincere gratitude to my thesis supervisor Dr. Leslie M. Landsberger, for his continued help, guidance and encouragement during the courses of this work. The hours of discussion and consultation with him had been the best times during my studies in Concordia University. I am very grateful to Dr. Mojtaba Kahrizi for his advice and guidance during the whole period of my M. A. Sc. Studies.

I would like to thank Dr. Abdel Essalik for his help and guidance during the whole period of this work. I really appreciate Dr. M. Paranjape's contribution and help during this work.

My sincere thanks to my brother Dr. Nehad Tashtoush, who introduced me to Dr. Leslie, and helped me to have successful beginning in my studies in Concordia University.

I express my sincerest thanks to my wife, who always encouraged me to go for better education.

Table of Contents

List of Figures........ix

List of Tables........xv

CHAPTER 1

INTRODUCTION

1.1 Introduction........1

CHAPTER 2

BACKGROUND AND LITERATURE REVIEW

2.1 Background........3

2.1.1 Micromachining and Bulk Micromachining........3

2.1.2 Background on Anisotropic Etching of Silicon........4

2.1.3 Background on Anisotropic Etching of Silicon in Tetra-Methyl Ammonium Hydroxide (TMAH).........6

2.1.4 Background on Basic electrochemistry........10

2.1.4.1 The Fundamentals of Electrochemistry........10

2.1.4.2 The Electrochemical Mechanism........11

2.1.4.3 Electrochemical Considerations........12

2.1.4.4 The Influence of Concentration and Temperature on cell Potential.. 14

2.1.4.5 Utilization of electrochemistry for chemical characterization. 17

2.1.4.6 Utility of Electrochemistry Methodologies.................................... 18

2.1.5 The Realization of the Silicon Etching Process in TMAH......................... 18

2.2 Literature Review of the Electrochemistry of Si and Si/Al in Anisotropic Etchants.. 22

2.2.1 The Etch Mechanism.. 22

2.2.2 Linear Sweep Voltammetry (LSV).. 32

2.2.2.1 Electrochemical etch-stop characteristics of TMAH:IPA solutions 32

2.2.2.2 Electrochemical etch-stop in TMAH without externally applied bias. .. 41

2.2.2.3 The galvanic cell passivation mechanism.. 45

CHAPTER 3

Experimental Measurements of Open-Circuit-Potential of Galvanic Cell of Si /Al in TMAH

3.1 Introduction. 51

3.2 Sample and Experiment Configuration.. 51

3.3 Sample Preparation Procedure. 54

3.4 Experimental Procedure... 58

3.5 Preliminary Control Tests 60

3.6 Results.. 62

3.6.1 Graphs of the experimental results.. 63

3.7 Observations and Contributions 73

CHAPTER 4

DISCUSSION

4.1 Measured Galvanic Cell Voltage Values 75

4.2 Bubbling Intensity 79

4.3 Comparison of Au/Si/TMAH and Al/Si/TMAH Galvanic Cells 80

4.4 Difference in n-type and p-type Bubbling Intensity] 81

4.5 The Difficulty of Etching Si without Etching Al 82

4.6 The Application of the Nernst Equation to the Si/TMAH System and Comparison to Experiment 82

4.7 Energy Band Diagrams For Si Anisotropic Etching in the Contexts of Equilibrium and non-equilibrium Electrochemical Conditions 88

4.8 Conclusions and Contributions 93

CHAPTER 5

CONCLUSIONS AND CONTRIBUTIONS
SUGGESTIONS FOR FUTURE WORK

5.1 Conclusions and Contributions 96

5.2 Suggestions for Future work 100

6. References 102

APPENDIX 1

The principles and operation of the Potentiostat 108

APPENDIX 2

Energy Band Models 114

APPENDIX 3

Pilot Tests: Linear-Sweep-Voltammetry (LSV) tests 151

List of Figures

Fig.2.1 Arrhenius curves for TMAH 25wt. %, Si (100) surface. [18] 9

Fig.2.2 Arrhenius curves for TMAH 15wt. %, Si (100) surface. [18] 9

Fig.2.3 The Electrochemical Experimental situation 14

Fig.2.4 Anodic Oxide Passivation I/V Characteristics, I/V curve for p-type Si in 44% KOH at 60°C. At the passivation potential (peak current) and including surface oxide is formed, the current drops to zero, and passivates the silicon to further etching. 26

Fig.2.5 Anodic Etch Stop at p/n Junction, electrical connections for an electrochemical etch-stop on a p/n junction by anodic oxide formation. V_P is that added as " four electrode" etch-stop to prevent leakage currents from prematurely etches stopping. 26

Fig.2.6 The room temperature (I-V curves) voltammograms for n-type (solid line) and p-type (dashed line) samples of <100> orientation. Denoted by n(100) and p(100), respectively. Here PP(n) and PP(p) refer to the Passivation Potential of the n and p-type samples, respectively, while V_{FB} is the flatband potential. The areas of the samples were similar and approximately equal to 1 cm^2. 30

Fig.2.7 Experimental setup for the etching tests. 35

Fig.2.8 Etch-rate *vs.* voltage characteristics of n-, and p-type silicon in: (a) 25 *wt.*% TMAH solution; (b) 25 *wt.*6Zt, 'TMAH: 17 *vol.%* IPA solution [45]. 37

Fig.2.9 A cyclic voltammogram of p-type Si (0.25 cm^2) in 25%TMAH at 80 °C, using an SCE as reference. [10] 43

Fig.2.10 Schematic representations of galvanic cell formation in a TMAH solution containing an oxidizing agent. (a) Shows the anodic current due to Si oxidation. (b) and (c) refer to the reduction of the oxidizing agent at gold. At operation point V_b the cathodic current is not sufficient to achieve passivation. By increasing the concentration of oxidizing agent (curve (c)) V_c reached and the silicon is passivated. [10] 46

Fig.2.11 The formation of a galvanic cell by short-circuiting a gold and a silicon electrode (A) or by evaporating gold onto a silicon wafer (B). [10] 48

Fig.2.12 The time dependence of the rest potential of a silicon electrode in a 25% TMAH solution. At t=0 a gold electrode connected to the Si was immersed in the solution. At t = 1.1 min the gold was withdrawn from the solution. The change in time scale should be noted. [10] 49

Fig.3.1 The schematic set up of the overall experimental configuration. 53

Fig.3.2 Shows schematically the sample configuration, indicating the important features. 54

Fig.3.3 The fabrication process steps 56

Fig.3.4 Variation of OCP vs. time (a) n-type Si, where temperature varies from 24.7 °C to 80.1 °C, in 25 wt.% TMAH (b) p-type Si, where temperature varies from 45.5 to 46.9 °C, in 25 wt. % TMAH 61

Fig.3.5 The experimental results for sample N2, n-type Si <100> in 25wt% TMAH at temperature range of 24.7-81.9 °C (a) OCP (Si) and OCP (Si +Al) vs. pH (b) OCP (Si) and OCP (Si +Al) vs. T (c) pH vs. T (d) pH and T vs. experimental time. 63

Fig.3.6 The experimental results for sample N3, n-type Si {100}, OCP (Si) and OCP (Si +Al) vs. experimental time, in 25wt.% TMAH. 64

Fig.3.7 The experimental results for sample N2, n-type Si <100> in 5wt% (a) OCP (Si) and OCP (Si +Al) vs. pH (b) OCP (Si) and OCP (Si +Al) vs. T (c) pH vs. T (d) pH and T vs. experimental time. 65

Fig.3.8 The experimental results for sample P2, p-type Si <100> in 25wt% TMAH (a) OCP (Si) and OCP (Si +Al) vs. T (b) OCP (Si) and OCP (Si +Al) vs. pH (c) pH and T vs. experimental time (d) pH vs. T. 66

Fig.3.9 The experimental results for sample P2, p-type Si {100}, OCP (Si) and OCP (Si +Al) vs. experimental time, in 25wt.% TMAH. 67

Fig.3.10 The experimental results for sample P3, p-type Si {100}, OCP (Si) and OCP (Si +Al) vs. experimental time, in 25wt.% TMAH. 67

Fig.3.11 The experimental results for sample P2, p-type Si <100> in 5wt% TMAH (a) OCP (Si) and OCP (Si +Al) vs. T (b) OCP (Si) and OCP (Si +Al) vs. pH (c) pH vs. T (d) pH and T vs. experimental time. 68

Fig.3.12 Bubbles level on n-type Si and Al working electrodes in 25wt.% TMAH. 69

Fig.3.13 Bubbles level on p-type <100>Si and Al working electrodes surfaces in 25wt.% TMAH. 70

Fig.3.14 Bubbles level on <100>Si and Al working electrode surfaces in 5wt.% TMAH. (a) n-type Si, (b) p-type Si. 71

Fig.3.15(a) The OCP measurements of only Al in 25wt.% TMAH (b) Bubbles level on Al working electrode surface in 25wt.% TMAH at 47 °C. 72

Fig.4.1 Comparison between Measured OCP and Nernst Equation OCP at the same pH and T values 87

Fig.4.2 The band Diagram of the structure Al/Si after immersion in the solution, the Fermi level of Al/Si (F_{ms}) aligned with the redox level of the solution (E_{sol}) in equilibrium system 89

Fig.4.3 Energy band diagram in context of non-equilibrium condition 90

Fig.4.4 The effective of the electrolyte potential variation with pH on energy band diagram in non-equilibrium condition. (a) This case For p-type Si in 25 wt.% TMAH (b) This case For p-type Si in 5 wt.% TMAH (energy level not to scale) 92

Fig.A1.1 The potentiostat circuit. 109

Fig.A1.2 The demonstration circuit of the potentiostatic measurements. 109

Fig.A1.3 Potential drops in the circuit with the potentiostat no longer matter, as the reference electrode draws no current. 110

Fig.A1.4 A simple experimental setup representation. 111

Fig.A1.5 *I-V* characteristics of n-type Si in TMAH 5 wt.% at 80 $^{\circ}C$. The potential is relative to the Ag/AgCl reference electrode. The exact magnitude of the current profile depends on the working electrode area 112

Fig.A2.1 Effects of bias at a p-n junction; transition region width and electric field, electrostatic potential, energy band diagrams, and particle flow and current directions within W for (a) equilibrium (b) forward bias, and (c) reverse bias. [43] 115

Fig.A2.2 The energy-band for metal-semiconductor junction before contact. For $\Phi_m<\Phi_s$. 118

Fig.A2.3 Variation of the metal-semiconductor work function potential difference Φ_{ms} with substrate doping concentration for Al-Si. [43] 119
Fig.A2.4 The energy-band diagram of metal-semiconductor after contact for $\Phi_m<\Phi_s$.. 120
Fig.A2.5The energy-band for metal-n-semiconductor junction with a negative applied voltage to the n-type (cathodic bias). for $\Phi_m<\Phi_s$. 121
Fig.A2.6 The energy-band for metal-n-semiconductor junction with a positive applied voltage to the semiconductor (anodic bias) . for $\Phi_m<\Phi_s$. 122
Fig.A2.7 The energy-band diagram shows the main parameters. 123
Fig.A2.8 Space charge and electric field distribution within the transition region of a p-n junction with $N_a>N_d$. 124
Fig.A2.9 The schematic of the metal-oxide-semiconductor configuration. 127
Fig.A2.10 Energy levels in metal-oxide-semiconductor structure prior to contact. 128
Fig.A2.11 Energy levels of metal-oxide-semiconductor structure in thermal equilibrium after contact. 131
Fig.A2.12 The Energy-band diagram of the metal-oxide-semiconductor structure with n-type substrate for a negative voltage applied to n-type (cathodic bias). 132
Fig.A2.13 The Energy-band diagram of the metal-oxide-semiconductor structure with n-type substrate for a positive voltage applied to n-type (anodic bias). 134
Fig.A2.14 The Energy-band diagram of the metal-oxide-semiconductor structure with n-type substrate for a "large" positive voltage applied to n-type (anodic bias). 135
Fig.A2.15 Energy band diagram of the metal-oxide-semiconductor structure at Flat band. 136
Fig.A2.16 The Combination the band Diagram of an Al/Si structure with the solution, the Fermi level of Al/Si (F_{ms}) separated with OCP vale from the redox level of the solution (E_{sol}). 138
Fig.A2.17 The effect of the pH and T on the OCP and E_{ss} 145
Fig.A2.18 The energy band diagrams that proposed by Nemirovsky (a) n-type Si (b) p-type Si. [47] 146
Fig.A2.19 The electrolyte potential with respect to vacuum *vs.* the variation of *p*H.(25 wt.% TMAH, p-type Si) 149

Fig.A3.1 Process steps, for the samples that Aluminum deposit over silicon and the samples that aluminum deposit over silicon and silicon oxide. 156
Fig.A3.2 The mask diagrams: (a1) for the front side of the structures code FsiBsi, (b1) for the front side structures code FoxAoxBsi and FoxAsiBox (a2) for backside of the structures to define Al contact area (a3) for the front side structures code FoxAsiBsi and FoxAsiBox where the Al in contact with SiO_2&Si, and (b3) for the front side structures code FoxAoxBsi and FoxAoxBox where the Al in contact with SiO_2. ... 157
Fig.A3.3 The amount of dissolved silicon required to passivate exposed aluminum for various TMAH concentrations.[48] 159
Fig.A3.4 The experimental setup for the electrochemical technique. 160
Fig.A3.5 Circuit diagram for potentiostatic measurements. 161
Fig.A3.6 Potential drops in the circuit with the potentiostat no longer matter, as the reference electrode draws no current. 162
Fig.A3.7 *I-V* characteristics of n-type Si in TMAH 5 wt.% at 80 $°C$. the potential is relative to Ag/AgCl reference electrode. The exact magnitude of the current profile depends on the working electrode area. 162
Fig.A3.8 Current-voltage characteristics of (100) n-type silicon for different concentrations of TMAH (25 wt.% TMAH, 5 wt.% TMAH, and 5 wt.% TMAH with dissolved silicon) at 80 °C. 163
Fig.A3.9 *I-V* characteristics Linear Sweep Voltammetry profile, using 25 wt.% TMAH, n-type Si{100}, pH = 13.4 at a temperature of 80 °C, (its code FsiBsi). 164
Fig.A3.10 *I-V* characteristics Linear Sweep Voltammetry profile, using 5 wt.% TMAH, n-type Si{100}, pH = 12.4 at a temperature of 80 °C. (code FsiBsi). 165
Fig.A3.11 *I-V* characteristics Linear Sweep Voltammetry profile, using 5 wt.% TMAH with dissolved Si, n-type Si{100}, pH = 11.7 at a temperature of 80 °C. (code FsiBsi). 165
Fig.A3.12 Current-voltage characteristics of n-type Si{100}, (front side) aluminum deposited on Si and SiO_2, (backside) open Si, in 5wt.% TMAH with dissolved silicon, at temperature 80 °C. (code FoxAsiBsi). 166

Fig.A3.13 Current-voltage characteristics of n-type Si{100}, (front side) aluminum deposited on SiO_2, (backside) open Si, in 5wt% TMAH with dissolved silicon, at temperature 80 °C. (code FoxAoxBsi). 166

Fig.A3.14 Current-voltage characteristics of n-type Si{100}, (front side)aluminum deposited on SiO_2, (backside) is covered with SiO_2, in 5wt% TMAH with dissolved silicon, at temperature 80 °C. (code FoxAoxBox). 167

Fig.A3.15 Current-voltage characteristics of n-type Si{100}, (front side) aluminum deposited on Si and SiO_2 (backside) is covered with SiO_2, in 5wt.% TMAH with dissolved silicon at 80 °C. (code FoxAsiBox) 167

Fig.A3.16 Current-voltage characteristics of n-type Si{100} (front side) open Si, (backside) open Si, in 5wt.% TMAH with dissolved silicon at 80 °C. (code FsiBsi). 168

Fig.A3.17 Current-voltage characteristics of n-type Si{100}, (front side) aluminum deposited on Si, (backside) is open Si, in 5wt.% TMAH with dissolved silicon at 80 °C. (code FsiAsiBsi) 168

Fig.A3.18 Current-voltage characteristics of p-type Si{100}, (front side) open Si, (backside) open Si, in 5 wt.% TMAH with dissolved silicon at 80 °C. (code FsiBsi). 169

Fig.A3.19 Current-voltage characteristics of p-type Si {100}, (front side) aluminum deposited on Si, (backside) is open Si, in 5wt.% TMAH with dissolved silicon at 80 °C. (code FsiAsiBsi) 169

List of Tables

Table 2.1 Etch rate of silicon on different concentration of TMAH [18]....................8
Table 2.2 surface condition as a function of experimental conditions [18]..................8
Table 2.3The standard emf series[21]. 16
Table 2.4 Measured values of the open-circuit potential (OCP) and the passivation potential (PP) of p- and n-type silicon in different TMAH solutions [45].............36
Table 2.5 Measured membrane thickness and roughness obtained by electrochemical etching in different TMAH solution. [45]..38
Table 2.6 The OCP and PP values Summarization of the literature........................50
Table 4.1 Summary of the OCP and PP values from the literature................................77
Table 4.2 The Galvanic cell results 78
Table A3.1 Sample Configurations 151
Table A3.2 Summary of the structure descriptions and their experimental results. 170
Table A3.3 Summary of the LSV results 171

Chapter 1

INTRODUCTION

Anisotropic etching of silicon is a common technique in the field of microsystems technology (MST). It is used to shape silicon to create microstructures, for microdevices such as microsensors and microactuators. It includes creating familiar cavities on Si{100}, bounded by flat, slow-etching {111} planes. It includes creating deep cavities in {110} silicon with vertical sidewalls defined by {111} planes [1,2]. It also includes the creation of other structures bounded by fast-etch planes [3]. Even though it has been used successfully in the field for several decades, the atomic mechanisms are still not well understood [4,5].

It is used in CMOS-compatible micromachining, often as a post-process after the CMOS- circuitry has been processed, including metals such as Al. Since TMAH (and some other common anisotropic etchants of silicon), etch Al rapidly, this can be a very constraining problem for designers of CMOS-compatible micro-systems. Many researchers have addressed this problem, [3,6,7], without clear resolution. In some etchant conditions, the Al etches rapidly, while in other etchant conditions neither Si nor Al is etched. Based on the observations of several researchers, whether or not etching occurs is not easily controlled [8]. In general, it has been found difficult to anisotropically etch cavities in Si with satisfactory etched surfaces, without etching Al. This work aims

to advance the knowledge related to the problem of Si/Al selectivity, by an experimental study of the electrochemistry of the Al/Si/TMAH system.

Chapter 2 reviews research literature related to anisotropic etching, with emphasis on electrochemical aspects and measurements. The proposed reaction mechanism by Seidel *et al* (1990) is the most commonly-accepted working hypothesis. Several researchers have proposed energy-band analyses for the Si/etchant system. The question of whether or not the etch reaction is in equilibrium is brought forth by Nemirovsky *et al* [9]. Several researchers have performed linear sweep voltammetry measurements in a variety of cases. Recently, galvanic-cell-potentials have been examined for the Au/Si/TMAH system.

After various pilot studies, this thesis focuses on galvanic-cell measurements, to represent the open-circuit potentials of Al/Si/TMAH experimental systems. Chapter 3 describes sample design aspects, sample preparation sequence, and experimental protocol, for galvanic cell experiments on Si/TMAH and Al/Si/TMAH systems. The temperature is varied, the TMAH concentration is varied, and both silicon dopant types are examined.

Chapter 4 discusses the validity of the experiments, and interprets the results in an electrochemical framework, comparing to specific results of other researchers. In particular, the results are compared and contrasted with those of Ashruf *et al* [10], on the Au/Si/TMAH system. The results are also examined with respect to the question of the equilibrium/non-equilibrium nature of the silicon etch reaction.

Chapter 5 lists the contributions of the thesis and suggestions for future work.

CHAPTER 2

BACKGROUND AND LITERATURE REVIEW

2.1 BACKGROUND

2.1.1 Micromachining and Bulk Micromachining

The fabrication of miniaturized mechanical structures on silicon is called micromachining; therefore, the micromachining can be classified in two categories:

2.1.1.1 Bulk Micromachining :

This technology based on making mechanical structures by etching single crystal silicon (SCS). The reason that this technique is called bulk Micromachining because the bulk of the silicon wafer is etched to a depth of tens of micrometers. In this technology, the fabricated parts are made of silicon itself or some other layers that are grown on silicon like thermal oxide or deposited like *LPCVD* oxide and silicon nitride. By using this technique a structure like cantilevers, bridges and membranes are made by masking such as silicon dioxide or of silicon itself with specific orientation [11].

2.1.1.2 Surface Micromachining

In this technology, three-dimensional structures are made of deposited thin films on the silicon substrate and they are released by selective etchants. The reason that this technique is called surface Micromachining (as opposed to bulk Micromachining) is because the substrate of the silicon is not affected and the etching is isotropic.

2.1.2 Background on Anisotropic Etching of Silicon

Anisotropic etching is one of the more important technologies in Micromachining. The anisotropic etchants have some common properties that make them very useful in micromachining these properties are:

1. Anisotropic: the etch rate of silicon is strongly dependent on the orientation of the surface to be etched.
2. Selectivity: the etch rate of the silicon much higher than that of the other material commonly used as etching mask like SiO_2 and SiN_4.
3. The etch rate of {100} n-type Si is lower than that for the {100} p-type Si, making it potentially useful for fabricating thin silicon membranes.

The driving force for the success of anisotropic etching is that it is one of a few microfabrication processes that permits extensive and relatively easy three-dimensional structuring of a substrate. There are essentially two forms of anisotropic etching:

2.1.2.1 Physical dry etching methods

This is including plasma etching, magnetron, reactive ion etching, synchrotron, ion milling,.. *etc.* In dry etching, high-energy ions physically collide with a substrate. Through momentum transfer, the impact kicks out a substrate atom, ion, or molecule. The displacement of substrate may be entirely due to impact as is the case in ion milling with an inert gas, or etching may be assisted through specific chemical reaction such as when reactive ion etching is used. However, for practical reasons anisotropic etching is usually limited to depths of less than $20\mu m$. Although the anisotropic nature of physical etching is important, of immediate interest to define is

the etching selectivity that dry etching demonstrates, particularly reactive ion etching (*RIE*). Although physical dry etching, particularly plasma and RIE, is standard fare in the commercial fabrication of integrated circuits (*IC*), its use in the fabrication of microstructures is still an emerging field.

2.1.2.2 Chemical anisotropic etchants

The term anisotropic etching is usually reserved for the selective wet chemical etching of single-crystalline material along certain crystallographic directions. Although anisotropic etchants are known for a number of different crystalline materials semiconductors have received the most research and commercial attention with, of course, silicon playing the leading role. Some of the more common anisotropic etchants for silicon are KOH, Ethylenediamine Pyrocatechol (EDP), tetra-methyl ammonium hydroxide (TMAH), and hydrazine.

In anisotropic etching of semiconductors with face-centered cubic lattices, like silicon (diamond structure) and GaAs (zinc blend structure), the etching of (111) crystal planes proceeds much more slowly than other crystal planes (i.e. (100) and (110)). Although other crystallographic orientations have been used to fabricated microstructures, these crystallographic orientations are, by far, the most commonly used. So, ***etch anisotropy is the variation of etch rate with direction in the crystal***.

In bulk micromachining, the etchant with different Si lattice surface gives the anisotropic etch characteristic. Mask shapes and etch anisotropy of Si in a particular etchant determine the final shapes of the three-dimensional structures achieved. Etch anisotropy can vary substantially with etchant, etchant concentration, temperature, and additives, leading to widely differing etched shapes [5,12], in both concave and convex structures.

2.1.3 Background on Anisotropic Etching of Silicon in Tetra-Methyl Ammonium Hydroxide (TMAH).

Anisotropic etching of silicon is of such fundamental importance in silicon micromachining that it has been studied and continues to be studied by many researchers. Yet, even with all the attention that it has received, there remain many difficulties, such as toxicity of the most commonly used etchants such as KOH and EDP (i.e. Ethylenediamine Pyrocatechol Water), where, TMAH is relatively less toxic alternative to other anisotropic etchants in contrast to KOH and EDP [13]. The disadvantages of TMAH are: it etches Al rapidly (EDP and hydrazine do not), this is particularly serious nuisance because the bonding pads in Can-MEMS die are made of *Al*, and, the ratio of etch rates, ER{100}/ER{111} is not overwhelmingly high (about 35:1), which is inconvenient in long etches, and the use of TMAH still requires a fume hood. The characteristics of tetra-methyl ammonium hydroxide (TMAH), having the molecular formula $\{(CH_3)_4\ NOH\}$, were investigated by a lot of researchers and they devoted most of their work, on the behaviour of the TMAH as an anisotropic etchant of silicon on various orientation (i.e. {100}, {110} and {111}) at various concentrations (for 25wt%, 15%wt, and 5wt%), by simple temperature dependence. The samples were cut from wafers low doping concentration with resistivity in the range of 0.2-70 Ω.cm n-type, single sided polished. All the samples were cleaned using the *RCA* cleaning before any etch process. Thermal oxide and silicon nitride are excellent masks for TMAH. In most of the experiments carried out thermal oxide was used as mask. The oxide was grown using wet oxidation at 1100°C for a sufficient length of time to grow thickness enough to be used as a mask. Common lithography procedures were used for generating the desired pattern on the polish side of the

samples. In all the cases, the oxide on the back of the samples was left to protect the backside of the samples from etching. The mask used for the measurement of the etch rate does not need to have a specific form. The only condition is that the open area of the silicon exposed to TMAH should be large enough so those etch-stop planes are not reached early. Before etching, the samples were immersed in dilute HF(1:10) for 30 seconds to remove native oxide. The samples used in the experiments were {100}, {110} and {111}. The specific concentrations of TMAH used were 25,15 and 5wt.%. The temperature under control for all of the experiments were 50, 60,70,80 or 90°C, a reasonable rapid etch rates are obtained at a temperatures greater than 60°C-70°C.[9,10,14,15,16,17] Etching was done for different lengths of time. After etching, all of the samples were rinsed with DI water for 10 to 20 seconds, dried with blow of nitrogen and examined through an optical microscope. Measurements of depth were also done by optical microscope, with an accuracy of $\pm 1\ \mu m$. After inspection the etched samples observed [18] that the surfaces of etched area of {100} samples were usually very clean and smooth and the etch depth was very uniform. In this respect, TMAH acts like KOH and EDP[19,20].

In the case of etching {110}surface, it observed the same phenomenon as by H. *Seidel et al* observed, the etched surface is quite rough and its roughness can even be seen with the naked eye. The depth of etch was also non-uniform. For the case of Si {111}, the etched area has a staircase appearance, to measure {111} etch rate, underetch rate of {111} walls were measured instead; the surfaces of the {111} walls which emerges in both {100} samples and {110} samples are all ver smooth and have a mirror-like quality [18].The difference of the etch rate of silicon in different

concentration of TMAH are shown in table 2.1 as result of S. Naseh research [18], and table 2.2 shows the surface condition as a function of experimental conditions for the same author.

Table 2. 1 Difference of etch rate of silicon on different concentration of TMAH [18].

TMAH (wt.%) Concentration	Si Orientation	T (°C)	Etch rate µm/hr unstirred	Etch rate µm/hr stirred
25	(100)	50	4.45	4.16
25	(100)	60	7.9	8.17
25	(100)	70	14.8	14.56
25	(100)	80	23.2	24.63
25	(100)	80	41.85	43.2
25	(110)	89.2	9.35	10.94
25	(110)	50	18.3	20.07
25	(110)	60	30.45	32.7
25	(110)	70	56.56	55.35
25	(110)	80	83.5	83.8
15	(100)	89.2	6.6	6.6
15	(100)	50	35	35
15	(110)	80	4.7	4.7
15	(110)	50	57	57
5	(100)	80	39 (large squares) 13 (small squares)	47 (large square) 35 (small squares)
5	(110)	80	48 (large squares) 21 (small squares)	62 (large squares) 41 (small squares

Table 2. 2 surface condition as a function of experimental conditions [18].

TMAH (wt.%) Concentration	Si Surface Orientation	T (°C)	State of Agitation	Results
25	{100}	50-90	Stirred &unstirred	smooth, uniform etch depth
25	{110}	50-90	Stirred &unstirred	Very rough, textured appearance
15	{100}	50,80	Stirred &unstirred	Uniform, etch depth, many hillocks
15	{110}	50,80	Stirred &unstirred	Very rough, Textured appearance
5	{100}	80	Stirred &unstirred	Very rough, Non-uniform etch depth
5	{110}	80	Stirred &unstirred	Very rough, Textured appearance

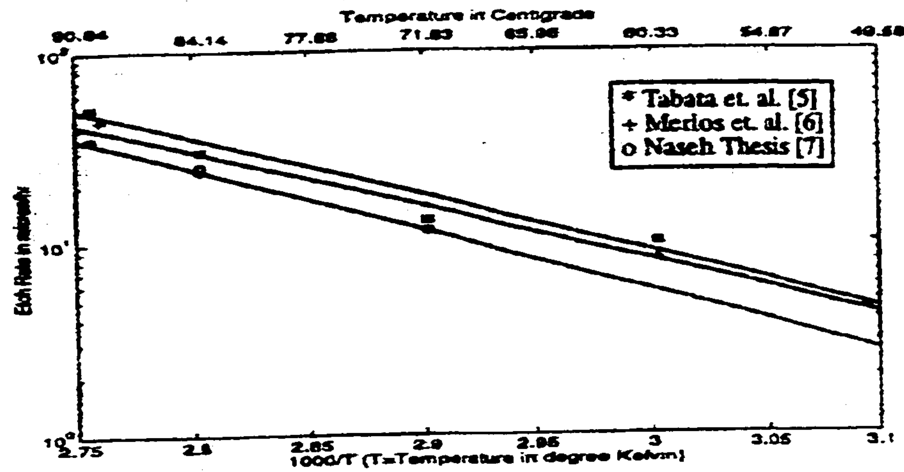

Fig.2.1 Arrhenius curves for TMAH 25wt. %, Si (100) surface. [18]

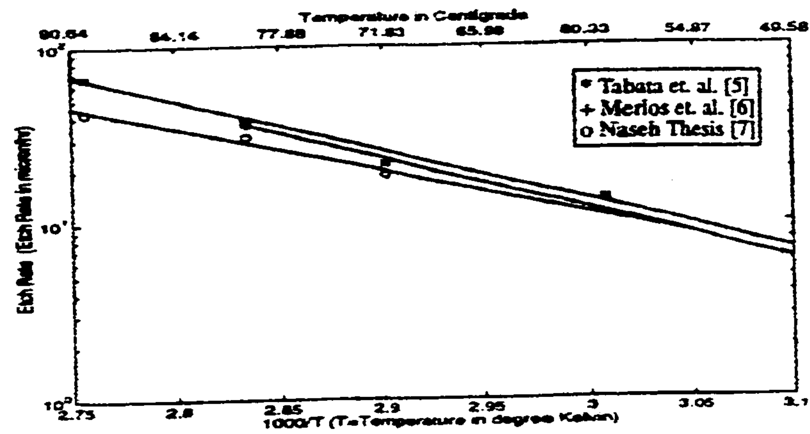

Fig.2.2 Arrhenius curves for TMAH 15wt. %, Si (100) surface. [18]

The same author also observed that the stirring of the solution at all temperatures does not have any effect on the etch rate of the TMAH at 15 and 25 wt.% concentrations. However, for the case of TMAH 5 wt.% stirring and also size of the etch window, as shown in table 2.1 have effect on the etch rate.

Etching of lightly-doping Si (100) surfaces in TMAH is also characterized by authors such as Tabata and Merlos the following figures will clarify the situation of the silicon from each perspective. Where Fig. 2.1 shows Arrhenius curve for TMAH 25wt.%, Si(100) surface, Fig.2.2 shows Arrhenius curves for TMAH 15wt.%, Si(100) surface [12].

In the above figures the results of other researchers are included for comparison. Arrhenius' formula is:

$$R = R_0 e^{\frac{-E_A}{kT}} \qquad \text{Eq.2.1}$$

Where R is the reaction rate, R_0 is called frequency factor [18], E_a is activation energy (eV), k=8.26 $\times 10^{-5}$ (eV) is Boltzman constant and T is temperature in Kelvin. This formula describes the relation between reaction rate and temperature. The units of R and R_0 can be chosen as µm/hr.

2.1.4 Background on Basic electrochemistry

2.1.4.1 The Fundamentals of Electrochemistry

Electrochemistry is the science of electron transfer across a solution-electrode interface. At the cathode, ions or molecules are transformed within the interface via reaction with electrons (from working electrode) to produce-reduced molecules or ions, for example:

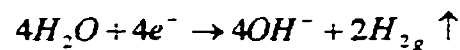

$$4H_2O + 4e^- \rightarrow 4OH^- + 2H_{2g} \uparrow$$

At the anode, molecules or ions (from the solution) are transformed within the interface to produce electrons (at working electrode surface) and oxidized ions and molecules, for example:

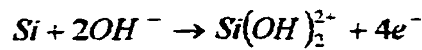

$$Si + 2OH^- \rightarrow Si(OH)_2^{2+} + 4e^-$$

The resultant electrons move from the anode through the wires of the external circuit to the cathode as electronic current (*mA*).

In electrochemistry cells electrons transfer occurs within the electrode-solution interface, with electron removal (oxidation) at the anode, and with electron introduction (reduction) at the cathode. The current through the solution is carried by the ions of the electrolyte, and the voltage limits are those for electron removal from and electron insertion into the solvent-electrolyte.

2.1.4.2 The Electrochemical Mechanism

The principal objective of modern electrochemistry is to study the behaviour and reaction of ions in a variety of environments. The information obtained has important applications to a wide variety of processes, including power cells, fuel cells catalysis, corrosion (etching), and the function of biological membranes. None of these processes is strictly an equilibrium process. Nevertheless, knowledge of equilibrium electrochemistry forms a basis for understanding non-equilibrium processes, and it has many important applications in its own right. The formulation of thermodynamics is directly applicable to the discussion of ions in solution. Only two changes of detail are necessary in order to accommodate the presence of charge. In the first place, ions interact electrostatically over long distances and so they deviate strongly from ideal behaviour even at very low concentrations. In the second place, ions respond to electric potentials and the presence of favorable potential decreases their chemical activity. When several phases are present (i.e. a metal electrode immersed in an electrolyte solution) each phase may be at a different potential. This remark lies at the

heart of electrochemistry. It's good to mention here, that the activity coefficient is the ions response to electric potentials arising from the presence of other ions, and the electrode potentials are the existence of different phases in contact [21].

2.1.4.3 Electrochemical Considerations

Etching (Corrosion) is defined as the destructive and unintentional attack of a metal; it is electrochemical and ordinarily begins at the surface. But etching processes are occasionally used to advantage. For example, etching procedures, as it will discuss later on in more details, make use of the selective chemical reactivity of grain boundaries or various microstructural constituents. For metallic materials, the corrosion process is normally electrochemical, that is, a chemical reaction in which there is transfer of electrons from one chemical species to another. Metal atoms lose or give up electrons in what is called an **oxidation reaction**. For example, the hypothetical metal M, which has a valence of ***n*** (or ***n*** valence electrons) may experience oxidation according to the reaction:

$$M \rightarrow M^{n+} + ne^- \qquad \text{Eq.2.2}$$

in which M becomes a n^+ positively charged ion and in the process loses its ***n*** valence electrons; e^- is used to symbolize an electron. Examples in which metals oxidize are:

$$Al \rightarrow Al^{3+} + 3e^- \qquad \text{Eq.2.3a}$$

$$Fe \rightarrow Fe^{2+} + 2e^- \qquad \text{Eq.2.3b}$$

The site at which oxidation takes place is called the **anode;** oxidation is sometimes called an anodic reaction or de-electronation. The electrons generated from each metal atom that is oxidized must be transferred to and become a part of another chemical species in what is termed a ***reduction*** or ***electronation*** reaction. For example,

some metals undergo etching (corrosion) in acid solutions, which have a high concentration of hydrogen (H^+) ions; the H^+ ions are reduced as follows:

$$2H^+ + 2e^- \rightarrow H_2 \uparrow \qquad \text{Eq.2.4}$$

and hydrogen gas (H_2) is evolved.

Other reduction reactions are possible, depending on the nature of the solution to which the metal is exposed. For an acid solution having dissolved oxygen, reduction according to:

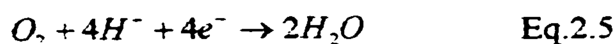

$$O_2 + 4H^+ + 4e^- \rightarrow 2H_2O \qquad \text{Eq.2.5}$$

will probably occur. Or, for a neutral or basic aqueous solution in which oxygen is also dissolved:

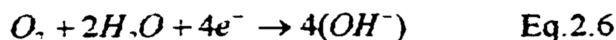

$$O_2 + 2H_2O + 4e^- \rightarrow 4(OH^-) \qquad \text{Eq.2.6}$$

any metal ion present in the solution may also be reduced; for ions that can exit in more than one valence state (multivalent ions), reduction may occur by:

$$M^{n+} + e^- \rightarrow M^{(n-1)+} \qquad \text{Eq.2.7}$$

in which the metal ion decreases its valence state by accepting an electron, or a metal may be totally reduced from an ionic to a neutral metallic state according to:

$$M^{n+} + ne^- \rightarrow M \qquad \text{Eq.2.8}$$

That location at which reduction occurs is called the **cathode**. Furthermore, it is possible for two or more of the reduction reactions above to occur simultaneously.

An overall electrochemical reaction must consist of at least one oxidation and one reduction, and will be the sum of them, often the individual oxidation and reduction reactions are termed ***half-reaction***. There can be no net electrical charge

accumulation from the electrons and ions; that is, the total oxidation must equal the total reduction, or all electrons through oxidation must be consumed by reduction, And this the main concept of ***Open Circuit Potential*** (OCP) at equilibrium circumstances.

2.1.4.4 The Influence of Concentration and Temperature on cell Potential

The potential difference of a cell measured at equilibrium (no current flow) and between platinum terminals is called the *electromotive force* of the cell. Fig.2.3 shows the setup for Linear Sweep Voltammetry (LSV).

This is commonly abbreviated to *e.m.f.* and this is also referring to the OCP in the Linear Sweep Voltammetry (LSV). The platinum electrode itself in electro-chemical cell does not take part in the electrochemical reaction; it acts only as a surface on which hydrogen atoms may be oxidized or hydrogen ions may be reduced.

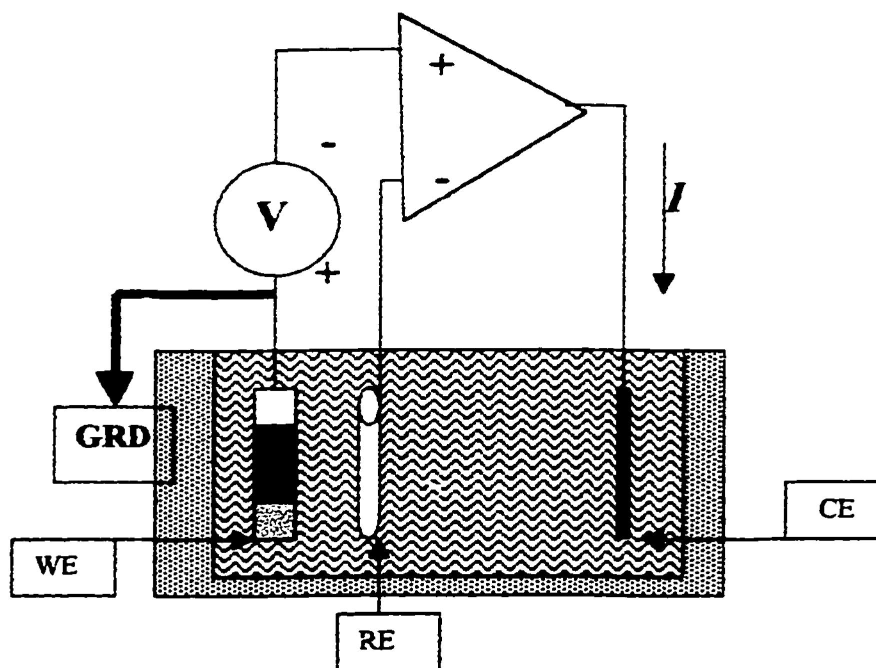

Fig.2.3 The Electrochemical Experimental situation

The electromotive force *e.m.f.* series (table 2.3)[21] are generated by coupling to the standard hydrogen electrode, standard half-cell for various metals and ranking them according to measured voltage. Table 2.3 represents the etching (corrosion) tendencies for the several metal those at the top (i.e. gold and platinum) are noble, or chemical inert. Moving down the table, the metals become increasingly more active, that is, more susceptible to oxidation. Sodium and potassium have the highest reactivities.

The voltages in table 2.3 are for the half reaction as *reduction reaction*, with the electrons on the left-hand side of the chemical equation; for oxidation, the direction of the reaction is reversed and the sign of the voltage changed.

Consider the generalized reaction involving the oxidation of metal M_1 and the reduction of metal M_2 as:

$$M_1 \rightarrow M_1^{n+} + ne^- \qquad -V_1^0 \qquad \text{Eq.2.9}$$

$$M_2^{n+} + ne^- \rightarrow M_2 \qquad +V_2^0 \qquad \text{Eq.2.10}$$

Where, V^0's are the standard potentials (i.e. as taken from the standard e.m.f series). Since metal M_1 is oxidized, the sign of V_1^0 is opposite to that as it appears in table 2.3. Addition of Eqs. 2.9 and 2.10 yields:

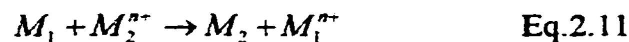

$$M_1 + M_2^{n+} \rightarrow M_2 + M_1^{n+} \qquad \text{Eq.2.11}$$

and the overall potential ΔV^0 is:

$$\Delta V^0 = V_2^0 - V_1^0 \qquad \text{Eq.2.12}$$

Table 2.3The standard emf series[21].

The-Etching tendencies	Electrode Reactions "reduction reactions"	Standard electrode Potential, V^{0} (v)
Increasingly inert (cathodic)	$Au^{+3} + 3e^{-} \rightarrow Au$	+1.420
Increasingly inert (cathodic)	$O_2 + 4H^{+} + 4e^{-} \rightarrow 2H_2O$	+1.229
Increasingly inert (cathodic)	$Pt^{2+} + 2e^{-} \rightarrow Pt$	~+1.2
Increasingly inert (cathodic)	$Ag^{+} + e^{-} \rightarrow Ag$	+0.800
Increasingly inert (cathodic)	$Fe^{3+} + e^{-} \rightarrow Fe^{2+}$	+0.771
Increasingly inert (cathodic)	$O_2 + 2H_2O + 4e^{-} \rightarrow 4(OH^{-})$	+0.401
Increasingly inert (cathodic)	$Cu^{2+} + 2e^{-} \rightarrow Cu$	+0.340
Reference Point	$2H^{+} + e^{-} \rightarrow H_2$	0.000
Increasingly active (anodic)	$Pb^{2+} + 2e^{-} \rightarrow Pb$	-0.126
Increasingly active (anodic)	$Sn^{2+} + 2e^{-} \rightarrow Sn$	-0.136
Increasingly active (anodic)	$Ni^{2+} + 2e^{-} \rightarrow Ni$	-0.250
Increasingly active (anodic)	$Co^{2+} + 2e^{-} \rightarrow Co$	-0.277
Increasingly active (anodic)	$Cd^{2+} + 2e^{-} \rightarrow Cd$	-0.403
Increasingly active (anodic)	$Fe^{2+} + 2e^{-} \rightarrow Fe$	-0.440
Increasingly active (anodic)	$Cr^{+3} + 3e^{-} \rightarrow Cr$	-0.744
Increasingly active (anodic)	$Zn^{2+} + 2e^{-} \rightarrow Zn$	-0.763
Increasingly active (anodic)	$Al^{3+} + 3e^{-} \rightarrow Al$	-1.662
Increasingly active (anodic)	$Mg^{2+} + 2e^{-} \rightarrow Mg$	-2.363
Increasingly active (anodic)	$Na^{+} + e^{-} \rightarrow Na$	-2.714
Increasingly active (anodic)	$K^{+} + e^{-} \rightarrow K$	-2.924

The *emf* series applied to highly idealized electrochemical cells (i.e. pure metal in $1M$ solutions of their ions, at 25°C). Altering temperature or solution concentration or using alloy electrodes instead of pure metals will change the cell potential, and, in some cases, the spontaneous reaction direction may be reversed.

Considering again the electrochemical reaction described by Equation Eq.2.11. If M_1 and M_2 electrodes are pure metals, the cell potential depends on the absolute temperature T and the molar ion concentration $[M_1^{n+}]$ and $[M_2^{n+}]$ according to the Nernst equation:

$$\Delta V = (V_2^0 - V_1^0) - \frac{RT}{nf} \ln \frac{[M_1^{n+}]}{[M_2^{n+}]} \qquad \text{Eq.2.13}$$

Where R is the gas constant, n is the number of electrons participating in either of the half-cell reactions, f is Faraday constant, 96,500 C/mol (i.e. the magnitude of charge per mole $=6.023 \times 10^{23}$ of electrons), at 25°C (about room temperature),

$$\Delta V = (V_2^0 - V_1^0) - \frac{0.0592}{n} \log \frac{[M_1^{n+}]}{[M_2^{n+}]} \qquad \text{Eq.2.14}$$

As expected for 1M concentrations of both ion types (that is, $[M_1^{n+}]=[M_2^{n+}]=1$), Eq.2.13 simplified to Eq.2.12.

2.1.4.5 Utilization of electrochemistry for chemical characterization.

Often the first step in the electrochemistry characterization of a compound is to ascertain its oxidation-reduction reversibility, the cyclic voltammetry is the most convenient and reliable technique for this and related qualitative characterization of a new system [22]. Because electrochemistry provides a unique controlled means of adding or subtracting electrons to or from a compound, it can be used to produce transiently stable species for study by other physical methods such as optical, ESR spectroscopy and mass spectroscopy. The state of utilization is such that for many

research group in the fields of organic and inorganic chemistry, electrochemistry has become a characterization tool as essential as infrared and NMR spectroscopy.

2.1.4.6 Utility of Electrochemistry Methodologies

Electrochemical methods firstly: are well established and use relatively inexpensive equipment to produce unique characterization information for molecules and chemical systems: qualitative (speciation), quantitative analytical data, thermodynamics data (equilibrium constant), and kinetic data (heterogeneous and homogeneous reaction rates). Secondly: electrochemical methods are sensitive; they are able to detect submicro-molar concentrations and sub-pico-mole amounts of electroactive material. Thirdly: electrochemical methods are selective; they are able to control the potential of an electrode, which makes it possible to determine the electrochemical spectrum of electroactive species in solution, analogous to probing the energy states of a molecule with light via spectroscopy [22,23].

2.1.5 The Realization of the Silicon Etching Process in TMAH

The reaction for silicon etching in alkaline solutions can be broken down into two separate Steps:

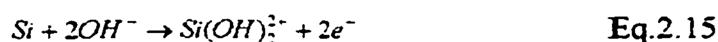

$$Si + 2OH^- \rightarrow Si(OH)_2^{2+} + 2e^- \qquad \text{Eq.2.15}$$

$$Si(OH)_2^{2+} + 4e^- + 4H_2O \rightarrow Si(OH)_6^{2+} + 2H_2 \qquad \text{Eq.2.16}$$

In the first step, as shown in Eq.2.15, electrons are injected into the conduction band of the Silicon. These are used in the reduction step Eq.2.16. Hydrogen forms as a byproduct. If the potential of the silicon is raised relative to the solution (made more anodic), the holes concentration at the surface goes up, and this corresponding for the

situation at the passivation potential (*PP*). The bias causes water molecules to electrolyze, and the resulting hydroxyl ions are attracted to the silicon surface, They then hydrolyze silicon atoms at the surface, which can be as shown in Eq.2.17:

$$Si^{2+} + 2(OH^-) \rightarrow Si(OH)_2 \qquad \text{Eq.2.17}$$

This silicon hydroxide slows the attack of the silicon surface by water molecules. Hydrogen gas is liberated from the $Si(OH)_2$, as shown in Eq.2.18, which causes the formation of silicon dioxide, in the electrochemical etch stop, this oxide is referred to as an anodic oxide.

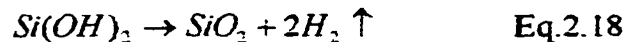

$$Si(OH)_2 \rightarrow SiO_2 + 2H_2 \uparrow \qquad \text{Eq.2.18}$$

This mechanism was also proposed by Glembocki [4], in which the rate-determining step (*RDS*) shifts between among chemical, electrochemical, or diffusion limited. It is interesting to note that despite the volume of work on the problem, the mechanism of the etching (corrosion) processes that take place is still not understood.

The most important question to consider is whether the rate-determining steps in etching reaction are chemical or electrochemical in nature. The most useful tool to distinguish between the two mechanism is to monitor the etch rate as a function of electrode potential. For the electrochemical RDS, the etch rate should be proportional to the concentration of free carrier at the surface, which varies exponentially with the potential drop across the space-charge layer. If the mechanism is chemical, then the only dependence on the electric field across the interface is expected that if the ionic diffusion across the passivating film is electric field assisted.

The most compelling argument in favor of a chemical mechanism for etching of Si in KOH is based on the results by Palik *et al* [4,24], that the etching is independent of carrier density for both n- type and p-type Si, up to concentration About $N=10^{19} cm^{-3}$. For $N>10^{19} cm^{-3}$, there is a dramatic decrease in etch rate, i.e. the etch-stop mechanism.

In the electrochemical mechanism, the experimental etch rates for both orientations and carrier types over a broad potential range. At the *OCP*, where the etching close to its maximum, the difference in the etch rates is small. But this difference increases substantially as one goes anodic and cathodic of the *OCP*.

All of the samples n-type Si (100) stopped etching at anodic biased, owing to passivation of the surface, the etch rates are finite near the passivation potential. At cathodic potentials, there is a substantial difference in the n-type and p-type etches rates. The p-type Si (100) samples continues to etch at a rate close to that of the *OCP* value, where as the n-type Si exhibits etch-stop.

At potentials anodic to the passivation potential (*PP*), the electrochemical hydrogen-evolution will be quenched and the equilibrium will shift to the formation of the oxide. Here, the *RDS* will change from being determined by the charge-transfer reactions at the surface to being controlled by diffusion across the oxide [25].

At the passivation potential (*PP*), the chemical oxidation process is the *RDS* and a connective layer is formed. In the n-type Si, however, there is a lack of holes and the reaction cannot readily proceed. Consequently, even at large anodic biases no appreciable oxide is grown. Cathodic to the passivation potential (*PP*), the semiconductor is in accumulation and majority carries become available at the surface

for reducing the solvent. At the *OCP*, the etching reaction, accompanied by H_2 evolution, will dominate. However, cathodic to *OCP*, hydrogen evolution will proceed not through the hydrolysis of Si-Si bonds (i.e. etching). But rather through the reduction of the solvent (electrolysis), in other word, the reaction, (i.e. in the n-type material) shifts to an electrochemical hydrogen-evolution reaction, resulting from the presence of majority carriers (electrons) at the surface. Etching will stop, and the hydrogen evolution will follow the conventional electric-field-mediated activation mechanism that is dominant on most metals and n-type semiconductors in an accumulation mode.

As was mentioned in the preceding section the etching process is normally electrochemical, that is, a chemical reaction in which there is transfer of electrons from one chemical species to another. The silicon etching process in TMAH has exactly the same mechanism. The mechanism of the etching process is fundamentally a charge-transfer mechanism, the SCS Etching takes place in four basic steps as described in detail by several authors [26,27]:

1. Injection of holes into the semiconductor to raise the silicon to a higher Oxidation state Si^{+}
2. The attachment of hydroxyl groups OH^- to the positively charged Si.
3. The reaction of the hydrated silicon with complexing agent in the solution.
4. The dissolution of the reacted products into the etchant solution.

This process implies that any etching solution must provide a source of holes as well as hydroxyl groups, and must also contain a complexing agent whose reacted species is soluble in the etchant solution.

2.2 Literature Review of the Electrochemistry of Si and Si/Al in Anisotropic Etchants.

2.2.1 The etch mechanism.

Several authors have proposed a lot schemes of chemical reactions [4,20,28], and experimental work of Palik and co-workers have revealed that OH^--groups play a key role in the chemical reaction [29,30]. Based on Palik's suggestion [31,32], Seidel *et al* proposed the following reactions [20,33]:

the first step is a reaction of a silicon atom, attached with two bonds to the solid and thus having two dangling bonds, with OH^- from the solution,

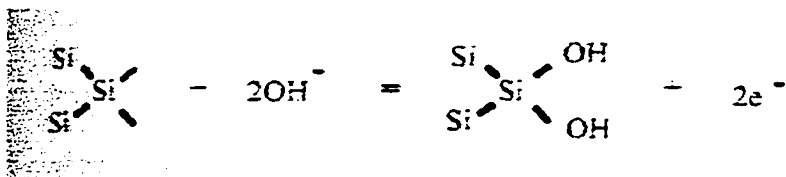

This reaction delivers two electrons to the solid which are thought to be confined to the surface of the silicon. The second step would be an ionization of the $Si[OH]_2$ complex, whereby two further electrons are delivered to the solid (i.e. *RDS*):

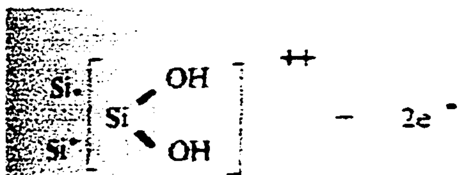

In the third step, the positively charged $Si[OH]^{++}$ complex reacts with two OH^- -ions from the solution:

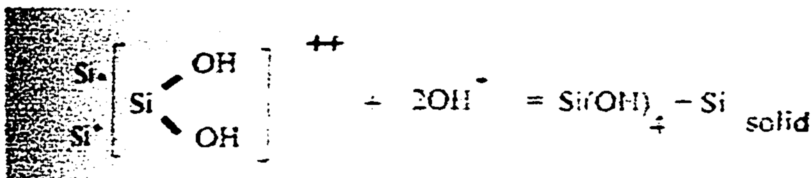

$Si(OH)_4$ is soluble. The molecule can leave the surface. However at the extremely low pH of the solution it is not stable but reacts according to

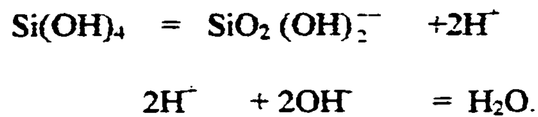

$$Si(OH)_4 \;=\; SiO_2\,(OH)_2^{--} \quad +2H^+$$

$$2H^+ \quad +2OH^- \quad = H_2O.$$

Finally, the four electrons at the silicon surface react with water:

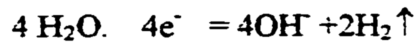

$$4\,H_2O.\quad 4e^- \;=4OH^- + 2H_2\uparrow$$

The second step is considered to be the Rate Determining Step (*RDS*). The difference between the (1 1 1) and the other faces is explained by Seidel *et al.* [20] by the fact that on the (1 1 1) the silicon atoms are bonded with three bonds to the solid, instead of only two bonds:

On the (100) face we have

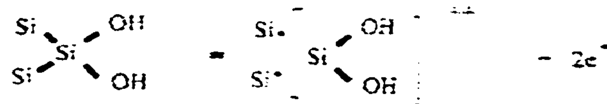

while on the (111) face we have:

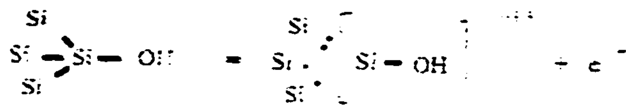

The dots indicate that the attachment of an OH radical changes the energy of the covalent bonds. The anisotropy of the etch-rate is now assumed to result from this energy change, it could depend on the number of OH radicals attached to the silicon

atom. If there is only one OH radical attached, Seidel *et al.* assume that the bond energy will be larger than in the case when there are two OH radicals.

This scheme seems to fit the observations of Palik *et al* quite well. It provides in principle an explanation of the B^{++} etch stop. But it is an electrochemical reaction, the rate of which should depend strongly on the density of electrons at the surface and therefore of the doping. Up to a concentration of 10^{18} atoms.cm^{-3} (donor or acceptor doping) ***the etch rate is independent of the doping.*** Glembocki *et al.* [4] and Allongue *et al* [28] conclude that there must be two parallel reactions: one chemical, without participation of charges and one electrochemical. Glembocki even suggests that at the *OCP* the reaction is entirely chemical.

Electrochemical etch-stops are probably the most common type of etch-stop under external control. However, despite the diversity, ease, and versatility of electrochemical methods these advantages are offset by one major disadvantage. An electrochemical etch-stop usually requires electrical connections to the substrate. This necessitates the obligatory use of cumbersome etch chucks, and fixtures to insulate and protect the electrical wiring from the etching solution. Until recently, this problem has been sufficiently troublesome to virtually eliminate all electrochemical etch-stop from serious consideration in production processing. However, this objection is coming under scrutiny by industrial concerns that see improvements in sensor quality and/or precision by the use of electrochemical etch stop techniques. In addition etching fixtures are becoming readily available items, eliminating many objections to electrochemical etch stops by making electrical connections convenient and compatible with current microfabrication processing. Also there have been some

attempts to eliminate the external wiring providing photovoltaic potentials via internal photodiodes or by a new contactless electrochemical etch-stop based on a gold/silicon/TMAH galvanic cell [10]. A series of electrochemical measurements have been performed on a variety of n-type and p-type Si of {100} orientation in KOH, EDP and hydrazine, more details will be later on.

The salient features of anodic passivation are shown in the current/voltage curve of Fig.2.4 for p-type silicon in KOH (n-type silicon shows similar behavior). However, at some characteristic passivation potential (PP), the current drops precipitously. The decrease in current is concurrent with the formation of a surface oxide and marks the cessation of silicon etching by anodic oxide passivation. To date silicon is the only semiconductor routinely utilizing etch stops by anodic oxide passivation. This is undoubtedly due to the ease with which a high quality surface oxide is formed on silicon. Anodic oxide formation on silicon occurs in almost all etchants. However, the degree of passivation (and etch stop) depends on the complexing strength of the particular etchant as well as the magnitude of the applied potential. EDP does not appreciable etch oxides and demonstrates a particularly high anodic passivation while KOH slowly etches oxides and shows a slightly lower passivation. Silicon also passivates in HF etchants, but the strong complexing strength of fluoride ions makes passivation problematic except in extremely dilute solutions and is also complicated by the formation of pores.

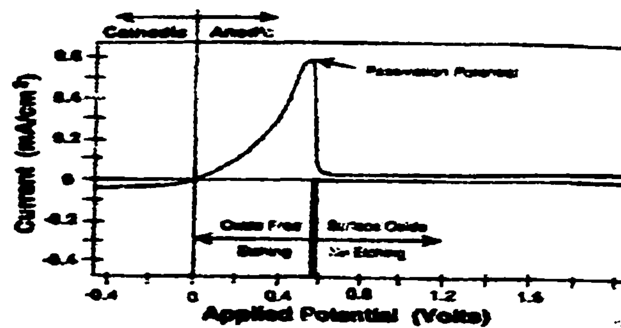

Fig.2.4 Anodic Oxide Passivation I/V Characteristics, I/V curve for p-type Si in 44% KOH at 60°C. At the passivation potential (peak current) and including surface oxide is formed, the current drops to zero, and passivates the silicon to further etching. [5]

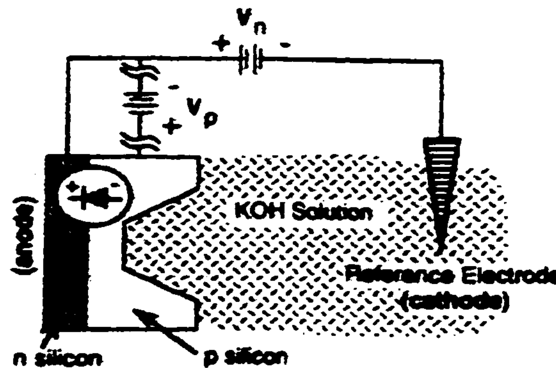

Fig.2.5 Anodic Etch Stop at p/n Junction, electrical connections for an electrochemical etch-stop on a p/n junction by anodic oxide formation. V_P is that added as " four electrode" etch-stop to prevent leakage currents from prematurely etches stopping. [5]

Waggener [14] was the first to propose using the passivation properties of silicon as an etch stop at a p/n junction. In the proposed arrangement an anodic potential in excess of the *passivation potential* (*PP*), V_n is applied directly to the n side of a p/n junction as shown in Fig.2.5. Although the n-type silicon is above the *passivation potential* (PP) and will not etch. The voltage drop across the reverse bias p/n junction leaves the p-type silicon floating at *Open-Circuit -Potentials* (*OCP*) and etching. The result is an etch stop on the n-type silicon. A number of microstructures

fabricated by anodic oxide passivation have been reported [35] using either KOH or EDP as the etchant.

Kloeck *et al* [35,36] have characterized the electrochemical passivation of silicon in KOH and its application to the fabrication of solid-state pressure sensors. They experienced several difficulties with the simple two-electrode electrical configuration. First, they found that small point defects in the electrical integrity of large area p/n junctions allowed sufficient leakage current across reversed biased p/n diode to raise the potential of p-type silicon above passivation and prevent etching long before the p/n junction was reached. Even when the junctions were good, surface leakage across the exposed portions of the p/n junction provided the necessary short to raise the p-type silicon above passivation. In addition, they also found that even when reverse bias electrical integrity was guaranteed, etching would sometimes cease microns before obtaining the p/n junction. To alleviate these problems they added an additional hard electrical connection directly to the p-type silicon to independently controlled its potential externally, V_p in Fig.2.5. The p-type silicon was then pinned at etching potentials and not allowed to float above the passivation potential according to the whims of uncontrolled parameters. They coined the additional electrical connection the four-electrode etch stop configuration, and found that etch stop occurred precisely at the metallurgic p/n junction independent of applied potentials, leakage currents, *etc*.

Later Andews and Turner [18,36] reported that the anomalous cessation of etching under the two electrode configuration resulted from transistor action created by the inadvertent formation of a bipolar transistor during the etch stop.

E. D. Palik[24,25,29,30,31] has with other researchers a big volume of work on silicon etching. The importance of Orientation Depending (*OD*) etching silicon technology has prompted them to study the etch mechanism with the aim of improving the *OD* etching of silicon sufficiently to meet the needs of the microstructure electronics of the future. Actually, the success of the *OD* for etching in Si device technology is due to the strong orientation dependence of aqueous KOH (and few non-aqueous combinations of organic oxidizing and complexing agents). They observed that for a large number of wafers of {100} and {111} orientation ranging in doping density from 10^{14} to 10^{21} cm^{-3} have been used to determine *I-V* curves. All {100} surfaces regardless of doping density or type below 10^{20} cm^{-3} show single *PP* peak while all {111} surfaces regardless of carrier density or type below 10^{20} cm^{-3} show double peaks.

Palik *et al* [24] did a study of the etch-Stop Mechanism in Silicon, too. Potentiostatic electrochemical, ellipsometric, and etch-rate measurements have been made on Boron and Phosphorus doped {100} and {111} silicon wafers. The current – voltage curves indicate that as the doping density increases, the separation of the open-circuit potential (*OCP*) and the passivation potential (*PP*) decreases sharply near a doping density of 10^{19} cm^{-3}. Also, Palik did an ellipsometric study of the etch-stop mechanism in heavily doped, the etch-stop phenomenon which occurs in both p-type and n-type Si when the doping density exceeds 10^{19} cm^{-3} has been studied ellipsometry. Biasing the samples both anodically and cathodically from open-circuit potential (*OCP*) causes layers to grow, which can then be observed to etch back when the applied potential is released. They lead to the conclusion that the p-type Si etch

stops because of spontaneous passivation which produces a thin oxide-like layer, while n-type Si shows a tendency to etch stop, probably owing to formation of a prepassive layer.

Fig.2.6 shows current-voltage characteristics and the bias dependence of the etch rates of <100> oriented n- and p-type low doped Si samples in aqueous KOH have been studied by O. J. Glembocki, R. E. Stahlbush, and M. Tomkiewicz [4]. They found that voltages cathodic of the open-circuit potential (*OCP*) have little effect on the p-type etch rates, while the n-type etching is stopped. Anodic of the open-circuit potential, both carrier types stop etching, owing to passivation of the surface. These results are used to characterize the rate-determining steps (*RDS*) of *the chemical or electrochemical reactions* that take place at the semiconductor surface at various biases. A mechanism is proposed in which the *rate-determining step (RDS) shifts between among chemical, electrochemical or diffusion limited.*

Another parameter, which is very important in electrochemical reactions at semiconductor electrodes, is the flatband potential. With electrolyte electroreflectance [31] and capacitance measurements, the flatband potentials have been determined for Si in 2*M* KOH and are V_{FB}=-1.0V and V_{FB}=-0.2V for n- and p-type samples, respectively. From these numbers they found that the p-type sample was in depletion (hole) during both etching and oxide growth. However, since there is evidence for Fermi-level pinning in p-type Si, its value of flatband is somewhat questionable. For the n-type sample, the situation is different and the data clearly show that flatband occurs between the *OCP* and the passivation potential. Therefore, the n-type sample is in electron accumulation during etching and in depletion at oxide producing potentials.

K. Sundaram and H. Chang [37] studied the anodic dissolution and passivation of n- and p-type Si in different concentrations of hydrazine solution and etching temperatures. During etching, performed at 70°C and 90.5°C, it was observed that the current-potential characteristics for both n- and p-type Si showed a current reduction after reaching a peak value. A linear *I-V* relation was observed for the room temperature etching. A mechanism, which accounts for the semiconductor energy level change solution as under different biasing conditions, was proposed them to give a qualitative explanation of the different *I-V* behaviors for n- and p-type semiconductors.

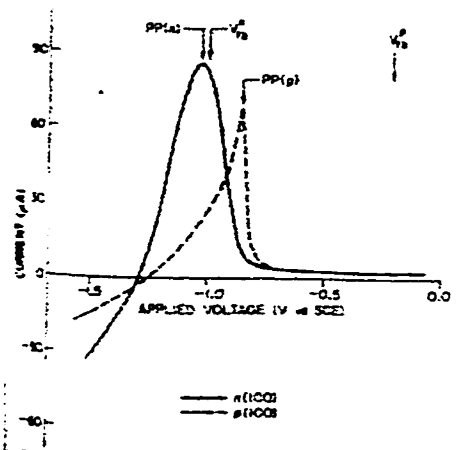

Fig.2.6 The room temperature (I-V curves) voltammograms for n-type (solid line) and p-type (dashed line) samples of <100> orientation. Denoted by n(100) and p(100), respectively. Here PP(n) and PP(p) refer to the Passivation Potential of the n and p-type samples, respectively, while V_{FB} is the flatband potential. The areas of the samples were similar and approximately equal to 1 cm^2. [37]

The importance of silicon micromachining in the fabrication of mechanical and electronic microstructure devices such as microsensors, transducers, and actuators has generated a growing interest in the anisotropic etching and passivation of silicon. The

advantages of using silicon as fabrication material are batch-fabrication capability, low cost, miniaturization of structures, and reproducibility of device characteristics.

The most commonly used etchants in electrochemical etching of silicon are ethylene diamine pyrocatechol (EDP) [19,20], aqueous potassium hydroxide (KOH) [14,24,29,30,31], hydrofluoric acid (HF) [15], and aqueous hydrazine ($N_2H_4H_2O$) [37]. Among them, the EDP and HF have lower etch rates and KOH has the potential problem of potassium ion contamination in semiconductor device fabrication processes. In contrast to these etchants, hydrazine has the fastest etch rate and no contamination problem. Therefore, K. Sundaram *et al* [37] proposed that hydrazine is the most suitable etchant for electrochemical etching of silicon.

The current-standard electrode potential (I-V_{sce}) characteristics and the relation between external applied potential and standard potential (V_{bia}-V_{sce}) for anodic etching of silicon in aqueous hydrazine ($N_2H_4H_2O$) were studied extensively by K. Sundaram [37]. Different n- and p-type silicon wafers with various doping concentrations were used. The I-V_{sce} and V_{bia}-V_{sce} characteristics were examined by anodic etching of silicon samples in various hydrazine solution concentrations and different etching temperatures. The etching behaviors for n- and p-type silicon wafers were different for anodic etching in hydrazine. A mechanism was proposed by Sundaram to give a qualitative explanation for different anodic etching behaviors of n-and p-type silicon. The etching and the etch-stop mechanisms are discussed based on the energy level approach both for n- and p-type silicon-hydrazine systems.

2.2.2 Linear Sweep Voltammetry

Cyclic voltammetry is an extension of linear sweep voltammetry (LSV) with voltage scan reversed after the current maximum (peak) of the reduction process has been passed. The voltage is scanned negatively beyond the peak and then reversed in linear positive sweep. Such technique provides even more information about the properties and characteristics of the electrochemical process and also gives insight into any complicating side processes such as pre-post-electron-transfer reactions well as kinetic consideration. Linear sweep voltammetry uses scan rate is 5 V s^{-1} . For scan rates above 1 V s^{-1} , a computer is required [22].

2.2.2.1 Electrochemical etch-stop characteristics of TMAH:IPA solutions

In bulk silicon micromachining, the interaction of the etchant with the different Si lattice surfaces gives the anisotropic etch characteristics. One of the key technologies in bulk micromachining of silicon sensors has been anisotropic wet etching in alkaline solutions [20,38]. This technique has been dominated by three extensively studied solutions: KOH[39], EDP [19] and hydrazine[37]. All of them, however, have some inherent drawbacks. EDP and hydrazine are toxic and therefore not easy to handle. KOH has excellent etching properties with respect to anisotropy, etch-rate and surface quality. The etch-stop at reverse-biased p-n junctions, especially, is a widely used technique for device fabrication [18,39]. However, the use of KOH is usually restricted to post-processing, as it is contaminating and therefore banned in clean rooms. L.M. Landsberger notified that even if used during post-processing, KOH and such alkali metals are not CMOS-compatible [40].

On one hand, the prospering field of integrated and smart sensors and actuators requires a fully compatible etchant for flexible processes. On the other hand, some techniques well established for conventional etchants, like the boron or electrochemical etch stop, are indispensable. Tetramethyl ammonium hydroxide (i.e. $(CH_3)_4NOH$) (TMAH) has previously been proposed as an alternative etchant [12,18,41,42]. It is easy to handle (non-toxic, non-explosive) and has satisfactory etching characteristics. An extensive study of electrochemical etching with TMAH is presented. Membranes and bridges were etched selectively with similar results to those for KOH. As TMAH is used as a resist strip in standard clean-room processing, it is an appropriate substitute for KOH for the implementation of smart sensors. It has been used successfully for the fabrication of a CMOS integrated pressure sensor and a CMOS-compatible backside-contacted ISFETs [43,44].

M. Acero *et al* did a study on the characteristics of electrochemical etching of silicon in concentrated (25 wt.%) and dilute (2.5wt.%) tetra-methyl ammonium hydroxide (TMAH) and in 25 wt.% TMAH: 17 vol.% isopropyl alcohol (IPA) solutions [45]. They have obtained *I-V* curves and the variation of the etch-rate in the <100> direction with the applied potential for n- and p-type silicon. They observed difference in the passivation potential (PP) of n- and p-type silicon is more significant for dilute TMAH solutions and is practically unaffected by the presence of IPA. The silicon etch-rate is smaller for n-type than for p-type silicon, the difference being more pronounced when no IPA is used. In any case, the etch-rate decreases abruptly at potentials anodic to the PP. Surprisingly, a pronounced decrease in the etch-rate of n-type silicon is observed for potentials negative with respect to the open-circuit potential (*OCP*). The results

obtained are applied to the fabrication of thin membranes and for monocrystalline silicon microbridges. The electrochemical etching behaviour of both p- and n-type silicon was determined by measuring current and etch-rate versus voltage. Then the etch-stop at reverse-biased p-n junctions was used for the fabrication of membranes and microbridges. Two different concentrations of TMAH, 25 and 2.5 wt.%, and a 25 wt.% TMAH:17 vol.% isopropyl alcohol (IPA) mixture were employed. Adding IPA reduces the undercutting of convex corners with respect to unmixed TMAH solutions, which is desirable for the etching of silicon masses or freestanding mesas.

The starting material for their experiment consisted of 300um thick, <100> oriented double-sided polished 100mm p- and n-wafers. The resistivities were 12-18 Ω cm and 3.S5.4 Ω cm, respectively. For all samples a field oxide was used as masking material.

M.C Acero *et al* [45] characterization was based on the experimental set-up that can be seen in Fig.2.7. The current and etch-rate versus voltage measurements were performed with a three-electrode set-up whilst the membranes and the bridges were etched using a *four-electrode arrangement*.[45]. During the etching, the wafers were mounted in a specially fabricated etching chuck, which sealed one side of the wafer and allowed electrical contact to the wafer sample on both sides. Slight nitrogen overpressure in the sealed etching chuck prevented possible liquid leakage. Electrochemical etching was controlled using a Tacussel PJT24-1 potentiostat. As reference electrode an Ag/AgCl type, whose working temperature extends up to 100°C, and a Pt counter electrode, supporting high currents, were chosen. All potentials presented in Acero study refer to the Ag/AgCl electrode [45]. The etching processes were performed in the dark, using a

tank equipped with a reflux condenser and with nitrogen bubbling. A temperature of 80°C was chosen for all experiments, controlled during the process to within ± 1°C.

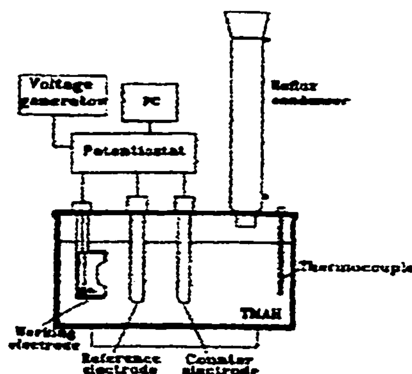

Fig.2.7 Experimental set-up for the etching tests. [45]

As the thermal oxide etch-rate of TMAH is very low (in the range of several tenths of Angstroms per hour), the native oxide was removed with a HF dip before etching. When etching with a four-electrode set-up, it is best to apply the etching first and then the passivation potential. If a surface to be etched is accidentally passivated a HF dip has to be done before starting again.

As a result of Acero *et al* study, he observed that with the usual *I-V* measurements the *OCP* (open-circuit potential) and the PP (passivation potential) were determined in the three-electrode configuration. The sweep rate was 25 mV s^{-1} and the range -2 to + 0.5 V. The results are listed in Table 2.4. They are in good agreement with data published by Tabata *et al.* [42].

As can be observed, the n-type silicon passivates at more anodic potentials than the p-type, for any TMAH concentration and with or without the presence of IPA. The difference in the passivation potentials is more pronounced for the 2.5 wt.% TMAH solution (0.27 V) than for the 25 wt.% TMAH (0.13 V) and TMAH IPA (0.12 V). In any

case it is not sufficient for passivating n-type silicon against p-silicon selectively by applying the same potential at both p- and n-type, i.e., by choosing a potential in between the two passivation potentials. With the same set-up the etch-rate versus voltage curves were obtained by etching for one hour at the applied voltage. From the etch depth, measured with a profilometer, the etch-velocity was calculated. Table 2.4 presents the results for the 25 wt.% TMAH and TMAH:IPA solutions.

Fig.2.8 shows that the etch-rate of n-type silicon is always lower than that of p-silicon, this fact being even more pronounced when etching without IPA. It is notable that there is a decrease of the etch-rate for both p- and n-type silicon for potentials cathodic to the OCP. This effect is much more pronounced for n-silicon, with practically negligible etch-rates. The same effect has been reported previously for KOH solutions [4].

Towards electrochemical micromachining, M. C. Acero *et al* notified that the samples for membrane fabrication were etched electrochemically with a four-electrode set-up, controlling the p-substrate at -1.5 V and biasing the n-wells at 0 V. TMAH concentrations varied from 25, 15 and 10 down to 2.5 wt.%. A single test was carried out in a 25 wt.% TMAH solution, applying a bias of -3 V to both types of silicon. When the etching reaches the space-charge layer of the n-region, the typical current peak appears, indicating the end of the process. The negligible etch-rate of n-type at potentials cathodic to the OCP was used for the fabrication membranes.

table 2.4 Measured values of the open-circuit potential (OCP) and the passivation potential (PP) of p- and n-type silicon in different TMAH solutions [45].

Etchant	Samples	OCP	PP
25 *wt. % TMAH*	n-Si	-1.68	-1.13
	p-Si	-1.69	-1.00
TMAH:IPA	n-Si	-1.66	-1.15
	p-Si	-1.66	-1.03
2.5 *wt. % TMAH*	n-Si	-1.48	-1.02
	p-S	-1.54, -1.34	-0.75

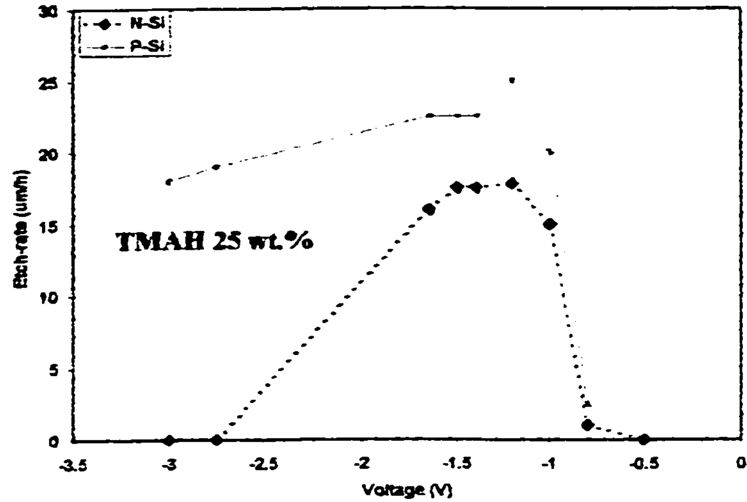

(a)

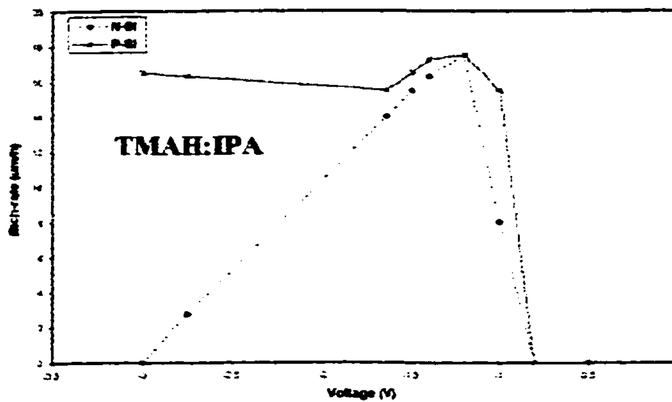

(b)

Fig.2.8 Etch-rate *vs.* voltage characteristics of n-, and p-type silicon in: (a) 25 *wt.*% TMAH solution; (b) 25 *wt.*% TMAH: 17 *vol.*% IPA solution [45].

The membrane thickness was measured optically with an accuracy of ±0.5 μm at five points of the wafer. Table 2.5 summarizes the results. In all cases the etching stops within the space-charge region, slightly before the 15.2 μm deep junction, agreeing with results obtained with KOH as etchant. For lower TMAH concentrations the membrane thickness increases slightly; however, the increase of the membrane roughness is much more pronounced. In the case of the 2.5 *wt.*% TMAH solution no membranes could be achieved, despite long over-etching. Significant etch-depth differences appeared and

stayed on the wafer and the surface had an aspect like "black silicon". In contrast, the surface quality of the samples etched with the 25 wt.% solution was excellent, as the measured roughness values demonstrate. Thc surface roughness of the sample etched at -3 V was also very low. Nevertheless, under the microscope it appeared black and porous, in contrast to the normally observed orange-peel surface.

The microbridges were fabricated using a four-electrode set-up. The voltage at the p-substrate was controlled at -1.5V whilst the n-bridges were biased at +1V. During the etching both silicon types were exposed to the solution. The p-type substrate was controlled at the etching potential while the n-doped bridges were biased by the applied passivation potential. Due to the 45° angle between bridges and {110} planes, the silicon underneath was etched away quickly, releasing the structures. The characteristics of electrochemical etching of silicon in concentrated 25 wt.% and diluted 2.5 wt. TMAH and in a TMAH:IPA solution have been presented. *I-V* curves have been obtained for n- and p-type Silicon showing a similar behavior to that of KOH solutions. Also the variation of the etch-rate in the <100> direction with the applied potential was studied.

Table 2.5 Measured membrane thickness and roughness obtained by electrochemical etching in different TMAH solution. [45]

TMAH (wt.%)	Voltage p/n (V)	Thickness (μm)	Roughness (μm)
2.5	-1.5/0		8.950 ± 4.81
10	-1.5/0	18.02 ± 0.370	0.834 ± 0.54
15	-1.5/0	17.80 ± 0.50	0.075 ± 0.03
25	-1.5/0	17.05 ± 0.25	0.057 ± 0.02
25	-3/-3	17.38 ± 0.40	0.043 ± 0.01

The results show that in the solutions used, for both p- and n-type silicon, passivation takes place at potentials more positive than the ***OCP***. The difference in the passivation potential of n- and p-type silicon is more significant for diluted TMAH

solutions and is practically unaffected by the presence of IPA. The silicon etch-rate is smaller for n-type than for p-type silicon, the difference being more pronounced when no IPA is used. In both cases, the etch-rate decreases abruptly for potentials anodic to the ***PP***. Surprisingly, a pronounced decrease in the etch-rate of n-type silicon was observed for potentials negative with respect to the ***OCP***.

Finally, the results obtained were applied to the fabrication of membranes and monocrystalline silicon microbridges using a four-electrode set-up. Membranes were etched using TMAH solutions with different concentrations. The etch-stop was detected by the appearance of the typical counter-electrode current peak, similar to that in KOH. In all cases it was observed that the etching stops slightly before the physical p-n junction within the space-charge region. It was demonstrated that membranes could also be etched electrochemically applying the same potential, cathodic with respect to the ***OCP***, to both types of silicon. Microbridges were produced making n-diffusions, which formed a 45° angle with the {110} planes, in p-type silicon. During the etching both types of silicon were exposed to the etchant.

2.2.2.2 Electrochemical etch-stop in TMAH without externally applied bias.

Anisotropic etching in tetra-methyl ammonium hydroxide (i.e. TMAH) has been attracting increasing attention as an alternative to KOH, since it is more compatible with a clean-room environment. It has similar etching properties to KOH, including electrochemical etch-stop capabilities although the etch-rate is slightly lower.

Fabrication of micromechanical structures (membranes and beams) with a reproducible thickness is usually accomplished by electrochemically controlled etching. This method requires an external contact to the n-type silicon to be passivated. There are

a few techniques available for fabricating micromechanical membranes of a given thickness based on an etch-stop in an anisotropic wet etchant. The simplest method is that of the timed etch-stop, where a silicon sample is immersed in the etchant for a predetermined time. This is effective for applications where the thickness control of the membrane is not critical. A better thickness control is achieved with the boron etch-stop, which can be used for single-clamped structure [19]. A high boron doping level (typically in excess of $10^{19}cm^{-3}$) decreases the etch rate of the silicon in alkaline etchant drastically because of Fermi-level effects. The high boron dose is known to introduce mechanical stress, which for double-clamped structures can result in buckling or even breaking of the structures. If membranes of a reproducible thickness are required the electrochemically-controlled etch-stop (ECES) can be used [39]. With this method excessive doping is not required. A wafer holder usually achieves an electrical contact to the wafer. This has two main disadvantages. First, the requirement to contact each wafer separately makes batch fabrication difficult. Secondly, the wafer holder itself can introduce mechanical stress into the silicon wafer because difference in the thermal expansion coefficients. For the fabrication of fragile structures this can seriously reduce the yield of the process. A technique has been reported by Peeters *et al.* [39] that accommodates boron etch-stop (which does not require external contacts) and ECES (which gives an accurate and reproducible thickness control) and eliminates the disadvantages (the need for high doping or a wafer holders). With a strong light source at the p-side of a platinum/n-bulk/p-epi-layer structure a photovoltage is generated across the p-n junction (hence the name "photovoltaic etch-stop technique"). Due to the photovoltage the n-type bulk is etched selectively with respect to the p-type epi-layer, resulting in a p-epi membrane.

Recently, a new contactless etch-stop method has been reported by French *et al.* using a p-type bulk and an n-type epi-layer [34]. A gold/chromium film is evaporated onto the n-type epi-layer, while an etch mask is patterned on the p-bulk side. The system is immersed in a TMAH solution and due to an internally generated voltage the n-epi-layer is biased positively. Etching of the p-type bulk proceeds until the p-n junction is reached, at which point etching stops, resulting in an n-epi membrane. A light source is not required, making the technique even more attractive for batch fabrication. This technique which is based on galvanic passivation of silicon has been reported by Ashruf *et al* [10] and they proposed an explanation of the etch-stop mechanism.

The electrochemical experiments were performed with a Bank POS73 Potentioscan. The cyclic voltammograms were measured at a scan rate of $20mV.s^{-1}$ in the dark. The working electrode consisted of a p-type silicon sample with an ohmic contact at the backside. The electrode was mounted with its surface (area $0.5\ cm^2$) facing upwards. A platinum counter electrode with a relatively large surface area ($4\ cm^2$) and a saturated calomel electrode (SCE) as reference were used.

Experiments were performed with <100> n- and p-type silicon wafers with a doping concentration of approximately $10^{15}\ cm^{-3}$ which were provided with a contact mask at one side and an etch mask at the other. Some p-type wafers were provided with an n-epi-layer ($10^{15}\ cm^{-3}$) at the front side in order to fabricate membranes. The masking material for the etchant was LPCVD silicon nitride with a thickness of 1000 Å. The metal films, 600 Å chromium which functioned as an adhesive layer, and 2000 Å gold, were evaporated onto the front side.

For all experiments commercially available tetra-methyl ammonium hydroxide (TMAH wt. 25%) was used. The solution was kept at a temperature of about 80°C using a double-walled glass vessel. Before the etching experiments the wafers were subjected to a 1% HF dip for 2min to remove the native oxide. The etched structures were analyzed with a SEM.

Basically, Ashruf *et al.*[10] proposed that to understand the *galvanic cell passivation mechanism* cyclic voltammograms of silicon (anodic passivation of Si) should be measured. The mechanism of the dissolution and passivation were discussed in detail by Palik *et al.* [4,29,31]. Ashruf *et al.*[10] observed for p-type (100) Si electrode in a 25% TMAH solution at 80°C, that the stable open-circuit potential (OCP) is -1.6 V (SCE). At this potential the semiconductor dissolves chemically at a rate that depends on the temperature and on the composition of the solution. At potentials more negative than the OCP, a small cathodic current is observed. As the potential is made positive with respect to the OCP, the current becomes anodic and increases markedly, as shown in Fig.2.9.

Silicon is electrochemically oxidized and the products dissolve in the solution. The mechanism of this reaction is complex, involving both electrochemical and chemical steps and it was proposed by Seidel *et al* [20].

For the sake of simplicity, Ashruf *et al.*[10] assumed that only valence band holes are involved, which react with hydroxide ions as follows [30]:

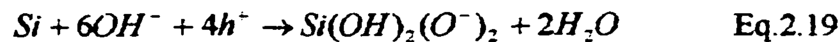

$$Si + 6OH^- + 4h^+ \rightarrow Si(OH)_2(O^-)_2 + 2H_2O \qquad \text{Eq.2.19}$$

At a critical current I_{pp}, corresponding to the passivation potential V_{pp}, an oxide layer is formed on the Si:

$$Si + 4OH^- 4h^+ \rightarrow SiO_2 + 2H_2O \qquad \text{Eq.2.20}$$

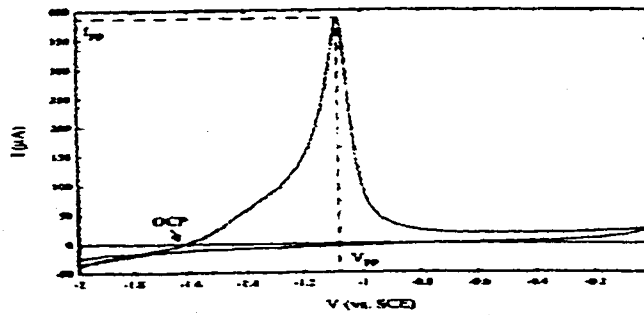

Fig.2.9 A cyclic voltammogram of p-type Si (0.25 cm²) in 25%TMAH at 80 °C, using an SCE as reference. [10]

The current drops markedly to a low value in the passive range. In this range the chemical etching of Si is also suppressed, since the etchant no longer has access to the Si-Si surface bonds. The current in the passive range is determined by the rate at which the oxide is dissolved chemically by the TMAH solution. On the return scan to negative potentials, the current remains low since the anodic oxide is etched back very slowly. To reactivate the surface and recommence chemical etching, the Si must be held at a negative potential to allow the oxide to dissolve.

A significant cathodic current is observed at negative potentials with n-type Si in TMAH solutions. This results from the electrochemical reduction of water to hydrogen, requiring conduction-band electrons. Apart from this process, which obviously does not occur at p-type Si, the forms of the current-potential curves of the two types of electrode are similar. The current to achieve passivation of n-type Si (I_{pp}) is generally similar to that required for p-type material.

2.2.2.3 The galvanic cell passivation mechanism

Silicon, chemically etching at the OCP in an electrochemical cell, can be passivated by applying a potential more positive than V_{pp} and by passing a current larger than I_{pp} through the cell. This means that some power is required to accomplish anodic

passivation. In principle, it should be possible to make use of a galvanic element to achieve the same effect without using an external source. In general, a galvanic cell consists of two electrodes, i.e., *the anode* at which an oxidation reaction occurs (electrons are generated) and *the cathode* at which the reduction reaction takes place (electrons are consumed). When the electrodes are short-circuited, stable *rest potential* is established, which can be measured with respect to a reference electrode. In the present case the Si electrode (anode) with ohmic contact is brought into electrical contact with an inert electrode (e.g., gold) at which an oxidizing agent A^{n+} can be reduced electrochemically (cathode):

$$A^{n+} + ne^{-} \rightarrow A \qquad \text{Eq.2.21}$$

The equation can be written in terms of holes:

$$A^{n+} \rightarrow A + nh^{+} \qquad \text{Eq.2.22}$$

The Nernst potential for the redox system A^{n+}/A must be more positive than the passivation potential of the Si [21]. The principle of galvanic passivation can be understood with the help of the current-potential curves indicated in Fig.2.10. Curve (a) shows schematically the anodic partial current as a function of potential for p-type Si in the etching solution without oxidizing agent. Curves (b) and (c) are those expected for the cathodic reduction of the oxidizing agent at the inert gold electrode. Since in the galvanic cell the electrons required for this reaction are supplied form the valence band of Si; the reduction is better described by reaction (4). In Fig.2.10 it is assumed that the rate of this reaction is controlled by *mass transport* of the oxidizing agent to the electrode and the current is, therefore, independent of the applied potential in a wide potential range. For

curve (c) the concentration of oxidizing agent is higher than for curve (b). The OCP of the Au electrode in the redox solution is the Nernst potential $V_{A^{n+}/A}$. When the two electrodes in the solution containing the oxidizing agent are short-circuited, holes injected by A^{n-} at the Au electrode Eq.2.22 should flow to the Si where they are available for electrochemical oxidation of the semiconductor (Eq.2.19 and Eq.2.20). In the case of the lower concentration of oxidizing agent (curve (b)) the maximum current that can be expected, assuming no ohmic losses in the galvanic cell, is the mass-transport-limited current I_b. From Fig.2.10 it can be seen that this is lower than the current required to passivate the Si (I_{pp}). When the two electrodes are short-circuited in this case, the potential of the Si is displaced from the OCP to the rest potential V_b. Note that at V_b, the anodic (hole consumption) and cathodic (hole generation) currents must be equal, since there is no external current source. The rate electrochemical dissolution of Si is enhanced due to galvanic element formation. Chemical etching of the Si is not changed. In the case of a higher concentration of the oxidizing agent, the maximum current I_c is larger than the passivation current. Short-circuiting the electrodes leads to the formation of an anodic oxide layer on the Si. Si potential is now in the passive range at V_c and the chemical etch rate of Si is negligibly low. The current required to maintain the passivated state at V_c is clearly very small.

Ashruf *et al.*[10] demonstrated the galvanic passivation works in practice by performing two types of measurement: (a) with separate p-type Si and Au electrodes and (b) with a Si wafer the front side of which was provided with a gold/chromium film. In both cases oxygen in the solution acted as oxidizing agent being reduced as follows:

$$O_2 + 2H_2O \rightarrow 4OH^- + 4h^+ \qquad \text{Eq.2.23}$$

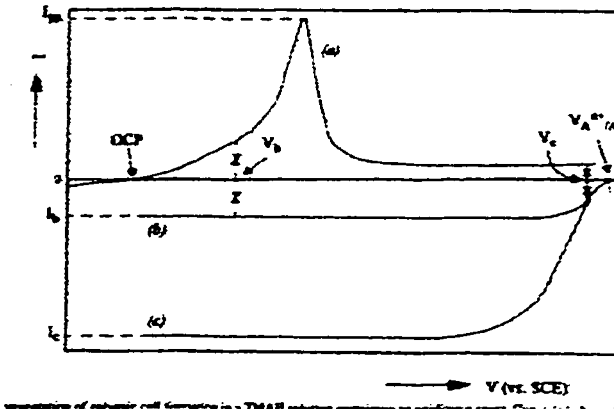

Fig.2.10 schematic representations of galvanic cell formation in a TMAH solution containing an oxidizing agent. (a) Shows the anodic current due to Si oxidation. (b) and (c) refer to the reduction of the oxidizing agent at gold. At operation point V_b the cathodic current is not sufficient to achieve passivation. By increasing the concentration of oxidizing agent (curve (c)) V_c reached and the silicon is passivated. [10]

The redox potential of the H_2O/OH^- couple at pH 14 (0.17V (SCE)) is more than one volt more positive than the Si passivation potential. In order to show that reaction (Eq.2.23) could provide sufficient current to passivate the Si, voltammograms of a Au electrode were measured in the TMAH solution. A mass-transport-limited current of about $300\mu A$ is observed. That this plateau current is indeed due to oxygen reduction is clear from curve (b), which was measured after oxygen was purged from the solution by argon bubbling. A reduction in current of about 80% is clearly observed. The increase in cathodic current at negative potentials and anodic current at positive potentials is due to hydrogen evolution and gold oxidation, respectively. However, the oxygen concentration

at the surface of the gold electrode immediately after immersion is the same as the concentration in the bulk solution. The initial rate of oxygen reduction is therefore considerably higher than the steady-state diffusion-controlled rate. As a result, the initial current should passivate the silicon.

To measure the change in rest potential of the system, Ashruf *et al.* [10] performed the following experiment. A silicon electrode was contacted externally to a gold electrode (see Fig.2.11). The silicon electrode was first immersed in the TMAH solution. The potential was measured with respect to a SCE using a high-impedance voltmeter. Next, the gold electrode was lowered into the solution and the change in potential was recorded. The measured potential is plotted as a function of time in Fig.2.12. The initial potential is typical for an active electrode (compare with the OCP in Fig.2.9) and chemical etching was obvious from the hydrogen evolution. As soon as the gold electrode entered the solution, the potential rapidly changed to about -0.4 V (SCE), which is well into the passive range. The potential stabilized quickly and remained constant. Clearly the Si had become oxidized and chemical etching stopped. When the gold electrode was removed from the solution a rapid decrease of the potential to -1V (SCE) could be observed. Note the difference in time scale in Fig.2.12. After disconnecting the circuit, the silicon does not immediately resume its initial OCP. This is due to the presence of the anodic oxide that was grown during passivation of the silicon. The time needed to re-establish the initial OCP is the etch-back time of the oxide. Ashruf *et al* [10] investigated the influence of the contacting area of the gold/chromium on the effectiveness of the etch-stop, and they observed that the contact area merely determines the series resistance between the electrodes (i.e. silicon and gold) and this has to be

sufficiently small to achieve passivation. When the contact/exposed silicon area ratio is above a small threshold value, the etch stop is effective. A p-n configuration can be used to fabricate n-type membranes in a way similar to the two-electrode ECES. With ECES a p-type wafer is provided with an n-epi-layer. The n-epi-layer is contacted and biased positively with respect to an inert counter electrode (usually platinum), which is immersed in the etchant.

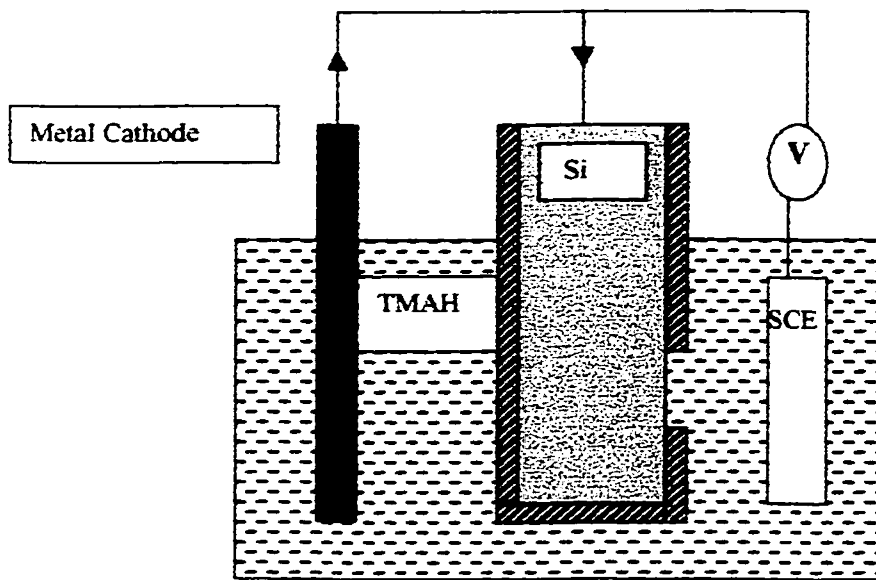

Fig.2. 11 The formation of a galvanic cell by short-circuiting a gold and a silicon electrode. (redrawn from [10])

Most of the potential drop in the reverse-biased p-n configuration is across the depletion region. The p-bulk floats at about the same potential as the etchant and etching proceeds until the depletion layer is reached. Since silicon biased positively with respect to the passivation voltage is passivated, etching stops at the point where the potential in the depletion layer is equal to the passivation potential. The result is an n-epi membrane.

Ashruf *et al* [10] were used the galvanic p-n etch-stop mechanism to fabricate silicon membranes. For the galvanic p-n etch-stop an n-type epi-layer is grown on a p-

type wafer. A gold/chromium film is evaporated on the surface of the epi-layer. A dielectric layer with etch windows on the p-bulk substrate ensures that the gold/exposed Si area ratio is high enough, so that the galvanic cell can provide the required passivation peak current. Initially, p-type Si is exposed to the etchant at one side and gold at the other.

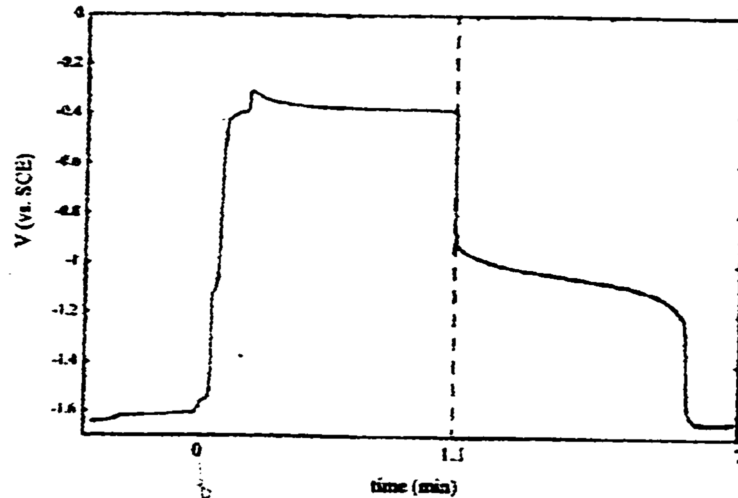

Fig.2. 12 The time dependence of the rest potential of a silicon electrode in a 25% TMAH solution. At t=0 a gold electrode connected to the Si was immersed in the solution. At t = 1.1 min the gold was withdrawn from the solution. The change in time scale should be noted. [10].

In order to passivate the Si a "hole" flux (equivalent to I_{pp}) must be supplied from the gold to the p-Si/etchant interface. However, the "hole" current is very small as the p-n junction is reverse biased. The p-type Si is etched until the junction is reached. At this point electrons are injected into the n-Si conduction band, giving rise to an anodic current and a passivating oxide layer is formed on the surface. The electrons are consumed al the gold electrode according to Eq.2.23 which can also be written in terms of electrons:

$$O_2 + 2H_2O + 4e^- \rightarrow 4OH^- \qquad \text{Eq.2.24}$$

Ashruf *et al* [10] notified that the etch rate of Silicon and silicon oxide in KOH solution is considerably higher than in a TMAH solution [20]. Due to a lower oxide etch rate, the passivation current is lower for TMAH and thus less current is required to passivate Si. Experiments with 33wt. KOH at 80°C showed that the galvanic etch-stop

was not effective using the same configuration and dimensions as with TMAH experiments. Table 2.6 shows the OCP and PP values summarization of the literature results.

- **Table 2.6 The OCP and PP values Summarized from the literature.**

The OCP and PP values in the literature.						
The reference	Etchant	<100>Si type	T (°C)	Reference Electrode	OCP (volt)	PP (Volt)
Acero [45]	TMAH 25wt.%	n-type	80	Ag/AgCl (0.222V)	-1.68	-1.13
Acero [45]	TMAH 25wt.%	p-type	80	Ag/AgCl (0.222V)	-1.69	-1.00
Ashruf [10]	TMAH 25wt.%	p-type	80	SCE (0.253V)	-1.6	-1.04
O.Tabata [42] *et al*	TMAH 22wt.%	p-type	80	Ag/AgCl (0.222V)	-1.66	-1.00
O.Tabata [42] *et al*	TMAH 22wt.%	n-type	80	Ag/AgCl (0.222V)	-1.72	-1.11
Acero [45]	TMAH 2.5wt.%	n-type	80	Ag/AgCl (0.222V)	-1.48	-1.05
Acero [45]	TMAH 2.5wt.%	p-type	80	Ag/AgCl (0.222V)	-1.54	-0.75
E.D. Palik[24]	KOH 2M	n-type	21	SCE (0.253V)	-1.34	-0.22
E.D. Palik[24]	KOH 2M	p-type	21	SCE (0.253V)	-1.05	-0.13
J. Faust[25]	KOH 2M	n-type	21	SCE (0.253V)	-1.32	-0.94
J. Faust[25]	KOH 2M	p-type	21	SCE (0.253V)	-1.07	-0.85
Glembocki[4]	KOH 2M	n-type	20	SCE (0.253V)	-1.3	-1.05
Glembocki[4]	KOH 2M	p-type	20	SCE (0.253V)	-1.25	-0.65
Sundaram[40]	Hydrazine 25%	n-type	70	SCE (0.253V)	-1.25	0.9
Sundaram[40]	Hydrazine 25%	p-type	70	SCE (0.253V)	-1.20	-0.4
B. Kloeck[39]	KOH 40%	n-type	60	SCE (0.253V)	-1.5	-1.2
B. Kloeck[39]	KOH 40%	p-type	60	SCE (0.253V)	-1.5	-1.00

CHAPTER 3

Experimental Measurements of Open-Circuit-Potential of Galvanic Cell of Si /Al in TMAH

3.1 INTRODUCTION.

After a series of pilot experiments involving linear-sweep voltammetry (see Appendix 3), these experiments were conceived to explore the behaviour of the open-circuit-potential (OCP) of Si and Si/Al in TMAH etchant. Both n-type and p-type silicon were used, 25wt% and 5wt% TMAH was used, and the temperature of the solution was swept from room temperature to 80 °C. Instead of the more-complicated linear-sweep voltammetry, simpler structures are used, and the OCP is estimated by inserting a (high-impedance) voltmeter between the working electrode (WE: Si/Al) and the reference electrode (RE).

3.2 SAMPLE AND EXPERIMENT CONFIGURATION.

The overall experimental configuration is schematically shown in Fig.3.1. Through this experiment the following tasks have been taken place:

- A temperature-compensated pH meter immersed in the solution monitored throughout the pH.

- The temperature was monitored throughout by a thermometer, inserted in the solution, and also by the pH meter.
- While the silicon sample was immersed in the solution, the *Al* bar was either immersed in the solution or removed from the solution, according to the protocol described below.
- The OCP measurements vs. time were reported, for various types of silicon (i.e. p- and n-type) at different values of pH and temperatures.

- The situation of the bubbles at the silicon working electrode vs. OCP values, at different temperatures was reported.
- The reliability and stability of the OCP values was studies for different types of silicon.
- The variation of the OCP values before and after the aluminum immersion in the etchant was reported.

In order to eliminate possible sources of error, a carefully-designed sample structure was used, based on the following criteria:

- In order to reduce the possibility of degrading a given sample during the experiment it was desired to keep the sample ohmic contact outside of the solution.
- It was also desired to maintain the exposed silicon area as constant as possible throughout experiments with a single sample.
- During each experiment the area not covered with oxide, not the insertion-depth of the sample, would control the sample area.

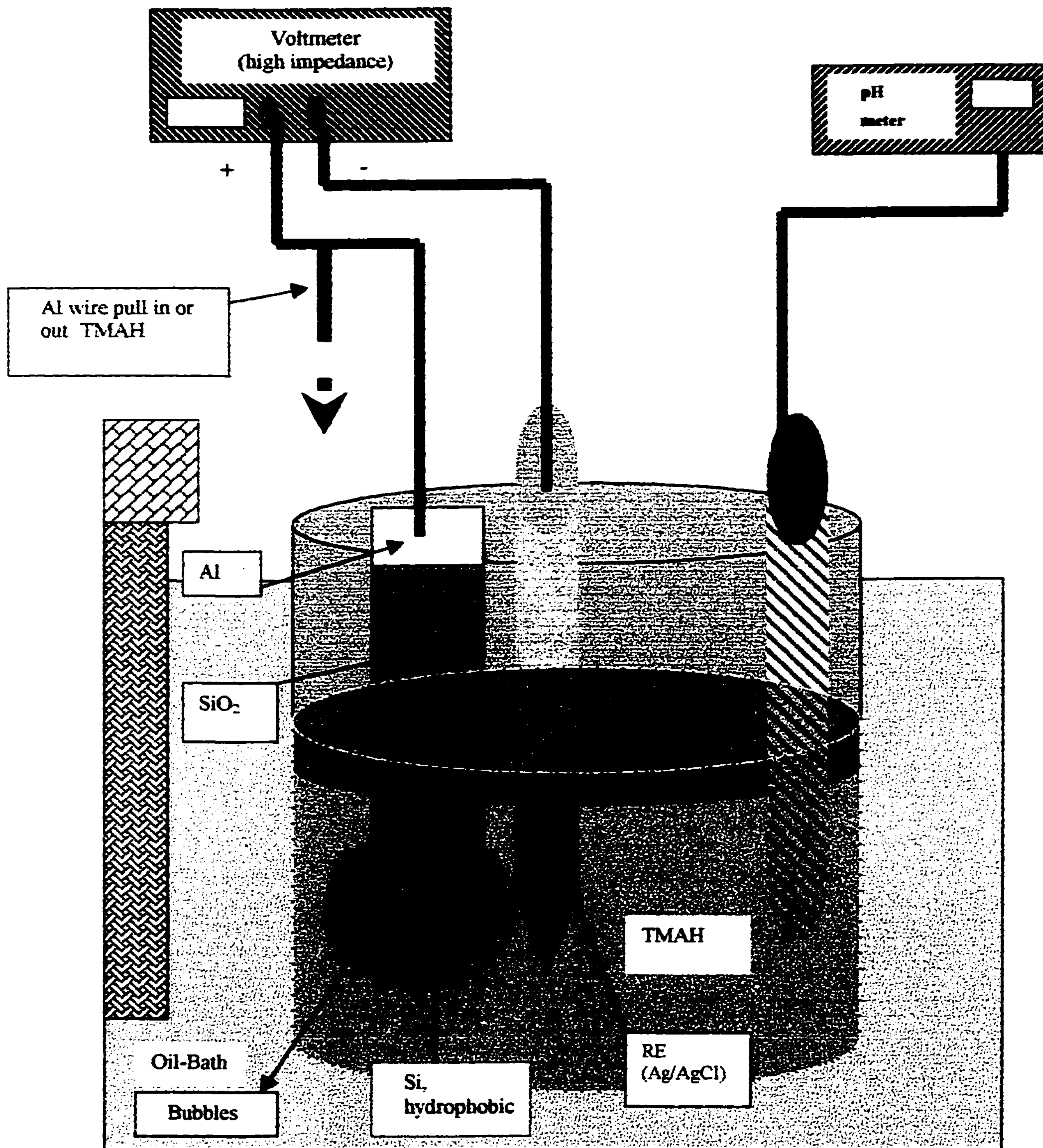

Fig.3.1 The schematic set up of the overall experimental configuration.

- The area not covered by oxide was kept large enough so that any change in exposed area by etching of the oxide at the edge of the masked area would represent an insignificant fraction of the total area.

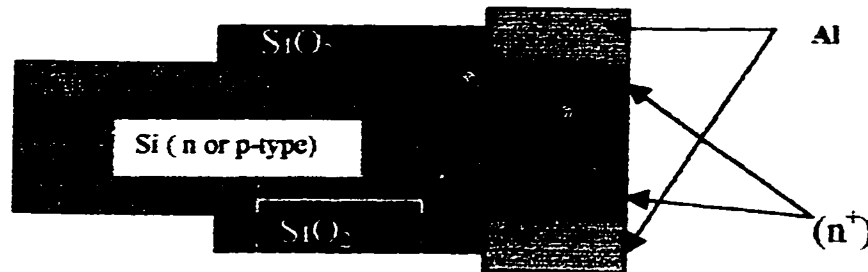

Fig.3.2 Shows schematically the sample configuration, indicating the important features.

3.3 Sample Preparation Procedure.

A special samples were fabricated for the purpose of this experiment, and the steps of this fabrication are as follows:

1. Two lightly-doped silicon wafers, 500-550 μm thick, single-side polished, were selected:

- One sample n-type Si <100>, 10-30 Ω-cm.
- One sample p-type Si <100>, 20-40 Ω-cm.

2. The wafers were cut into strips about 0.5" wide and 3" long. Two strips of each doping-type were made. See Fig.3.3(a).

3. Each strip was marked with a unique ID on the backside, indicating n- or p-type Si and an ID number.

4. The samples were cleaned, using the following typical steps:

- 1:1 H_2SO_4:H_2O_2 ratio, 5 minutes on hot plate, boiling, Then rinses in DI water.
- 1:1:5 HCl:H_2O_2:H_2O ratio, 5 minutes on hot plate, boiling, Then rinses in DI water.
- 1:1:5 NH_4OH:H_2O_2:H_2O ratio, in room temperature for 5 minutes.
- 1:50 dilute HF:H_2O, ratio, dip for 30-60 seconds. Then rinse in DI water.
- Dry the sample by blowing N_2.

5. Thermal Oxidation at 1100 °C in wet O_2 ambient for 2.07 hr, to grow about 1μm (as a thick masking oxide). All of the samples were oxidized in the same run See Fig. 3.3(b).

6. On each sample, a small area of SiO_2 was etched off from one end, about 0.25", in dilute (1:50) HF, until the silicon became hydrophobic. See Fig.3.3(c).

7. These exposed ends of the samples were covered with sources of heavy doping:

- Phosphosilicate gel for n-type samples.
- Boronsilicate gel for p-type samples.

(a)

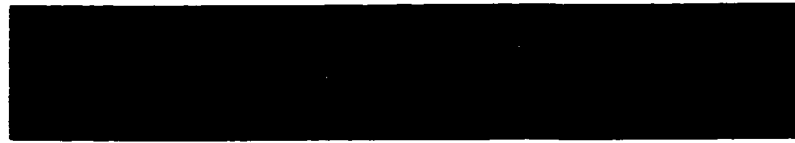

(b)

(c)

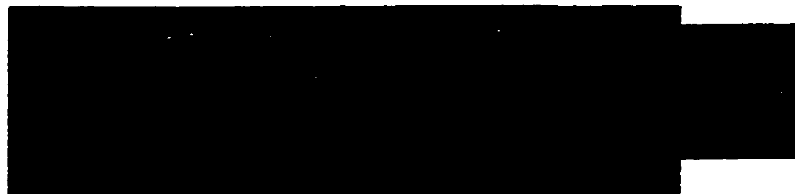

(d)

SiO_2

Al

Si (n or p-type)

SiO_2

(n^+)

(e)

Fig.3.3 The fabrication process steps

8. The samples were then put into the diffusion furnace at 1100 °C for 2.5 hr, in order to diffuse to a junction depth about 2.6 μm.
9. The resulting phosphosilicate glass and boronsilicate glass were etched off using 1:4 HF:NH_4F. and 1:50 HF:H_2O, respectively. Leaving heavily-doped bare silicon at the exposed ends of the samples.
10. Positive photoresist (Microposit 1350J, Shiply, MA. USA) was applied manually to the entire sample, both front and backsides, except for the heavily doped ends.
11. The samples were baked for 20 min at 95 °C.
12. Aluminum was evaporated onto the samples to a thickness of about 5 μm to both front and backsides of the samples.
13. The photoresist was removed in acetone, lifting with it the excess *Al* that did not contact the silicon. See Fig. 3.3(d).
14. The samples were alloyed in N_2 gas flow through the sealed reactor tube for 2 min., when the temperature reaches 350 °C then the ambient change to nitrogen/hydrogen, when the temperature 450 °C is attained, begin alloy timing for 30 min at 450 °C.
15. Positive photoresist was painted on the mid-section of each (strip-shaped) sample, such that a large area at the non-aluminized end is not covered with photoresist (an area about 2 cm up the strip, and including the full width of the strip, both sides of the wafer).
16. Bake the photoresist for 30 min at 95 °C.
17. The exposed SiO_2 at the non-aluminized end of each strip was etched off by dipping in dilute HF:H_2O (1:50) until the silicon became hydrophobic.
18. The photoresist was removed by acetone. See Fig.3.3(e).
19. The samples are ready for the experiments.

3.4 EXPERIMENTAL PROCEDURE

The following experiment has been done to estimate the open circuit potential (OCP) of the cell for different concentrations of TMAH, without using the potentiostat. The pH and temperature were measured simultaneously. We found that both the pH and the OCP varied with temperature.

This experiment differs significantly from the previous experiments using the potentiostat in several ways, for example the connection between the silicon and the wire was done directly using an alligator-clip without silver paste or platinum wires.

The experimental procedure was as follows:

1. For all the experiments, commercially-available tetra-methyl ammonium hydroxide (TMAH) $\{(CH_3)_4NOH\}$ at 25wt% was used. (Purchased from Moses Lake Industrial INC. USA). 5wt% TMAH was obtained by diluting the 25wt% TMAH with DI water (i.e. 100 ml of 25wt% TMAH to 400 ml DI water).
2. Select a sample created as described above.
3. The native silicon oxide (SiO_2), which might be on the bare surfaces, is removed by etching in (HF/H_2O) solution (1/50) at room temperature, followed by a rinse and storage in DI water.
4. Immerse the reference electrode (RE) (i.e. Ag/AgCl) in the solution, and connect it to the ground of the digital voltmeter.
5. Immerse the thermometer in the solution, and monitor the temperature of the solution, beginning near room temperature (25°C).
6. Immerse the pH meter (Corning pH meter 445, Corning Electrode cat. No.

476436, USA) in the solution, and begin observing the pH meter reading at room temperature.

7. Connect alligator-clip to one bare end of the Si sample.
8. Immerse the other end of the sample into the solution, making sure to immerse the entire bare silicon portion (so that the area of exposed silicon remains constant). Then the readings begin recording from all of the meters (i.e. Voltmeter, pH meter, and thermometer) and observing the bubble situation at the silicon working electrode.
9. After recording the three readings, electrically connect an Al wire to the wire between silicon and voltmeter. Then immerse the other end of the aluminum into the solution, and record voltmeter, pH and T.
10. Heating the solution using oil-bath raises the temperature. The above readings are taken roughly.
11. After the temperature reaches a maximum 80 °C, the oil-bath is turned off, and the solution is allowed to cool. Again, the same readings are taken periodically.

3.5 Preliminary Control Tests

In order to validate certain aspects of the sample configuration, experimental set-up and procedures, several preliminary tests were done:

1. Ohmic contact was tested on several of the aluminized samples. This was done by carefully using the probe station and hp Hewlett Packard 4155A, semiconductor parameter analyzer, serial No. JP10A00907, Japan.
2. In order to verify whether the position of the sample in the solution made a difference, the sample was moved laterally by several cm while immersed in the solution, such that the distance from the working electrode changed by several cm. This was done at a range of T = 45.5-47.1 °C. The measured OCP was not found to change by more than 0.2 mV.
3. In several early tests, upon immersion of the sample into the etchant, it was found that the OCP was unstable and un-repeatable for several minutes. After some minutes, the OCP dramatically change to a more-realistic value, and bubbling began on the immersed Si surface. Fig. 3.4 shows an example of this behavior. It was found that this unreliable stage of operation was eliminated by immersion of the sample in dilute HF immediately before (within 5 minutes before) immersion into the etchant.
4. Position of sample in the solution was found to affect OCP negligibly.
5. Native oxide was found to be a significant issue. Fig.3.4b shows manifest this issue. The sample should be dipped in HF solution (1:50) at room temperature to remove all of the native oxide that might be grown over the silicon surface.

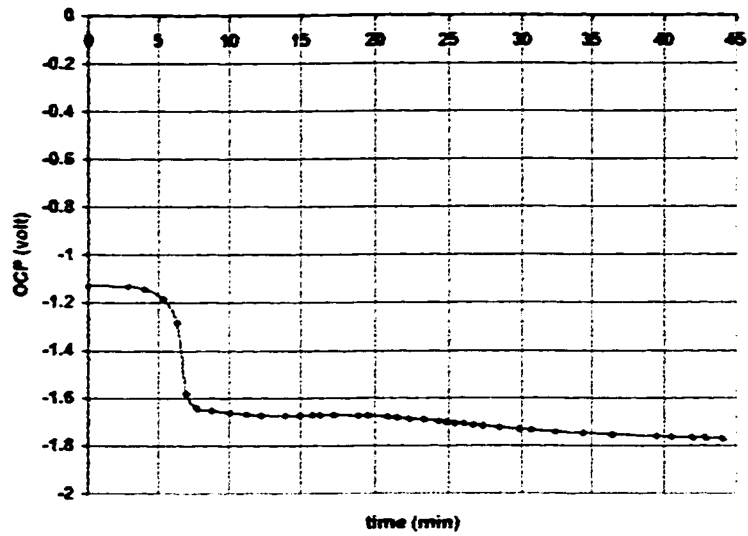

(a)

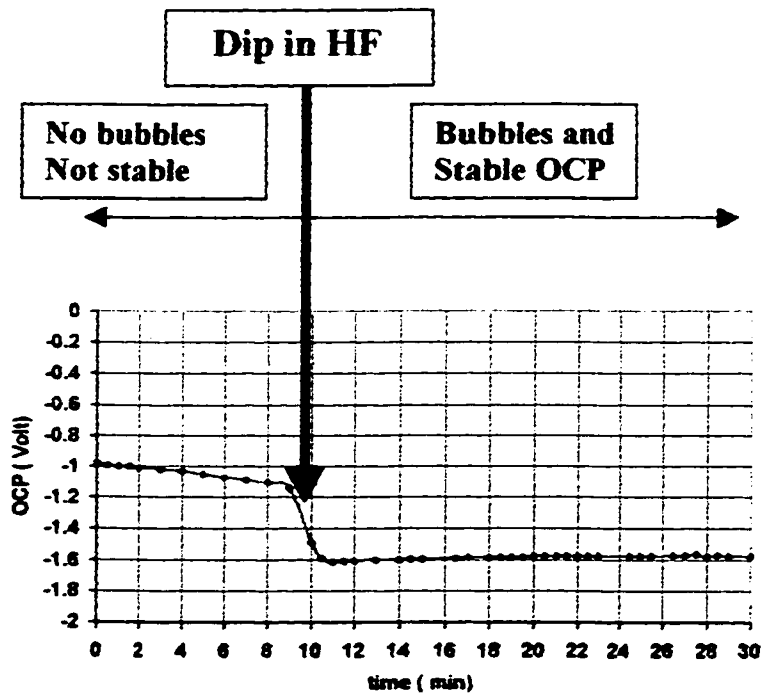

(b)

Fig.3.4 Variation of OCP vs. time (a) n-type Si, where temperature varies from 24.7 °C to 80.1 °C, in 25 wt.% TMAH (b) p-type Si, where temperature varies from 45.5 to 46.9 °C, in 25 wt. % TMAH.

3.6 RESULTS.

The following main experimental sequences were executed:

- Sample N2, n-type Si <100>/Al in 25wt% TMAH.
- Sample N3, n-type Si <100>/Al in 25wt% TMAH.
- Sample N2, n-type Si <100>/Al in 5wt% TMAH.
- Sample P2, p-type Si <100>/Al in 25wt% TMAH.
- Sample P2, p-type Si <100>/Al in 25wt% TMAH
- Sample P3, p-type Si <100> /Al in 25wt% TMAH.
- Sample P2, p-type Si <100> in 5wt% TMAH.

For each case mentioned above, several graphs are presented:

- pH and T vs. experimental time.
- pH vs. T.
- OCP (Si) and OCP (Si +Al) vs. pH.
- OCP (Si) and OCP (Si +Al) vs. T.

3.6.1 GRAPHS OF THE EXPERIMENTAL RESULTS.

1. The experimental results for sample N2, n-type Si <100> in 25wt% TMAH at temperature range of 32.9-81.9 °C. (see Fig.3.5)

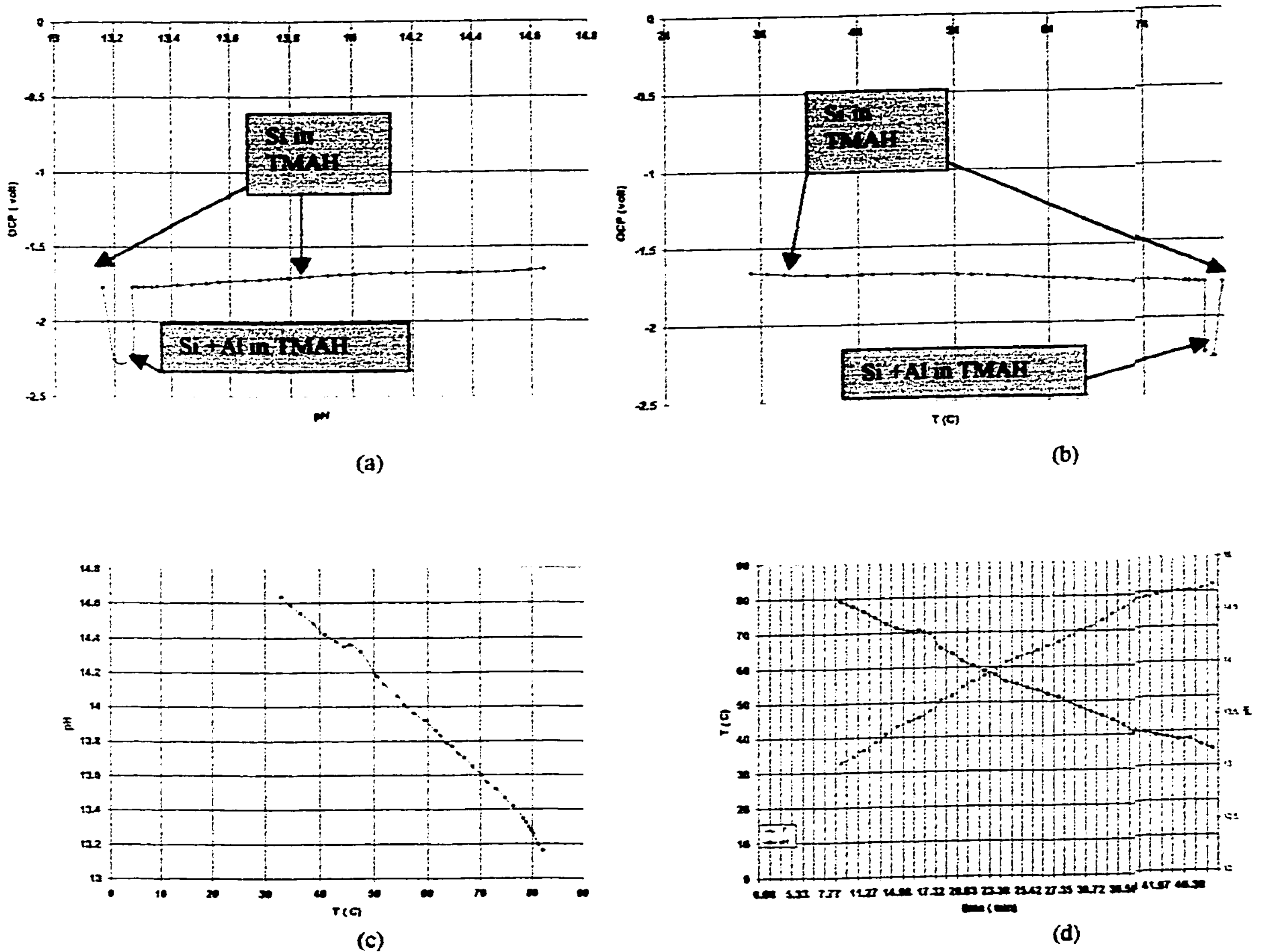

Fig.3.5 The experimental results for sample N2, n-type Si <100> in 25wt% TMAH at temperature range of 24.7-81.9 °C (a) OCP (Si) and OCP (Si +Al) vs. pH (b) OCP (Si) and OCP (Si +Al) vs. T (c) pH vs. T (d) pH and T vs. experimental time.

2. The experimental results for sample N3, n-type Si {100}, in 25wt.% TMAH at constant temperature ~47 °C. (see Fig.3.6)

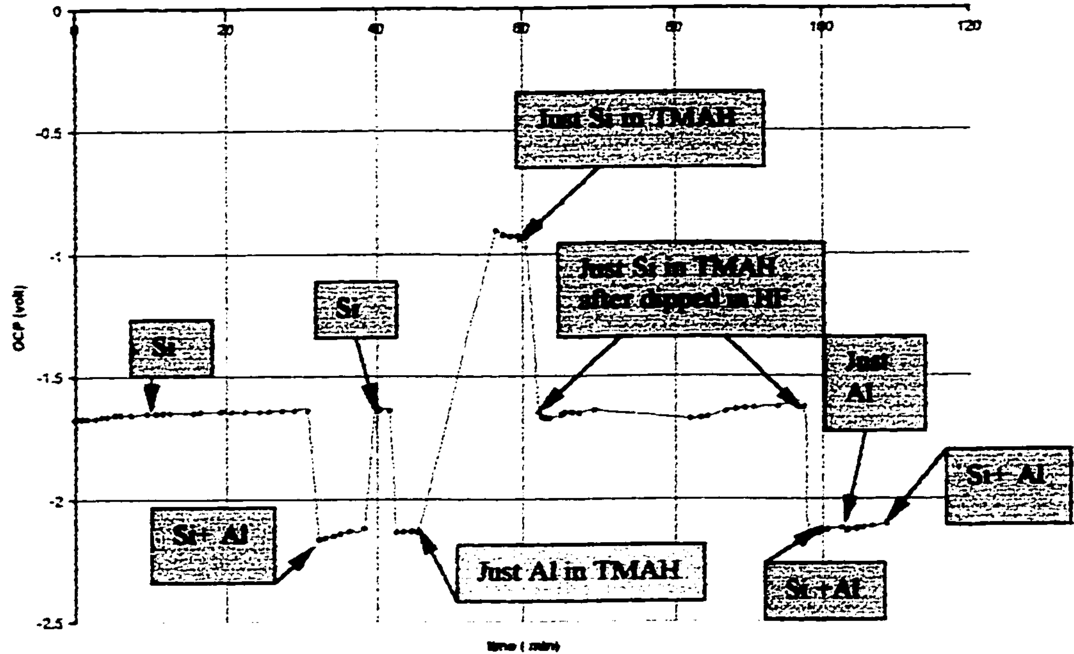

Fig.3.6 The experimental results for sample N3, n-type Si {100}, OCP (Si) and OCP (Si +Al) vs. experimental time, in 25wt.% TMAH.

3. The experimental results for sample N2, n-type Si <100> in 5wt. % TMAH at temperature range of 43.7-81.0 °C. (see Fig.3.7)

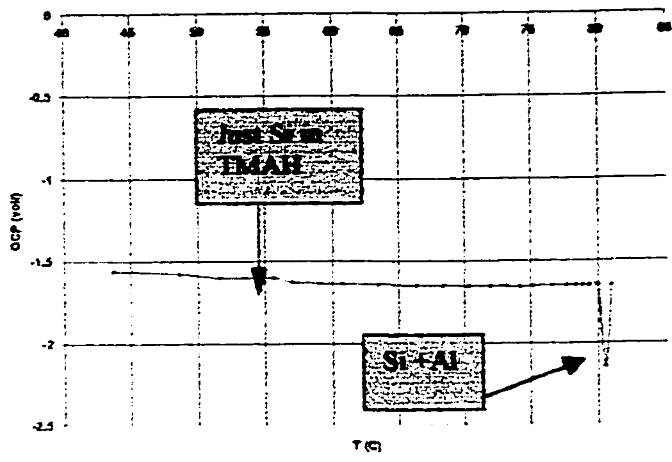

(a)

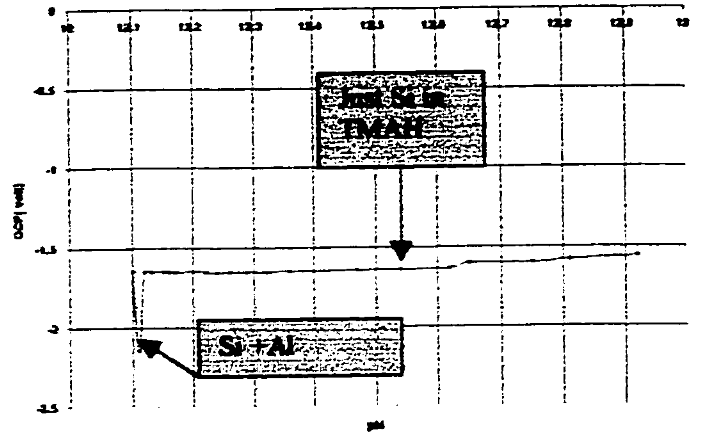

(b)

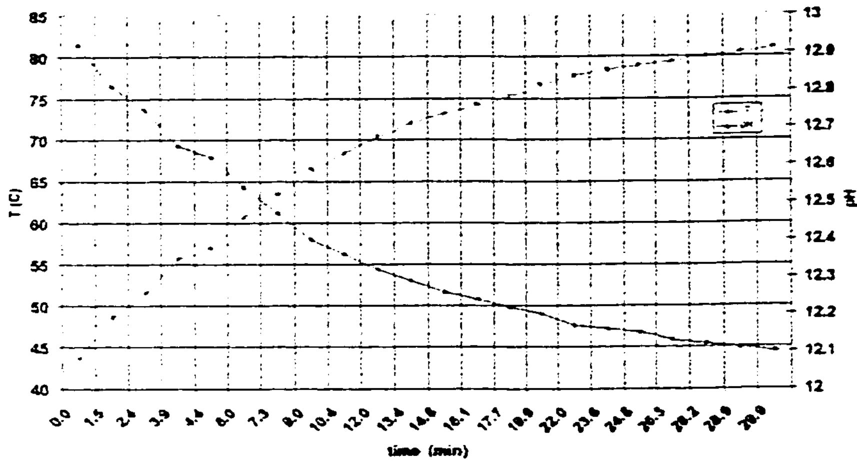

(c)

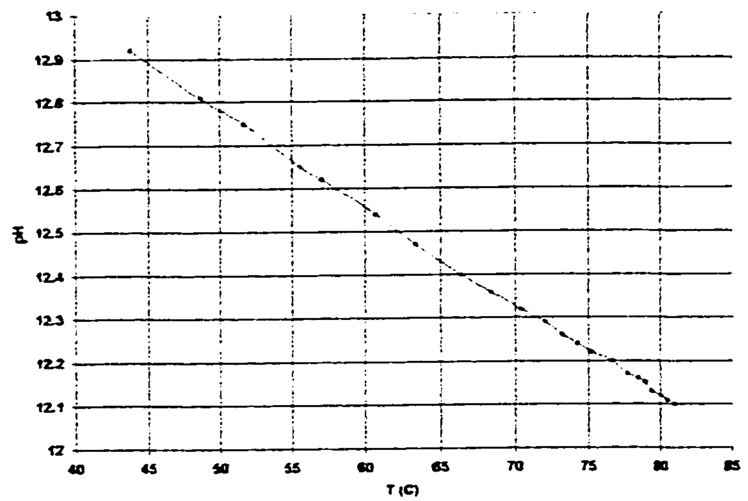

(d)

Fig.3.7 The experimental results for sample N2, n-type Si <100> in 5wt% (a) OCP (Si) and OCP (Si +Al) vs. pH (b) OCP (Si) and OCP (Si +Al) vs. T (c) pH vs. T (d) pH and T vs. experimental time.

4. The experimental results for sample P2, p-type Si <100> in 25wt% TMAH at temperature range of 30.4-83.7 °C. (see Fig.3.8)

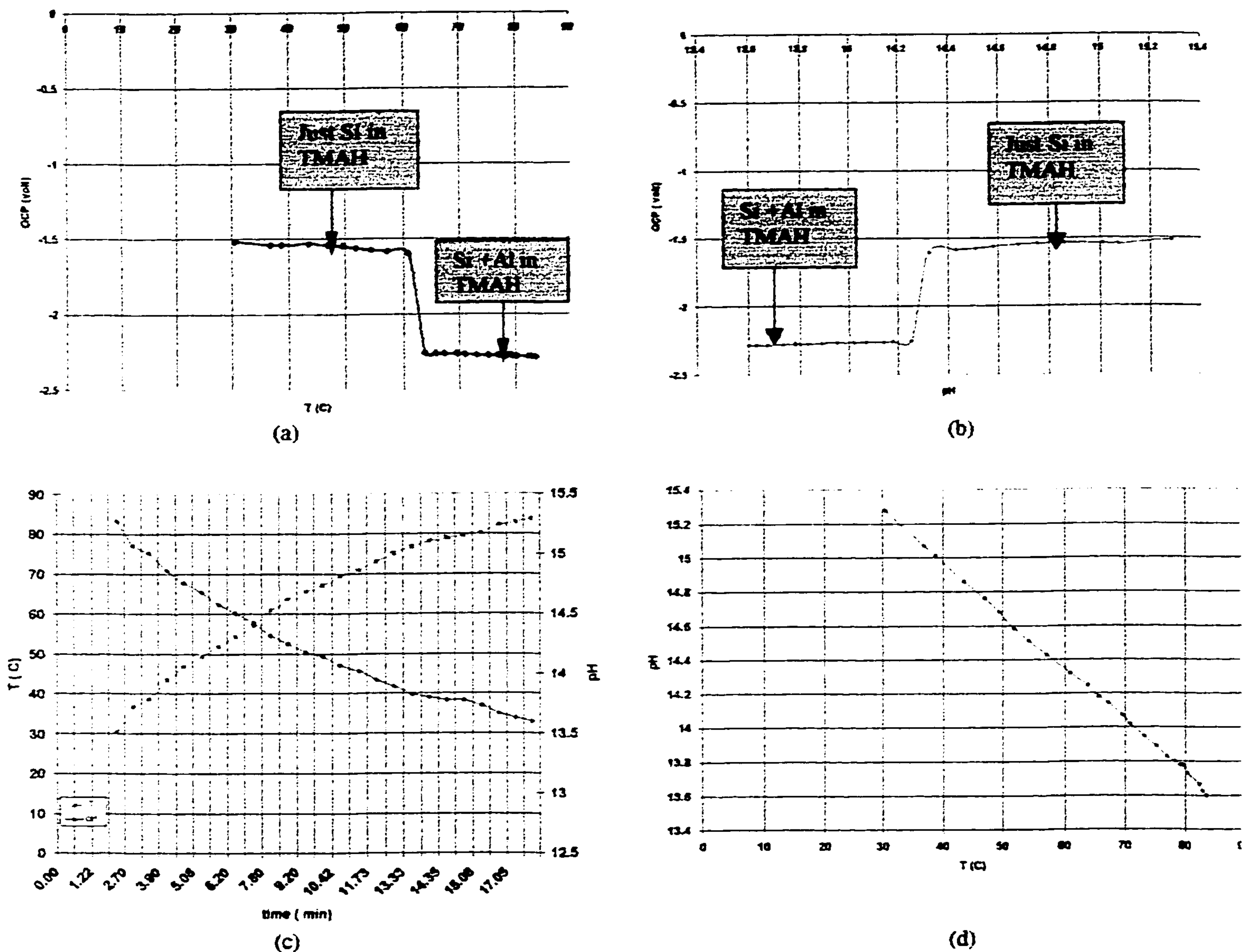

Fig.3.8 The experimental results for sample P2, p-type Si <100> in 25wt% TMAH (a) OCP (Si) and OCP (Si +Al) vs. T (b) OCP (Si) and OCP (Si +Al) vs. pH (c) pH and T vs. experimental time (d) pH vs. T.

5. The experimental results for samples P2 and P3, p-type Si {100} in 25wt.% TMAH at constant temperature ~47 °C. (see Fig.3.9 and Fig.3.10, respectively).

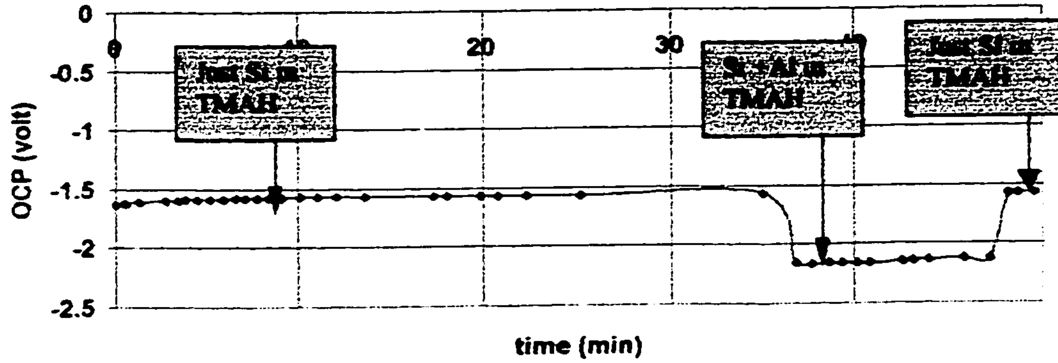

Fig.3.9 The experimental results for sample P2, p-type Si {100}, OCP (Si) and OCP (Si +Al) vs. experimental time, in 25wt.% TMAH.

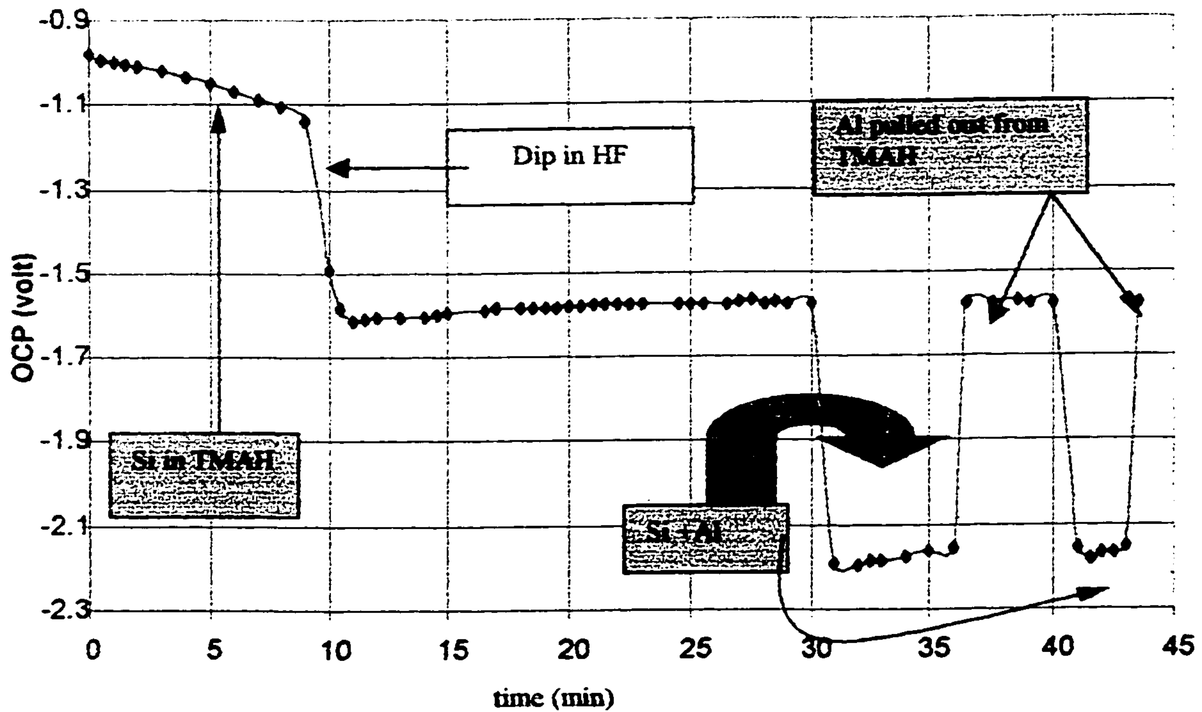

Fig.3.10 The experimental results for sample P3, p-type Si {100}, OCP (Si) and OCP (Si +Al) vs. experimental time, in 25wt.% TMAH.

6. The experimental results for sample P2, p-type Si <100> in 5wt% TMAH at temperature range of 21.3-80.1. (see Fig. 5.11)

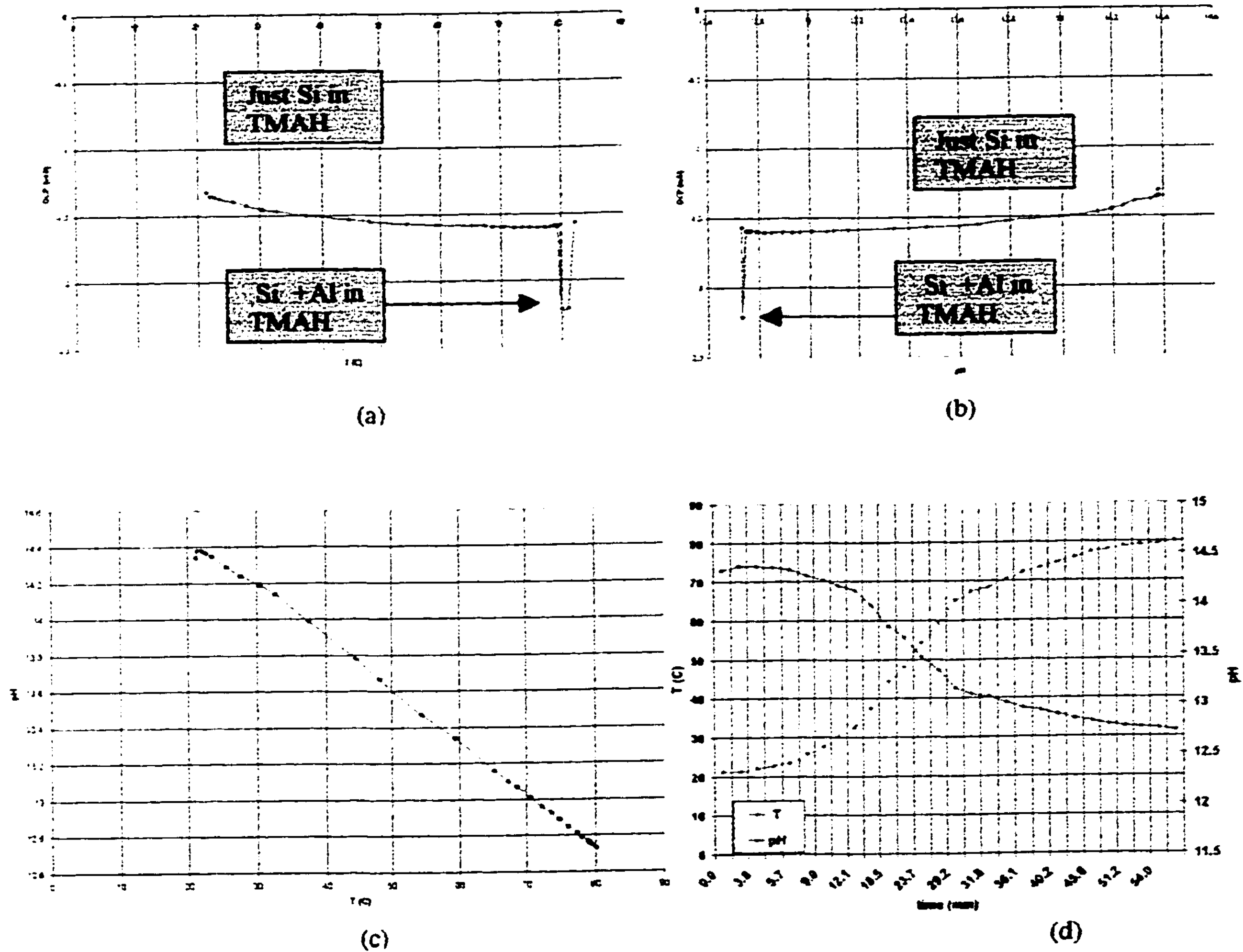

Fig. 5.11 The experimental results for sample P2, p-type Si <100> in 5wt% TMAH (a) OCP (Si) and OCP (Si +Al) vs. T (b) OCP (Si) and OCP (Si +Al) vs. pH (c) pH vs. T (d) pH and T vs. experimental time.

7. Bubbles level on n-type <100>Si and Al working electrode surfaces in 25wt.% TMAH, where the level of the bubbles indicating and demonstrating in the following table: (see Fig.3.12)

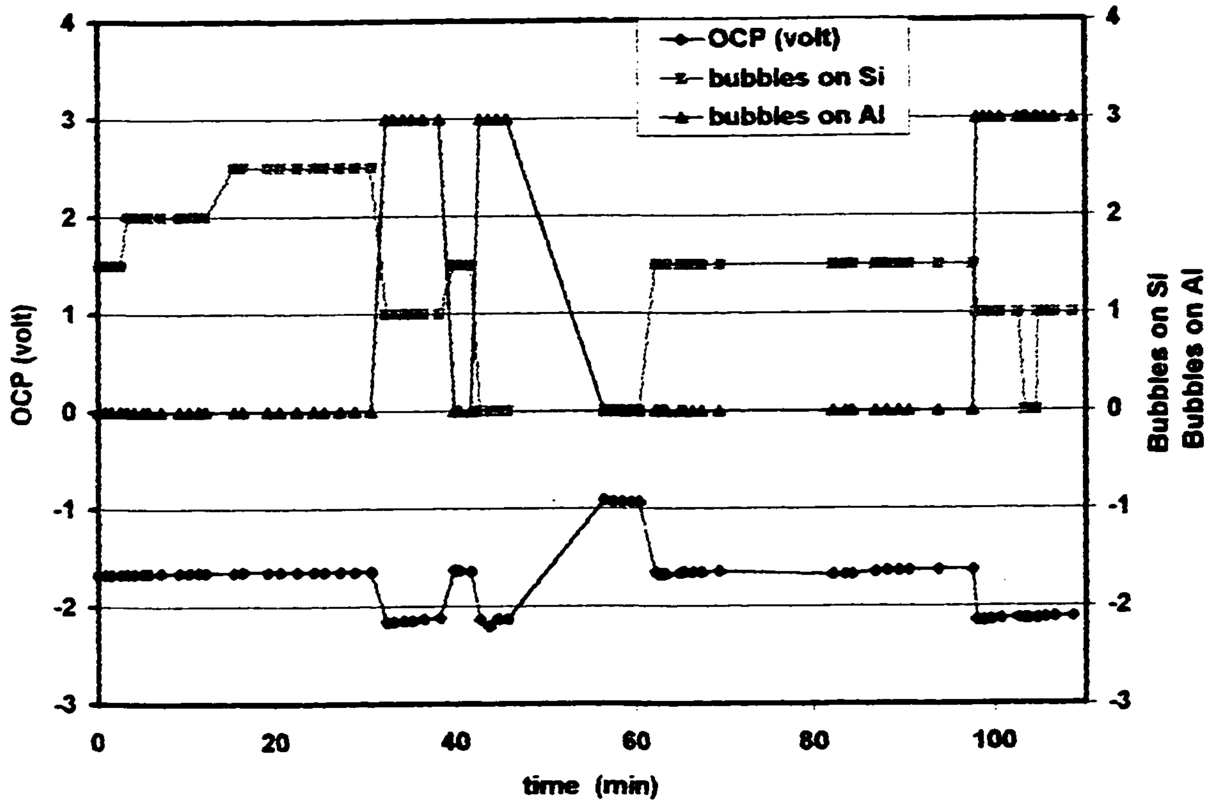

Fig. 3.12 Bubbles level on n-type S <100> and Al working electrodes surfaces in 25wt.% TMAH.

Bubbles level	No bubbles	Low bubbles	Medium	High	Very High	vigorous
	0	1	1.5	2	2.5	3

8. Bubbles level on p-type <100>Si and Al working electrodes surfaces in 25wt.% TMAH, where the level of the bubbles indicating and demonstrating in the following table: (see Fig.3.13)

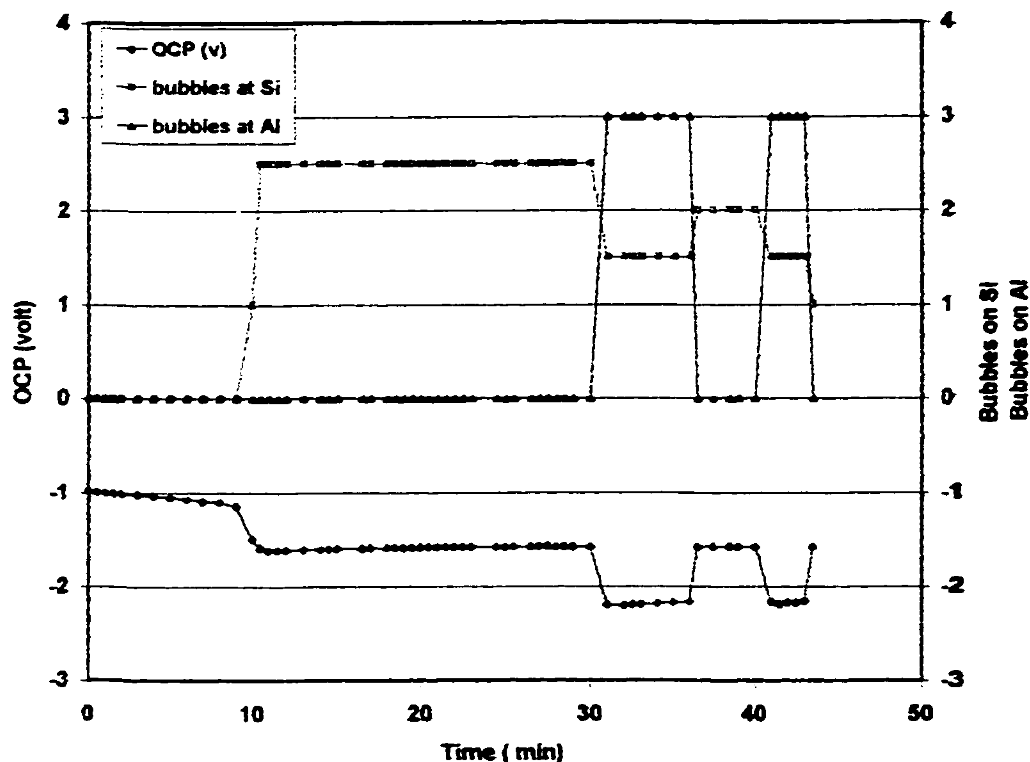

Fig. 3.13 Bubbles level on p-type S <100> and Al working electrodes surfaces in 25wt.% TMAH.

Bubbles level	No bubbles	Low bubbles	Medium	High	Very High	vigorous
	0	1	1.5	2	2.5	3

9. Bubbles level on p- and n-type <100>Si and Al working electrode surfaces in 5wt.% TMAH, where the level of the bubbles indicating and demonstrating in the following table:(see Fig.3.14)

Bubbles level	No bubbles	Low Bubbles	Medium	High	Very High	vigorous
	0	1	1.5	2	2.5	3

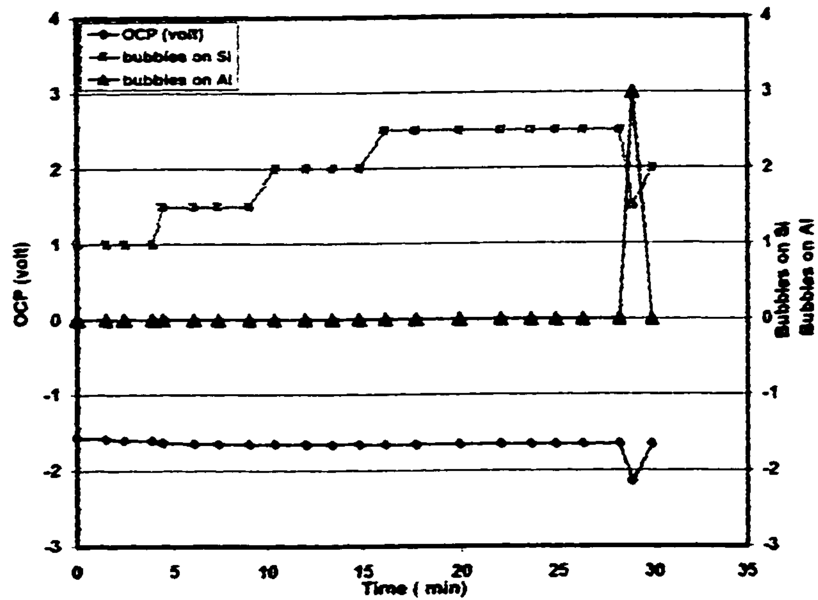

(a)

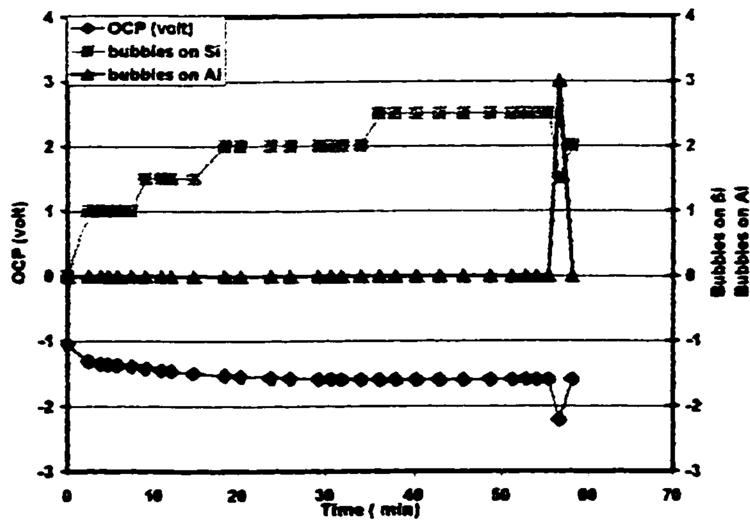

(b)

Fig. 3.14 Bubbles level on <100>Si and Al working electrodes surfaces in 5wt.% TMAH. (a) n-type Si, (b) p-type Si.

10. The OCP measurements of only Al (i.e. no Si) working electrode surface in 25wt.% TMAH at constant temperature ~ 47 °C, and the level of the bubbles indicating and demonstrating in the following table:(see Fig.3.15(a) &(b))

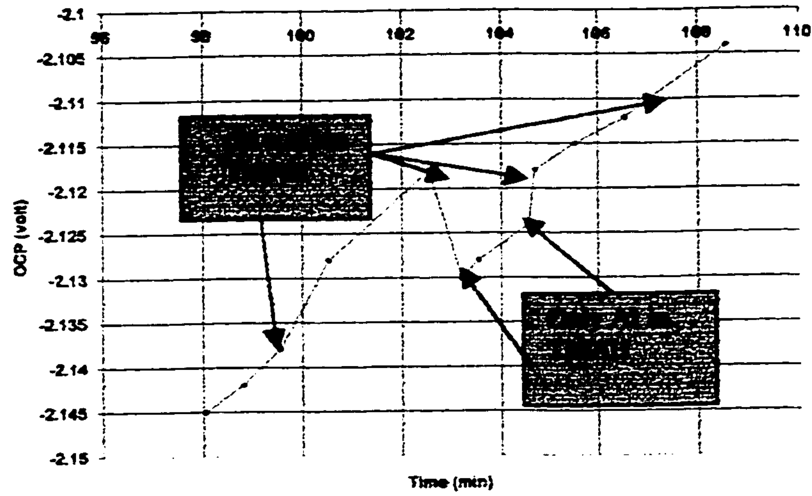

(a)

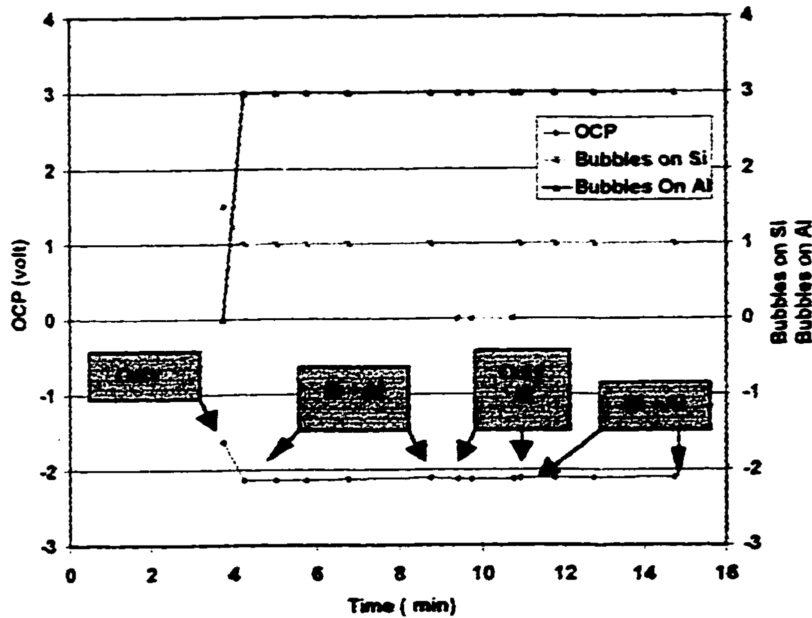

(b)

Fig. 3.15 (a) The OCP measurements of only Al in 25wt.% TMAH (b) Bubbles level on Al working electrode surface in 25wt.% TMAH at 47 °C.

Bubbles level	No bubbles	Low bubbles	Medium	High	Very High	vigorous
	0	1	1.5	2	2.5	3

3.7 OBSERVATIONS AND CONTRIBUTIONS

The observations and contributions from this Chapter can be summarized as follows:

1. The potential of Si/TMAH and Si +Al/TMAH etching systems were measured under open-circuit conditions using a high-impedance voltmeter in a simple scheme. This is taken as a measurement of the open-circuit potential (OCP) of the electrochemical cell.
2. Several aspects of the experimental scheme were validated; ohmic contact of the samples, relative insensitivity to position of the electrodes in the etchant solution.
3. These electrochemical potential measurements, and the etch reaction itself, are found to be very sensitive to the presence of even a very thin native oxide layer on the exposed silicon, especially at lower temperatures. This effect can be removed by a simple HF dip within 5 minutes prior to immersion in the etching cell. The establishment of satisfactory etching conditions and a stable OCP are correlated with the generation of many tiny bubbles at the Si surface being etched, in both n-type and p-type cases.
4. The measured OCP is found to be in the approximate ranges of -1.5V to -1.7V for Si/TMAH, and -2.1V to -2.3V for Si +Al/TMAH, for lightly-doped silicon in the temperature range between room temperature and ~80 °C.
5. The measured OCP of the Si/TMAH25wt% system is found to vary up to approximately ~0.1V over the temperature range from ~30 °C to ~80 °C for both

n-type and p-type silicon. As the temperature rises, the OCP becomes more negative.

6. The OCP values for n-type silicon tended to be on the order of ~0.1V more negative in the n-type cases than in the p-type cases.
7. The OCP values for 25wt% TMAH tended to be more negative than for 5wt% TMAH. The difference was on the order of ~0.05 to 0.1 V.
8. When Al, electrically connected to the Si, was simultaneously dipped into the solution, immediate dramatic changes were observed:

- The bubbles at the Si were immediately reduced, and more-vigorous bubbling was observed at the immersed Al.
- The OCP immediately became substantially more negative, by approximately 0.5-0.7V.
- On most occasions, after the immersion of Al, the OCP of Si alone became somewhat more positive.

9. The OCP of only Al (no Si) in the solution was distinguishable and observed within the experimental of this work, from the OCP measured with both Si and Al in the solution simultaneously, and Si and Al individually and separately.

CHAPTER 4

DISCUSSION

In this Chapter, the following aspects are discussed:

- The stability and validity of the galvanic cell voltage measurements.
- The relation of the experimental cases to the location and qualitative intensity of the reaction, as seen in the bubbling intensity.
- Comparison and contrast of the two cases of Al/Si/TMAH and Au/Si/TMAH (Ashruf *et al* [10]).
- The difference between n-type and p-type cases, as seen in the bubbling intensity.
- The difficulty of etching Si without etching Al.
- The application of the Nernst Equation to the Si/TMAH etching system, and comparison to experiment.
- The irreversibility of the etch reaction is Si in alkaline solutions.
- The energy band diagrams of the etching situation in the contexts of equilibrium and non-equilibrium electrochemical conditions.

4.1 Measured Galvanic Cell Voltage Values

In all cases measured, the removal of a native oxide layer by a dilute-HF-dip within 5 minutes of immersion in the TMAH was sufficient to achieve a stable galvanic cell voltage, within ± 50 mV over many minutes of measurement, at a given temperature. This finding allowed meaningful measurement of stable potentials for a variety of experimental cases, for different temperatures, etchant concentrations,

immersed sample configurations, and silicon dopant type. For example, Fig.3.9 and Fig.3.10 showed that the cell potential for p-type silicon at ~47 °C in high-concentration TMAH was in the range of −1.55V to −1.6V, while the cell potential for Al and p-Si was near −2.2V.

Since the presence of the voltmeter (connected in series in the measurement circuit), guarantees that virtually zero current will flow, the cell potentials are equivalent to open-circuit potentials (OCP) of the electrochemical cell, and can be reasonably compared with the OCP as measured by linear-sweep voltammetry by other researchers (as reviewed in Chapter 2, and summarized in Table 4.1).

- These galvanic cell OCP measurements, summarized in Table 4.2, were found to be in general agreement with the literature values (Table 4.1) for electrochemical etching of silicon in TMAH.
- These galvanic cell measurements showed more-negative OCP's in high-concentration TMAH than in low-concentration TMAH, for a given silicon dopant type. This is clearly consistent with the literature values in Table 4.1.
- These galvanic cell measurements showed more-negative OCP's with n-type silicon than with p-type silicon, for a given TMAH concentration. This is consistent with the high-concentration data in Table 4.1.
- These galvanic cell measurements showed more-negative OCP's at higher etchant temperatures, for a given sample and etchant.
- The general range of values for the galvanic cell measurements around 80 °C (approximately −1.6V to −1.8V), is in rough agreement with the range (-1.48V to −1.72V) in Table 4.1.

- **Table 4.1 The OCP and PP values Summarized from the literature.**

The OCP and PP values in the literature.						
The Reference	**Etchant**	**<100>Si type**	**T (°C)**	**Reference Electrode**	**OCP (volt)**	**PP (Volt)**
Acero [45]	TMAH 25wt.%	n-type	80	Ag/AgCl (0.222V)	-1.68	-1.13
Acero [45]	TMAH 25wt.%	p-type	80	Ag/AgCl (0.222V)	-1.69	-1.00
Ashruf [9]	TMAH 25wt.%	p-type	80	SCE (0.253V)	-1.6	-1.04
O.Tabata [42] *Et al*	TMAH 22wt.%	p-type	80	Ag/AgCl (0.222V)	-1.66	-1.00
O.Tabata [42] *Et al*	TMAH 22wt.%	n-type	80	Ag/AgCl (0.222V)	-1.72	-1.11
Acero [45]	TMAH 2.5wt.%	n-type	80	Ag/AgCl (0.222V)	-1.48	-1.02
Acero [45]	TMAH 2.5wt.%	p-type	80	Ag/AgCl (0.222V)	-1.54 -1.34	-0.75
E.D. Palik[24]	KOH 2M	n-type	21	SCE (0.253V)	-1.34	-0.22
E.D. Palik[24]	KOH 2M	p-type	21	SCE (0.253V)	-1.05	-0.13
J. Faust[25]	KOH 2M	n-type	21	SCE (0.253V)	-1.32	-0.94
J. Faust[25]	KOH 2M	p-type	21	SCE (0.253V)	-1.07	-0.85
Glembocki[4]	KOH 2M	n-type	20	SCE (0.253V)	-1.3	-1.05
Glembocki[4]	KOH 2M	p-type	20	SCE (0.253V)	-1.25	-0.65
Sundaram[40]	Hydrazine 25%	n-type	70	SCE (0.253V)	-1.25	0.9
Sundaram[40]	Hydrazine 25%	p-type	70	SCE (0.253V)	-1.20	-0.4
B. Kloeck[39]	KOH 40%	n-type	60	SCE (0.253V)	-1.5	-1.2
B. Kloeck[39]	KOH 40%	p-type	60	SCE (0.253V)	-1.5	-1.00

Table 4.2 The Galvanic cell results

25wt.% TMAH								5wt.% TMAH							
n-type <100>Si				p-type <100>Si				n-type <100>Si				p-type <100>Si			
T (°C)	OCP (V) Si alone	T (°C)	OCP (V) Si + Al	T (°C)	OCP (V) Si alone	T (°C)	OCP (V) Si + Al	T (°C)	OCP (V) Si alone	T (°C)	OCP (V) Si + Al	T (°C)	OCP (V) Si alone	T (°C)	OCP (V) Si + Al
32.9	-1.652	-	-	30.4	-1.512	-	-	-	-	-	-	21.4	-1.319	-	-
-	-	-	-	36.8	-1.54	-	-	-	-	-	-	25.7	-1.393	-	-
-	-	-	-	38.7	-1.538	-	-	-	-	-	-	30.4	-1.454	-	-
-	-	-	-	43.5	-1.533	-	-	43.7	-1.561	-	-	37.4	-1.498	-	-
45.5	-1.671	-	-	46.9	-1.538	-	-	-	-	-	-	44.4	-1.53	-	-
50.5	-1.674	-	-	49.4	-1.544	-	-	48.6	-1.582	-	-	48	-1.547	-	-
-	-	-	-	51.9	-1.56	-	-	51.6	-1.604	-	-	-	-	-	-
55.7	-1.682	-	-	54.4	-1.575	-	-	55.6	-1.6025	-	-	54.4	-1.568	-	-
-	-	-	-	57.2	-1.582	-	-	-	-	-	-	-	-	-	-
61.5	-1.697	-	-	60.9	-1.6	-	-	60.7	-1.642	-	-	59.3	-1.576	-	-
-	-	-	-	-	-	63.7	-2.259	-	-	-	-	-	-	-	-
65.7	-1.714	-	-	65.4	-1.657	65.6	-2.261	66.4	-1.652	-	-	65.2	-1.588	-	-
-	-	-	-	-	-	67.1	-2.263	-	-	-	-	-	-	-	-
-	-	-	-	-	-	69.4	-2.265	-	-	-	-	-	-	-	-
70.2	-1.731	-	-	-	-	70.8	-2.267	70.4	-1.656	-	-	70.5	-1.596	-	-
-	-	-	-	-	-	73	-2.27	-	-	-	-	74.8	-1.6	-	-
-	-	-	-	-	-	75.1	-2.274	75.2	-1.656	-	-	-	-	-	-
76.2	-1.754	-	-	76.1	-1.66	-	-	-	-	-	-	-	-	-	-
-	-	-	-	-	-	76.8	-2.276	-	-	-	-	-	-	-	-
-	-	-	-	-	-	78.2	-2.278	-	-	-	-	-	-	-	-
-	-	-	-	-	-	79	-2.271	-	-	-	-	-	-	-	-
-	-	-	-	-	-	79.5	-2.28	79.4	-1.652	-	-	79.4	-1.593	-	-
80.1	-1.77	80.1	-2.222	80	-1.66	80.3	-2.281	80	-1.652	80.5	-2.144	80.1	-1.592	80	-2.21
81.9	-1.77	81.0	-2.248	-	-	82.3	-2.283	81	-1.652	-	-	-	-	81.1	-2.212

The above-outlined agreement between measured cell values and literature results, supports the validity of the experiments and sample-design concepts.

- The OCP's measured when the Al and Si were simultaneously immersed in the TMAH were always substantially more negative, around –2.1V to –2.3V, although they did not seem to follow the trends outlined for Si-only immersion. The OCP's measured with Al-only were negligibly different from those measured with both Al and Si in the solution. Fig.3.15a shows the very small change in OCP (~0.01V) when the Si was removed from the solution while the Al was left in the solution.

4.2 Bubbling Intensity

Along with the OCP measurements, the bubbling intensity was qualitatively observed on bare silicon regions and on the Al bar, when immersed in the TMAH. The bubbling intensity is taken to represent the intensity of the etch reactions at the Si and/or Al. The bubbles coming from the silicon are reasonably assumed to be hydrogen (see equations Eq.2.15 and Eq.2.16). The bubbling intensity was observed and recorded as being on one of 6 levels, ranging from "no bubbles" to "vigorous".

When both Si and Al were simultaneously immersed in the solution, the bubbling was always most intense on the Al, consistent with the Al/TMAH half-reaction being more active than the Si/TMAH half-reaction. Furthermore, the intensity of bubbling at the Al was essentially the same for the two cases Al-only and Al/Si in the etchant.

4.3 Comparison of Au/Si/TMAH and Al/Si/TMAH Galvanic Cells

The galvanic cell used in these experiments was very similar to that used by Ashruf *et al* [10], except that the metal used was Al instead of Au. The standard electrode potentials (V_o in Table 2.3) indicate that Al (V_o = -1.662V) is electrochemically much more active than Au (V_o = +1.420) under standard conditions (at room temperature).

Ashruf *et al* [10] indicate that the insertion of the Au into the solution for 1.1 minutes, at the same time as the Si, had two main effects:

- The measured OCP jumped from ~-1.6V to ~-0.3V, while the Au was in the solution.
- The silicon was found to have been passivated after the Au was removed, as seen by the relatively long time needed to re-establish the original -1.6V OCP.

In the Al/Si/TMAH cell measurements in this work, the insertion of the Al into the solution, at the same time as the silicon had somewhat different effects:

- The measured OCP jumped from ~-1.6V to ~- 2.2V, while the Al was in the solution. This is essentially the same value as was recorded with Al-only.
- Even though the Al was inserted into the solution for periods of time substantially longer than 1.1 minute, the stable value near -1.6V was re-established quickly after the Al was removed.

Thus, the silicon was <u>**not**</u> found to have been passivated after the Al was removed. This situation is consistent with the following electrochemistry-based understanding.

- The Al is more reactive than the Si, since the overlay potential of the electrically-connected Al/Si becomes more negative, and the electrochemical system is dominated by the presence of the Al.
- It is sensible that the Si was not passivated during the Al immersion in the solution, because the OCP of the Al/Si was moved from -1.6V to a more negative value, farther away from the passivation potential (PP) and oxide-formation potential (OFP) seen in typical LSV curves discussed in Appendix 1. On the other hand, the OCP of Au/Si was moved to ~-0.3V, which is in the oxide-formation regime of the LSV curves.

4.4 Difference in n-type and p-type Bubbling Intensity

When the Al was inserted into the etchant solution at the same time as the Si, the bubbling intensity was clearly reduced in all cases, representing a reduction in etch reaction. However, the reduction in bubbling at the Si was more dramatic in the n-type case than in the p-type case. In these cases, the measured OCP was always in the range of -2.1V to -2.3V, substantially more negative than the OCP found for Si-only. These differences in bubbling are consistent with the previous observations of Glembocki *et al* [4] and Acero *et al* [45], who found that at potentials more cathodic than the OCP, the etching of n-type Si was stopped, while etching of p-type Si was not dramatically affected.

4.5 The Difficulty of Etching Si without Etching Al.

The difficulty of etching silicon without etching Al can be understood to be a reasonable consequence of the above observations.

- The etch reaction on the Si (as seen in the bubbles) was reduced or stopped when we inserted the Al.
- The presence of Al, in the solution at the same time as the Si, electrically connected to the Si, substantially alters the electrochemical situation during a silicon etches.
- The Al is electrochemically more active than the Si, and acts to shift the potential of the Al/Si sample away from the Si-only OCP, which acts to dramatically reduce the etch reaction at the Si.

4.6 The Application of the Nernst Equation to the Si/TMAH System and Comparison to Experiment

The effect of the concentration on the cell potential can be calculated from the Nernst Equation,

$$E_{cell} = E^{o}_{cell} - \frac{2.303RT}{nf}\log Q \qquad \text{Eq.4.1}$$

Where, E_{cell} is the actual cell potential, E^{o}_{cell} is the standard potential, R is the gas constant in energy units (joules). T is the absolute temperature (^{o}K), f is the Faraday constant = 96500 $C/mol\ e^{-}$. n is the number of moles of electrons transferred in the cell reaction, and Q is the reaction quotient for the reaction.

$$E^{o}_{cell} = E^{o}_{red} - E^{o}_{ox} \qquad \text{Eq.4.2}$$

$$Q = \frac{[OH^-]^2[Si(OH)_2^{2+}]}{[H_2O]^4} \qquad \text{Eq.4.3}$$

The reaction of an electrochemical cell always involves a combinations of two redox half-reactions such that one species oxidizes needs a second species to give the respective redox products, these two redox half-reactions are represented as follows:

1) **The oxidation Reaction**

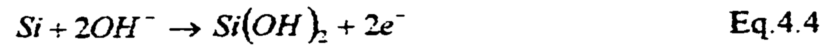

$$Si + 2OH^- \rightarrow Si(OH)_2 + 2e^- \qquad \text{Eq.4.4}$$

$$Si(OH)_2 \rightarrow Si(OH)_2^{2+} + 2e^- \qquad \text{Eq.4.5}$$

The overall oxidation reaction is:

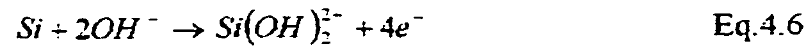

$$Si + 2OH^- \rightarrow Si(OH)_2^{2-} + 4e^- \qquad \text{Eq.4.6}$$

2) **The Reduction Reaction**

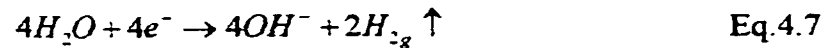

$$4H_2O + 4e^- \rightarrow 4OH^- + 2H_{2g} \uparrow \qquad \text{Eq.4.7}$$

Thus the overall cell reaction can be expressed by a balanced chemical equation:

3) **The overall reaction is**

$$Si + 4H_2O \rightarrow Si(OH)_2^{2-} + 2OH^- + 2H_{2g} \uparrow \qquad \text{Eq.4.8}$$

Metal hydroxides are strong bases- they are completely dissociated. This means that the hydroxide ion concentration in the solution is $[Si(OH)_2^{2-}]=[OH^-]^2$. [46,47,48]

Now, substitute in Eq.4.1 we obtain:

$$E_{cell}=E^o_{red}-E^o_{ox}-\frac{2.303RT}{4f}\log\frac{[OH^-]^2[Si(OH)_2^{2-}]}{[H_2O]^4} \qquad \text{Eq.4.9}$$

Now, the equilibrium constant; K_{eq} for this system is;

$$K_{eq}=\frac{[H_3O^+][OH^-]}{[H_2O]^2} \qquad \text{Eq.4.10}$$

The Ion-product constant of water, symbolized as K_w, is given by,

$$K_w=K_{eq}\times[H_2O]^2=[H_3O^+][OH^-] \qquad \text{Eq.4.11}$$

The values of K_w and K_{eq} vary with temperature, because they are depending on the molarity.

Therefore,

$$[H_2O]^2=\frac{K_w}{K_{eq}} \qquad \Rightarrow[H_2O]^4=\frac{K_w^2}{K_{eq}^2} \qquad \text{Eq.4.12}$$

and

$$[OH^-]=\frac{K_w}{[H_3O^+]} \qquad \Rightarrow[OH^-]^2=\frac{K_w^2}{[H_3O^+]^2} \qquad \text{Eq.4.13}$$

$$[Si(OH)_2^{2-}] = [OH^-]^2 = \left[\frac{K_w}{[H_3O^+]}\right]^2$$

By substituting these equations. in Eq.4.9

$$E_{cell} = E^o_{red} - E^o_{ox} - \frac{2.303RT}{4f}\log\frac{[OH^-]^2[Si(OH)_2^{2+}]}{[H_2O]^4}$$

we will obtain,

$$E_{cell} = E^o_{red} - E^o_{ox} - \frac{2.303RT}{4f}\left\{\log[OH^-]^2[Si(OH)_2^{2-}] - \log[H_2O]^4\right\}$$

thus,

$$E_{cell} = E^o_{red} - E^o_{ox} - \frac{2.303RT}{4f}\log\left\{\log[OH^-]^2 + \log[Si(OH)_2^{2-} - \log[H_2O]^4\right\}$$

$$E_{cell} = E^o_{red} - E^o_{ox} - \left\{\frac{2.303RT}{4f}\left\{\log\frac{[OH^-]^2}{\log[H_2O]^4} + \log[Si(OH)_2^{2-}\right\}\right\}$$

$$E_{cell} = E^o_{red} - E^o_{ox} - \left\{\frac{2.303RT}{4f}\left\{\log K^2_{eq} - 2\log[H_3O^+] + \log[Si(OH)_2^{2-}\right\}\right\} \quad \text{Eq.4.14}$$

but, $[Si(OH)_2^{2-}] = [OH^-]^2 = \left[\frac{K_w}{[H_3O^+]}\right]^2$

Therefore,

$$E_{cell} = E^o_{red} - E^o_{ox} - \left\{\frac{2.303RT}{4f}\left\{\log K^2_{eq} - 2\log[H_3O^+] + \log K^2_w - 2\log[H_3O^-]\right\}\right\}$$

$$E_{cell} = E^o_{red} - E^o_{ox} - \left\{\frac{2.303RT}{4f}\left\{\log K^2_{eq}K^2_w - 4\log[H_3O^+]\right\}\right\}$$

where,

$$pH = -\log[H_3O^+]$$ Eq.4.15

by substituting Eq.4.15 in Eq.4.14; we obtain,

$$E_{cell} = E^{\circ}_{red} - E^{\circ}_{ox} - \left\{ \frac{2.303RT}{4f} \{\log K^{2}_{eq} K^{2}_{w} + 4pH\} \right\}$$ Eq.4.16

$$E_{cell} = E^{\circ}_{red} - E^{\circ}_{ox} - \left\{ \frac{2.303RT}{4f} \log K^{2}_{eq} K^{2}_{w} + \frac{(2.303)RT}{f} pH \right\}$$ Eq.4.17

Some conversion factors:

1. $f = 96500 C / mole^- = 96500 J / V$
2. $T(k^\circ) = T(C^\circ) + 273.15$
3. $\ln x = 2.303 \log x$
4. $R = 8.3144 J mol^{-1} K^{-1}$

The etching reaction of the Si (n-type or p-type) in Alkaline Solutions (i.e. TMAH) is irreversible, based on reaction products (i.e. complex ions), as it clears in the following equation reactions:

Etching Si: $Si + 2OH^- \rightarrow Si(OH)_2^{2+} + 2e^-$ Eq.4.18

$Si(OH)_2^{2+} + 4e^- + 4H_2O \rightarrow Si(OH)_6^{2+} + 2H_2$ Eq.4.19

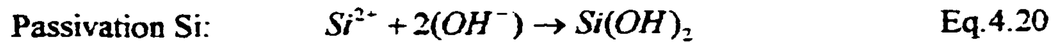

Passivation Si: $Si^{2+} + 2(OH^-) \rightarrow Si(OH)_2$ Eq.4.20

$Si(OH)_2 \rightarrow SiO_2 + 2H_2 \uparrow$ Eq.4.21

Since these half-reactions have as products complex ions which are prone to further decomposition, it is likely that this reaction system is an irreversible, non-

equilibrium process. This assertion can be verified by the experimental data in this work. Fig.4.1 shows the relevant comparison.

- The OCP calculated from Nernst Equation is based on measured pH and T.
- The Nernst-based OCP increases with T.
- The experimentally-measured OCP decreases with T.
- The magnitude of change with T is substantially different between the two cases.

The data supports hypothesis that Nernst Equation does not apply, and that this oxidation reduction process is an irreversible non- equilibrium case.

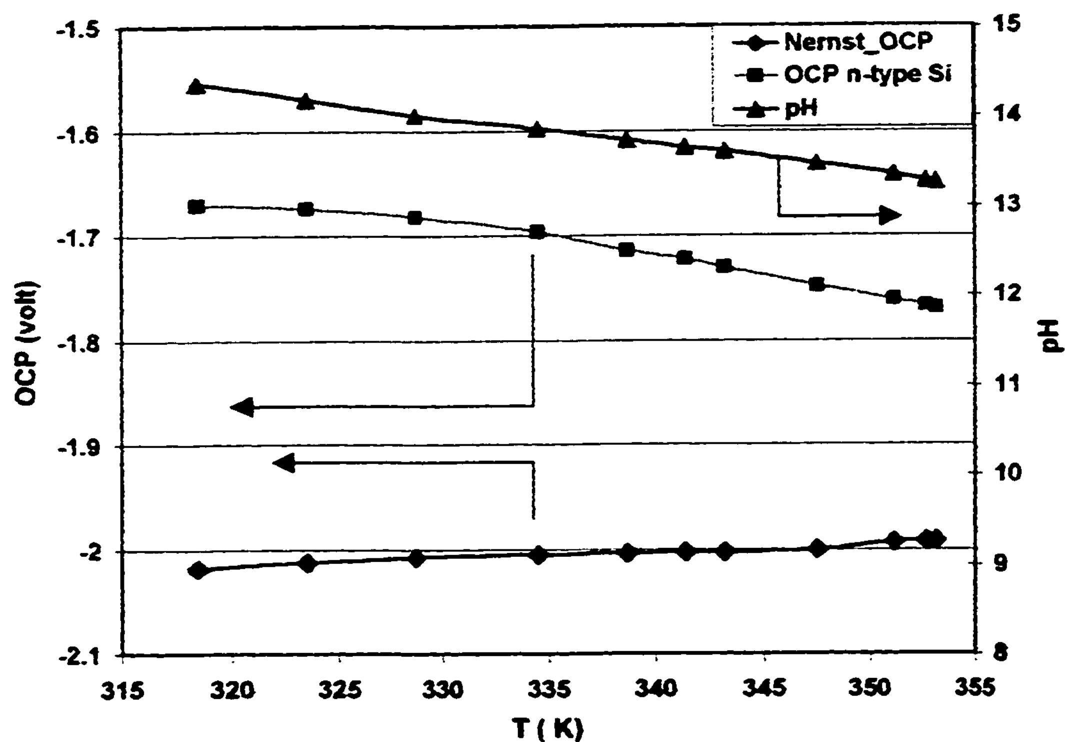

Fig.4.1 Comparison between Measured OCP and Nernst Equation OCP at the same pH and T values.

4.7 Energy Band Diagrams For Si Anisotropic Etching in the Contexts of Equilibrium and Non-Equilibrium Electrochemical Conditions

In the recent paper by Nemirovsky & Bahar [9], a non-equilibrium electrochemical model was proposed for the anisotropic etching of silicon. They explain that the Si/electrolyte system is not in thermodynamic equilibrium during etching, even at the open-circuit potential. They assert that the etching reaction involves two electrode reactions, the reduction of water molecules and the oxidation of silicon, whose balance constitutes a steady-state, instead of thermodynamic equilibrium.

Their experiments conclude several points of interest in this analysis:

- Their measured OCP represents the difference between Fermi levels in the silicon and solution in steady state.
- Their difference in OCP between lightly-doped n-type and p-type silicon should be low. For example, for n- and p-type doping at 10^{15} cm^{-3}, OCP-n was ~10mV more negative than OCP-p.
- The OCP should vary only mildly with temperature, with p-type more positive than n-type. OCP variations of tens of mV per 20 °C were reported, with OCP becoming more negative with increasing T.

Since these concepts and observations are compatible with the experimental data discussed in section 4.1, and with the analyses of section 4.6, relevant band diagrams are developed here.

The main concepts related to the energy band diagrams in equilibrium conditions are developed in Appendix 2. The Fermi level and the redox level would be aligned under equilibrium conditions. This situation is depicted in Fig.4.2.

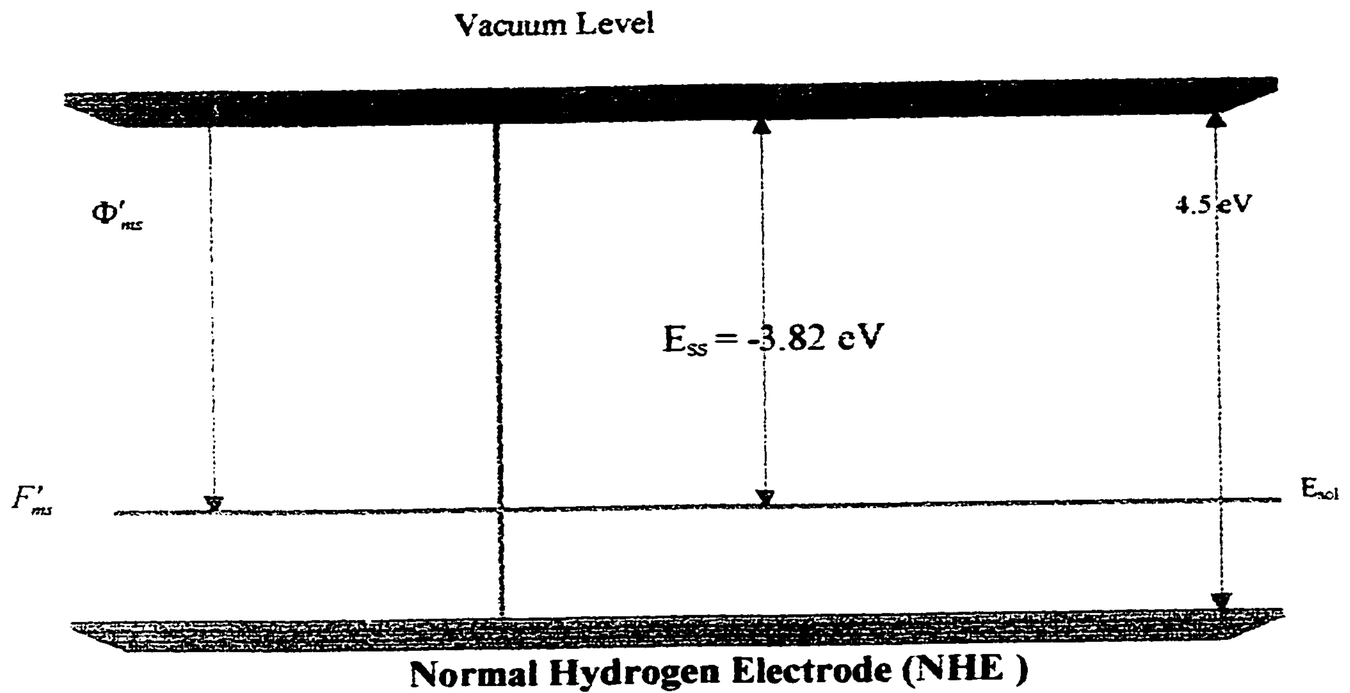

Fig.4.2 The band Diagram of the structure Al/Si after immersion in the solution, the Fermi level of Al/Si (F_{ms}) aligned with the redox level of the solution (E_{sol}) in equilibrium system.

However, as suggested by Nemirovsky *et al* [9], under non-equilibrium conditions, the Fermi level and redox levels will not be aligned. This situation is depicted in Fig.4.3. This case is likely to be more realistic, in view of the analyses of Section 4.6, which indicate that the Al/Si/TMAH system is a non-equilibrium system.

Fig.4.4 depicts two cases from table 4.2, for p-type Si in 25 wt.% TMAH, and for p-type Si in 5 wt.% TMAH which are in account with this principle.

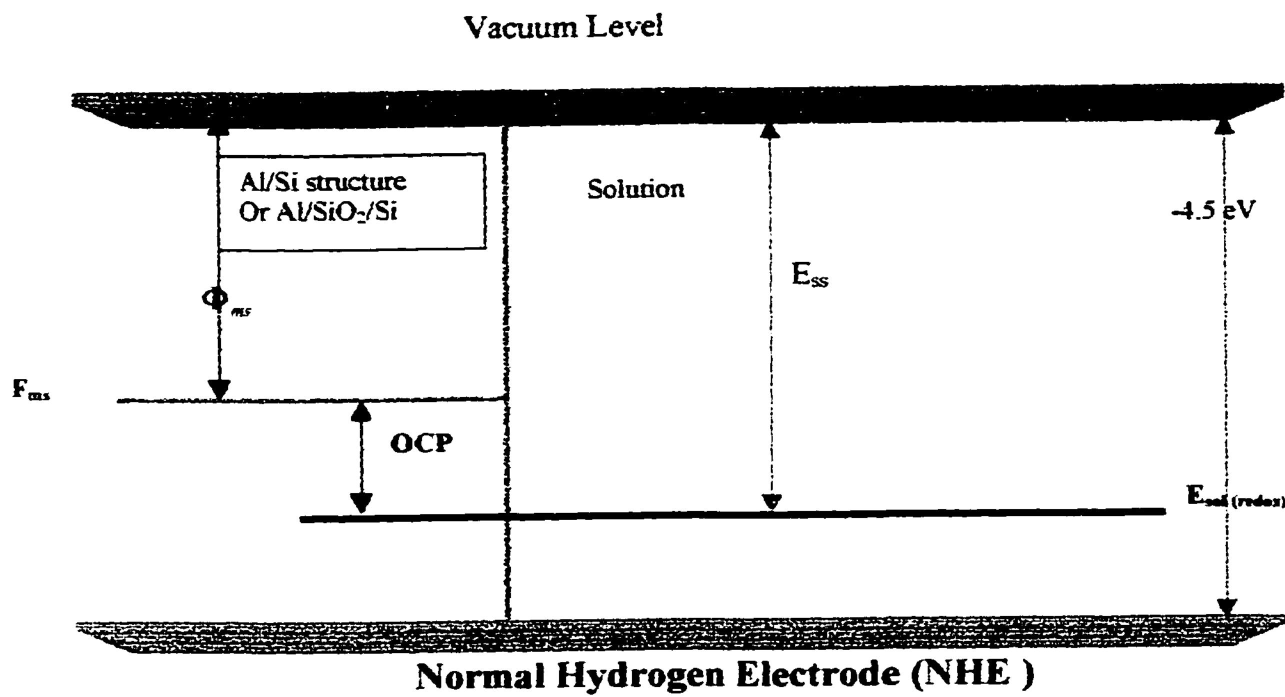

Fig.4.3 Energy band diagram in context of non-equilibrium condition.

Vacuum Level

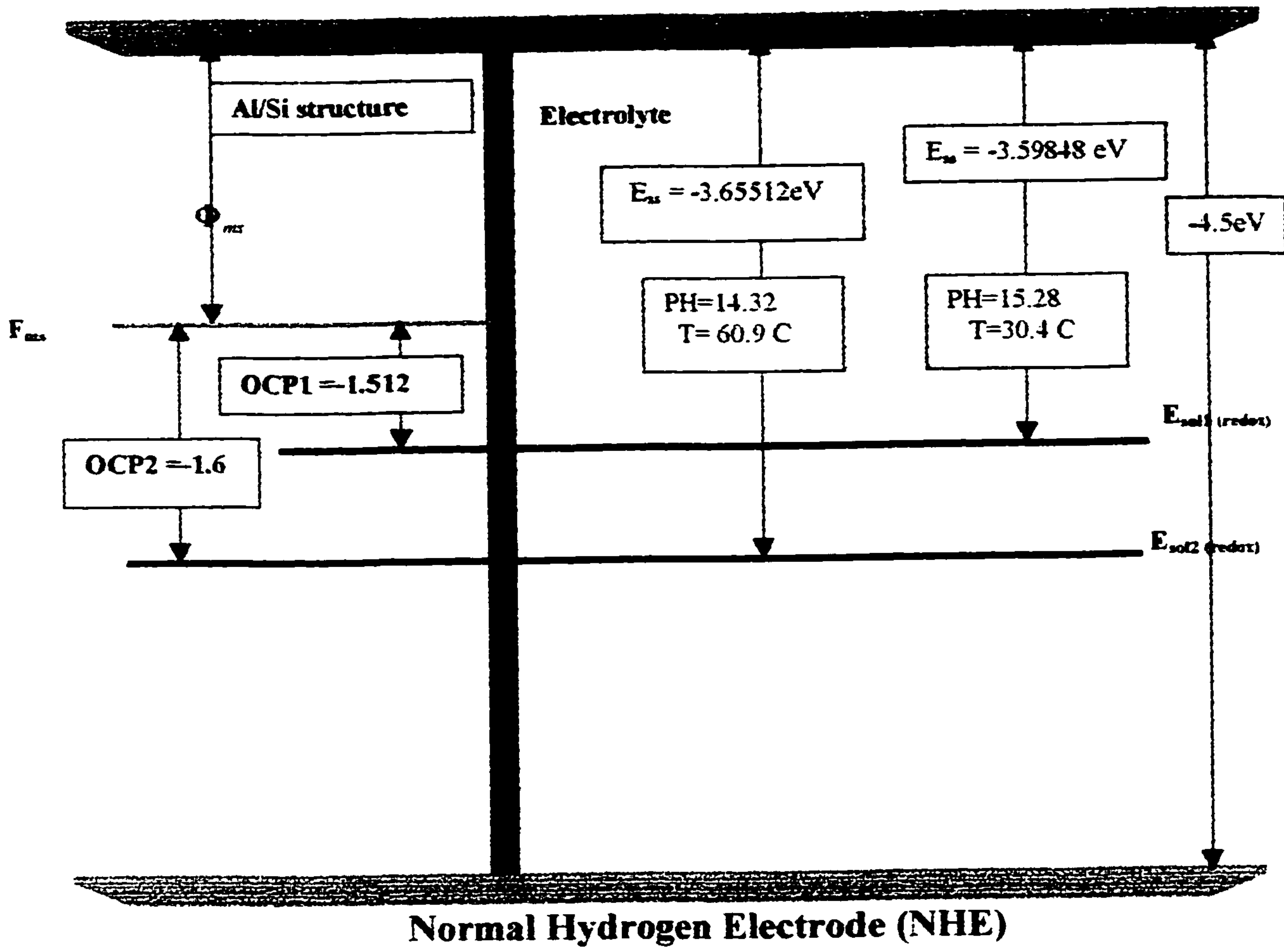

(a)

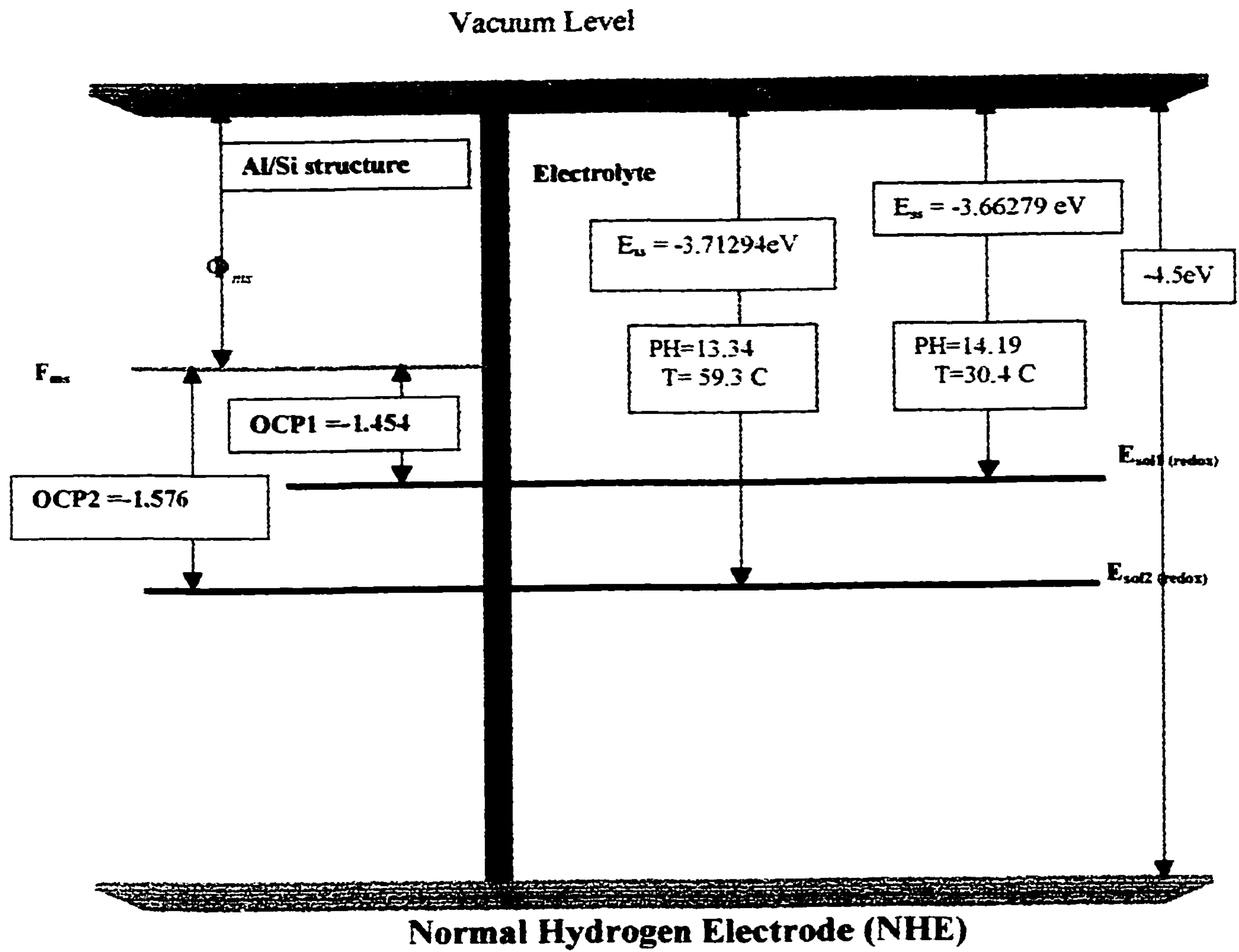

(b)

Fig.4.4 The effective of the electrolyte potential variation with pH on energy band diagram in non-equilibrium condition. (a) This case For p-type Si in 25 wt.% TMAH (b) This case For p-type Si in 5 wt.% TMAH (energy level not to scale).

4.8 Conclusions and Contributions

- The simple galvanic cell measurement scheme was found to be effective.

- The measured OCP values for silicon in TMAH were found to be in general agreement with results found by other researchers.

- The presence of alminum in the solution, electrically connected to the silicon, shifts the overall OCP to a more-negative potential, which reduces the etch rate of the silicon, especially n-silicon, while the aluminum is etched. The difference in behaviour between n-type and p-type is consistent with the previous work of Glembocki *et al* [4],and Acero *et al* [45].

- The galvanic cell measurements of Al/Si/TMAH, are consistent with a coherent electrochemical understanding initiated by the experiments of Ashruf *et al* [10] on Au/Si/TMAH.

- The measurements are consistent with aluminum being electrochemically more active than silicon.

- The silicon anisotropic etch reaction in alkaline solutions is not reversible and the Nernst equation does not hold. This is confirmed by quantitative analysis of the experimental data.

CHAPTER 5

CONCLUSIONS, CONTRIBUTIONS AND SUGGESTIONS FOR FUTURE WORK

5.1 CONCLUSIONS AND CONTRIBUTIONS

The observations and contributions from **Chapter 3** can be summarized as follows:

1. The potential of Si/TMAH and Si +Al/TMAH etching systems were measured under open-circuit conditions using a high-impedance voltmeter in a simple scheme. This is taken as a measurement of the open-circuit potential (OCP) of the electrochemical cell.

2. Several aspects of the experimental scheme were validated; ohmic contact of the samples, relative insensitivity to position of the electrodes in the etchant solution.

3. These electrochemical potential measurements, and the etch reaction itself, are found to be very sensitive to the presence of even a very thin native oxide layer on the exposed silicon, especially at lower temperatures. This effect can be removed by a simple HF dip within 5 minutes prior to immersion in the etching cell. The establishment of satisfactory etching conditions and a stable OCP are correlated with the generation of many tiny bubbles at the Si surface being etched, in both n-type and p-type cases.

4. The measured OCP is found to be in the approximate ranges of -1.5V to -1.7V for Si/TMAH, and -2.1V to -2.3V for Si +Al/TMAH, for lightly-doped silicon in the temperature range between room temperature and ~80 °C.

5. The measured OCP of the Si/TMAH25wt% system is found to vary up to approximately ~0.1V over the temperature range from ~30 °C to ~80 °C for both n-type and p-type silicon. As the temperature rises, the OCP becomes more negative.

6. The OCP values for n-type silicon tended to be on the order of ~0.1V more negative in the n-type cases than in the p-type cases.

7. The OCP values for 25wt% TMAH tended to be more negative than for 5wt% TMAH. The difference was on the order of ~0.05 to 0.1 V.

8. When Al, electrically connected to the Si, was simultaneously dipped into the solution, immediate dramatic changes were observed:

- The bubbles at the Si surface were immediately reduced, and more-vigorous bubbling was observed at the immersed Al.

- The OCP immediately became substantially more negative, by approximately 0.5-0.7V.

- On most occasions, after the immersion of Al, the OCP of Si alone became somewhat more positive.

- The OCP value of only Al (no Si) in the solution was distinguishable and observed within the experimental of this work, from the OCP measured with both Si and Al in the solution, simultaneously and Si and Al, individually and separately.

The observations and contributions from **Chapter 4** can be summarized as follows:

- The simple galvanic cell measurement scheme was found to be effective.

- The measured OCP values for silicon in TMAH were found to be in general agreement with results found by other researchers.

- The presence of alminum in the solution, electrically connected to the silicon, shifts the overall OCP to a more-negative potential, which reduces the etch rate of the silicon, especially n-silicon, while the aluminum is etched. The difference in behaviour between n-type and p-type is consistent with the previous work of Glembocki *et al* [4],and Acero *et al* [45].

- The galvanic cell measurements of Al/Si/TMAH, are consistent with a coherent electrochemical understanding initiated by the experiments of Ashruf *et al* [10] on Au/Si/TMAH.

- The measurements are consistent with aluminum being electrochemically more active than silicon.

- The silicon anisotropic etch reaction in alkaline solutions is not reversible and the Nernst equation does not hold. This is confirmed by quantitative analysis of the experimental data.

5.2 SUGGESTIONS FOR FUTURE WORK

The involvement of electrochemistry in anisotropic etching of silicon is very important, both because it is necessary to resolve the selective etching of silicon without etching Al, and because it must be considered in the study of the fundamental atomic mechanisms, which are still not well understood. Future study would investigate in more depth several aspects of the problem:

- The impact of the area of exposed Al on the electrochemical behaviour. This may affect the relative dominance of the Al half-reaction, since the area controls the current.

- The impact of controlled levels of illumination. It was observed during this work that shielding the sample cell from the light affected the measurements. This effect is also considered by various authors in the literature, and is likely to be important.

- The relationship between pH and electrochemical parameters on the etch anisotropy, since the pH varies with T, and the electrolyte potential of the etchant is a

strong function of pH. Particularly important would be the relationship of etchant concentration between etch rate, OCP, pH and T

REFERENCES

[1] Don L. Kendall, "Vertical Etching of Silicon at Very high Aspect Ratio," Ann. Rev. of Material Science, 9 (1979), pp. 373.

[2] Allen J. Bard, "Encyclopedia of Electrochemistry of the elements," Vol. V, pp. 287-291.

[3] Osamu Tabata, "pH-controlled TMAH etchants for Silicon Micromachining," Sensors and Actuators, A 53, pp. 335-339, 1996.

[4] O. J. Glembocki, R. E. Stahlbush, M. Tomkiewicz, "Bias-Dependent Etching of Silicon in Aqueous KOH," Journal Electrochemical Society, vol. 132, no.1, pp.145 (1985).

[5] Scott D. Collins, "Etch Stop Techniques for Micromachining," J. Electrochemistry Soc., Vol. 144, No. 6 June 1997.

[6] A. Pandy, L.M. Landsberger, B. Nikpour, M. Paranjape, M Kahrizi, "experimental investigation of high Si/Al selectivity during anisotropic etching in TMAH," (1997).

[7] Gregory T. A. Kovacs, "Micromachining Transducers Sourcebook," ISBN 0-07-290722-3, 1998.

[8] Sung B. Lee, and Davorin Babic, "Investigation of Al Selectivity in Si Doped TMAH Solutions by Raman Spectroscopy," Chicago, Illinois 60607, USA.

[9] Y. Nemirovsky and A. El-Bahar, "the non-equilibrium band model of silicon in TMAH and in anisotropic electrochemical alkaline etching solutions," Sensors and Actuators, 75, pp. 205-214, 1999.

[10] C.M.A. Ashruf, P J. French, P. M.M. C. Bressers, P.M. Sarro, J.J. Kelly, "a new contactless electrochemical etch-stop based on a gold/silicon/TMAH galvanic cell," Sensors and Actuators A66, pp.284-291, (1998).

[11] Gregory T. A. Kovacs, Nadim I. Maluf, and Kurt E., "Bulk Micromachining of Silicon," proceedings of the IEEE, Vol. 86, No. 8, Aug. 1998.

[12] L. M. Landsberger, M. Kahrizi and M. Paranjape, S. Naseh, "Variation of Underetched Planes Appearing in Bulk Micromachining Silicon Using TMAH Etchant," Sept. (1996).

[13] Mitsuhiro Shikida, Kazuo Sa'ato, Kenji Tokoro, and Daisuke Uchikawa, "Comparison of Anisotropic Etching Properties between KOH and TMAH Solutions," Chikusa, Nagoya, Japan.

[14] H. A. Waggener, "electrochemical control of silicon," Bell Systems Technical Journal, vol. 49, no.3, pp. 473,1970.

[15] P. C. Searson, X. G. Zhang, "The Anodic Dissolution of Silicon in HF Solutions," J. Electrochemical Soc., Vol. 137, No. 8, August 1990.

[16] N. F. Raley, Y. Sugiyama, and Van Duzer, "(100) Silicon Etch-Rate Dependence on Boron Concentration in Ethylenediamine-Pyrocatechol-Water Solutions," J. Electrochemistry Soc., Vol. 131, No.1, Jan. 1984.

[17] Lai-cheng Chen, Minjan Chen, Chenhsin Lien, and Chi-Chao Wan, "the band Model and the etching Mechanism of Silicon in Aqueous KOH," J. Electrochemistry Soc., Vol. 142, No.1, Jan. 1995.

[18] S. Naseh, "Experimental Investigation of Anisotropic Etching of Silicon in TMAH," thesis, Aug. 1995.

[19] H. Seidel, L, Csepregi, A. Heuberger, H. Baumgaertel, "Anisotropic Etching of Crystalline Silicon in Alkaline Solutions: *II.* Influence of Dopants," Journal of the Electrochemical Soc., vol. 137, no. 11, pp. 3626-3633,1990.

[20] H Seidel, L. Csepregi, A. Heuberger, H. Baumgaertel, "Anisotropic Etching of Crystalline Silicon in. Alkaline Solutions: *I.* Orientation Dependence and

Behavior of Passivation Layers," Journal of the electrochemical Soc., vol.137, no. 11, pp. 3612-3626,1990.

[21] William D. Callister, "Materials science and engineering," 4th ed. John Wiley & Sons (1997).

[22] Donald T. Sawyer, Andrzej Sobkowiak, Julian L. Roberts, and Jr. "Electrochemistry for chemists," 2nd edition, ISBN 0-471-59468-7,1995.

[23] A.Viktor Myamlin, Yurii V Pleskov, "Electrochemistry of Semiconductors," Institute of Electrochemistry Academy of Sciences of the USSR, Moscow, Chpt. 1, pp. 30.

[24] E. D. Palik, J. W. Faust, H. F. Grey and R. F. Green, "Study of Etch-Stop Mechanism in Silicon," J. electrochemical Soc., vol. 129 no. 9,p. 2051,1982.

[25] J. W. Faust, Jr. and E. D. Palik, "Study of the Orientation dependent_etching and Initial Anodization of Si in Aqueous KOH," Journal Electrochemical Society, Vol. 130, no.6, pp.1413, (1983).

[26] W. Kern, "Chemical etching of silicon, germanium Gallium arsenide, and gallium phosphide," Microsensors, p.43, 73 1978.

[27] S. K. Ghandhi, "The Theory and Practice of Microelectronics," Microsensors, p.43, 73 1978.

[28] P. Allongue, V. Kosta-Kieling and H. Gerischer, J. Electrochemical Society, 140, pp1009, (1993).

[29] C.M.A. Ashruf, P J. French, P.M. Sarro, M. Nagao, M. Esashi, "fabrication of micromechanical structures with a new contactless electrochemical etch-stop," transducers '97, pp.703-706.

[30] E. D. Palik, H. F. Gray, and P B. Klein. "A Raman study of Etching Silicon in Aqueous KOH," Journal Electrochemical Society. Vol. 130. no.4, pp.956-959, (1983).

[31] E. D. Palik, V. M. Bermudez, O J Glembocki, "Ellipsometric Study of the Etch-Stop Mechanism in Heavily Doped Silicon," Journal of the Electrochemical Society vol. 132, no. 1, pp. 135, 1985.

[32] E. D. Palik, O J Glembocki, and I. Heard, Journal of the Electrochemical Society vol. 134, no. 1, pp. 405, 1987.

[33] Miko Elwenspoek, "Micromechanics Etching of Silicon," Chpt.2, 3 and 4.

[34] P J. French, M. Nagao, M. Esashi, "electrochemical etch-stop in TMAH without externally applied bias," Sensors and Actuators A56, pp.279-280, (1996).

[35] P. Hartman, "in Crystal Growth, An Introduction," North Holland, Amsterdam, P. Bennema, and J. P. Van Der Eerden, "in Mophology of crystals," ed. I. Sunagawa,pp.1.

[36] Sundaram and H. Chang, "Electrochemical Etching of Silicon by Hydrazine," J. Electrochemical Soc., Vol. 140, No. 6, June 1993.

[37] K. E. Bean, IEEE trans. "Electron. Devices," Ed-25, 1185 (1978).

[38] Ben Kloeck, Scott D. Collins, Nico F. DE Rooji, and Rosemary L. Smith, "Study of Electrochemical Etch-Stop for High-Precision Thickness Control of Silicon Membranes," Trans. Electron Devices, vol. 36, no.4, pp. 663-669, April 1989.

[39] L. M. Landsberger and A. Pandy, "Post-Process Anisotropic Etching in TMAH," Etching of CMC-Mitel Die and Wafers, 1997.

[40] L. M. Landsberger, S. Naseh, M. Kahrizi and M. Paranjape, "On Hillocks Generated During Anisotropic Etching of Si in TMAH," J. of Microelectromechanical Sys., Vol. 5,No.2, June 1996.

[41] O. Tabata, R. Asahi, H. Funabashi and S. Sugiyama, "Anisotropic etching of silicon in $(CH_3)_4NOH$ solutions," Sensors and Actuators (Transducers '91), San Francisco, CA, USA, June 24-28, 1991, pp. 811-814.

[42] A. Merlos, E. Cabruja, J. Esteve, "New technology for easy and full IC-compatible fabrication of backside-contacted ISFETs," Sensors and Actuators B 24-25, pp. 228-231 (1995).

[43] E. H. Klaassen, Richard J.Reay, Christopher S.G. Kovacs, "Micromachined thermally isolated circuits," Sensors and Actuators A58, pp. 43-50, (1997).

[44] M.C. Acero, J. Esteve, Chr. Burrer, and A. Götz, "Electrochemical etch-stop characteristics of TMAH:IPA solutions," Sensors and actuator A46-47,pp. 22-26 (1995).

[45] James E. Brady and Gerard E. Humiston, "General Chemistry principles and structure," 3th ed. John Wily & SONS, New York, 1982.

[46] James E. Brady, John R. Holum, "Fundamentals of chemistry," 3th edition, John Wiley & sons, QD31.2 B69 1988.

[47] R.A Day, Jr. A. L. Underwood, "quantitative Analysis," 5th edition, ISBN 0-13-746728-1 01, 1986.

[48] S.M. Sze, "Physics of semiconductor Devices," John Wiley & Sons, Inc., New York (1981).

[49] Donald A. Neamen, "Semiconductor Physics and Devices *Basic principles*," Chpts.5, 7, 9 and 12.

[50] P. Schweitzer, editor Marce, "Corrosion and Corrosion Protection Handbook," Dekker, Inc., NewYork, pp. 487, 1983.

[51] Ben G. Streetman, "Solid State Electronic Devices," 4th edition, Simon & Schster co., New Jersey 1995, Chpts. 3,5 and 8.

[52] R. Memming, "in comprehensive treatise of electrochemistry," vol. 7, B.E. Conway, J. O'M. Bockris, E. Yeager, S.U.M. Khan, and R.E White,Editors,pp.535, Plenum Press, NewYork (1983).

[53] E. D. Palik, O J Glembocki, and I. Heard, Journal of the Electrochemical Society vol. 134, no. 1, pp. 405, 1987.

[54] U. Schnakenberg, W. Benecke, P. Lange, "TMAHW Etchants for Silicon Micromachining," Sensors and Actuators, ch287-5, 1991.

[55] Mitsuhiro Shikida, Kazuo Sa'ato, Kenji Tokoro, and Daisuke Uchikawa, "Comparison of Anisotropic Etching Properties between KOH and TMAH Solutions," Chikusa, Nagoya, Japan.

[56] Jacob Millman, "Microelectronics Digital and analog Circuits and systems," ISBN 0-07-Y66410-2, Chpt. 4 1985.

[57] Miko Elwenspoek, "Micromechanics Etching of Silicon," Chpt.2, 3 and 4.

[58] J. W. Faust, Jr., and E.D. Palik, J. Electrochemical Soc., Vol. 130, pp. 1413 (1983).

[59] S. Roy Morrison, "electrochemistry at semiconductor and oxidized metal electrodes," chpts.2-8, (QD 553 M6) plenum press, NewYork 1980.

[60] Madou Marc, "Fundamentals of Micromachining," ISBN 0-8493-9451-1, 1997.

[61] Sung B. Lee, and Davorin Babic, "Observation and Characterization of Aluminum Passivation in Silicon Doped KOH Solutions," Chicago, Illinois 60607, USA.

Appendix 1

The Principles and Operation of the Potentiostat

For all the experiments commercially available tetra-methyl ammonium hydroxide (TMAH) $\{(CH_3)_4NOH\}$ of 25 wt. % was used. A concentration of 5 wt. % was obtained by diluting the TMAH with DI water. The later one was used with dissolved silicon, because the amount of the silicon that should be dissolved in the TMAH to passivate the aluminum is potentially function to the concentration of the TMAH. The temperature in these experiments was at 80 ^{o}C. In order to perform an electrochemical technique its goal, it is necessary to accurately maintain the potentials on the electrodes (i.e. WE, CE, and RE) in a solution. This can be achieved using a potentiostat. A variety of circuits suitable for potential control (i.e. potentiostat) have been constructed from operational amplifiers. One typical example shown in Fig.A1.1. The operational of this circuit can be understood best by keeping in our mind the fact that the operational amplifier reacts in the manner required to maintained zero potential difference between it inputs [44].

This device utilized to accurately control the potentials between a solution and electrodes inside it, by supplying a necessary current in either direction, to

move the working electrode away from its open circuit potential (i.e. OCP) as shown in Fig.A1 2. This device should be used because an external applied potential will not accurately determine the potential across the electrode-solution interface, due to current-dependent potential drops elsewhere in the circuit, as shown in Fig.A1 3. Therefore, a potentiostat should be used to apply accurate potentials between a working electrode and reference electrode [44].

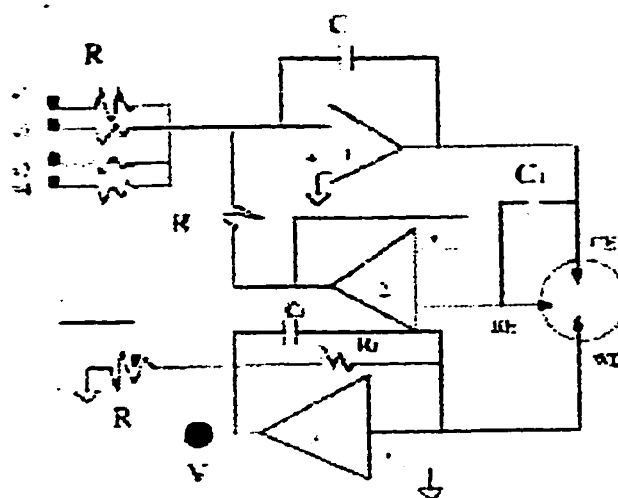

Fig.A1 1The potentiostat circuit.[51]

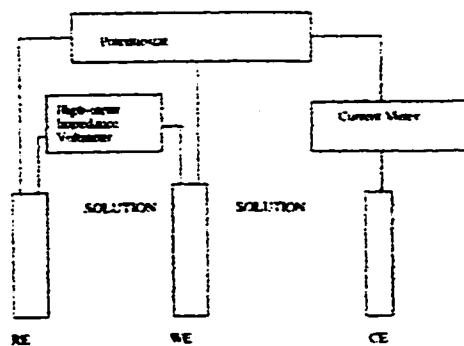

Fig.A1 2 The demonstration circuit of the potentiostatic measurements.[51]

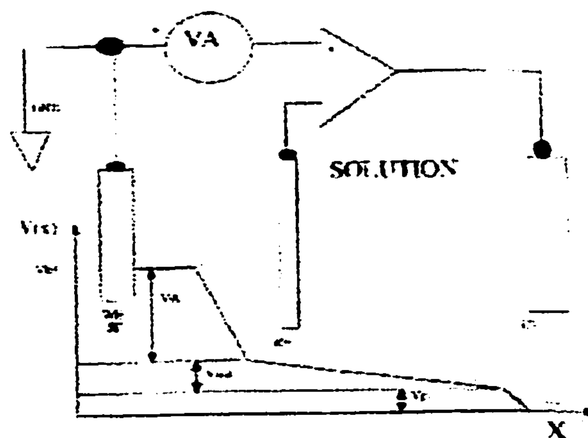

Fig.A1 3 Potential drops in the circuit with the potentiostat no longer matter, as the reference electrode draws no current.[44]

The potentiostat drives currents into the counter electrode (i.e. CE, Pt). Such that the potential between the reference electrode (RE) and the working electrode is brought to the desired value, in other word; the counter electrode drives the solution, such that the potential between the working and the reference electrodes is maintained at negative potential. The counter electrode is typically made of an inert material, such as platinum. The reference electrode (i.e. RE), silver/silver-chloride (Ag/AgCl), pseudo-reference electrode was used in these experiments. This electrode is selected because they maintained relatively stable interfacial potentials over varying current densities, although in this application, the reference currents are very small. The reference electrode draws no current, since it is connected to the inverting input of the operational amplifier as shown in Fig.A1 3. This electrode should be situated as close as possible to the working electrode and much better if it attaches to the top of the ceramic package for three purposes; firstly: to ensure that it is close enough to the Si (WE), without shorting to any of the other connections. Secondly: this is necessary because any potential drops

through the solution, between the working and counter electrodes introduce an error in the applied potentials. Thirdly: this will minimize the ohmic drop through the solution, between the working and reference electrodes.

The working electrode (WE) is the material that is to be maintained at the correct potential, in this case, n- and p-type silicon were used

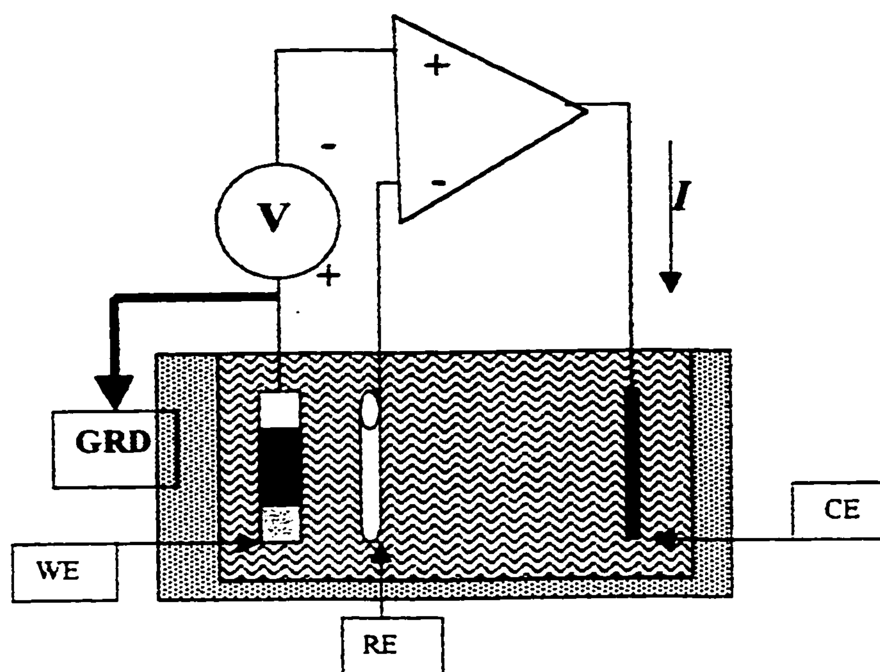

Fig.A1.4 A simple experimental setup representation.

Individually. Negative feedback applied to the operational amplifier forces the voltage drop at the working electrode to the applied voltage (*V*), regardless of resistive and other losses due to the counter electrode and bulk solution, as shown in Fig.A1.4. Note that in this configuration there are two ground points, the first is the potentiostat system electrical ground, which indicated by the grounding symbol connected to the n-

type Si (i.e. WE), and the second ground is the solution reference point, which it is Ag/AgCl electrode.

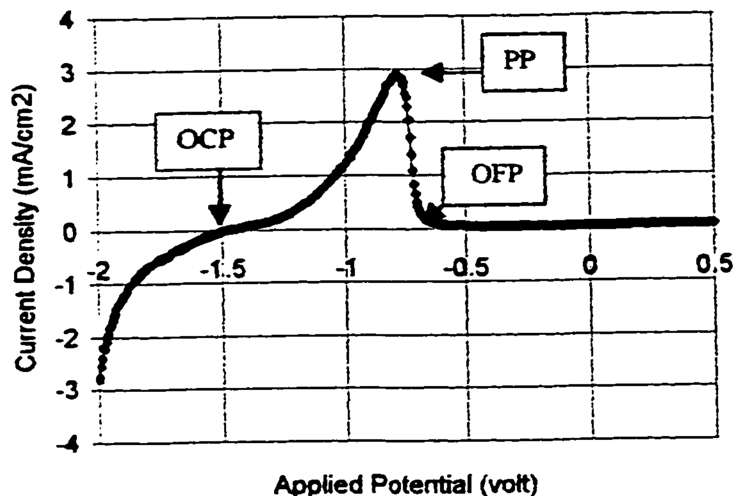

Fig.A1.5 *I-V* characteristics of n-type Si in TMAH 5 wt.% at 80 ^{o}C. The potential is relative to the Ag/AgCl reference electrode. The exact magnitude of the current profile depends on the working electrode area.

The LSV measurements were done using potentiostat model SR830 DSP lock-in amplifier, manufacturer SRS, USA. The potential between the WE and RE is swept from negative to positive, with scan rate of 5mV/s, to generate *I-V* curves. A typical plot of current density vs. applied potential is shown in Fig.A1.5. Such a graph indicate three particularly important potentials [4], the open-circuit potential (OCP), the passivation potential (PP), and the oxide-formation potential (OFP). The open-circuit potential (OCP), is the potential on the WE when there is no net current flow. This is not a thermal equilibrium, but is a steady-state [10] of electrochemical processes between the WE and

electrolyte, such that $I = 0$ mA. At this potential, the etch rate is usually at or near its maximum value [4], and decreases at more anodic or cathodic potentials. At the passivation potential (PP), the electrode current begins to drop, and the etch process is more and more inhibited for potentials more positive (more anodic). At the oxide formation potential, the etching is stopped.

APPENDIX 2

ENERGY BAND MODELS

As reviewed in Chapter 2, standard electrochemistry considers simple situations of a metal in contact with an electrolyte. Replacing the metal by a semiconductor (e.g. silicon) brings the complication of an energy band structure into the picture. The presence of another conductive material (Al) on the immersed structure; can cause even further complications. The analyses in this chapter aim to support the experiments reported in Appendix 3 and Chapter 3. Various sample structures are described in Appendix 3 and Chapter 3, with Si, SiO_2 and Al, in various configurations etching in TMAH. Accordingly, the energy bands of certain basic arrangements are analyzed here:

- The p-n junction,
- The metal-semiconductor junction,
- The alloyed metal-semiconductor junction
- The Al/SiO_2/Si configuration (the MOS Capacitor).

These analyses are then considered in the context of equilibrium electrochemistry, where the potential in the solution is relevant. Finally, a recently published journal article by Nemirovsky *et al* is discussed [9], where the hypothesis of non-equilibrium electrochemistry is raised.

A2.1 The p-n Junction

In general, the **p-n junction** can be understood beginning with a qualitative description of current flow in a biased junction. Since an applied voltage changes the electrostatics potential barrier and thus the electric field within the transition region, one can expect changes in the various components of current at the junction Fig.A2.1. In addition, the separation of the energy bands is affected by the applied bias, along with the width of the depletion region. The electrostatics potential barrier at the junction is lowered by a forward bias V_f from the equilibrium contact potential V_0 to the smaller value V_0-V_f. This lowering of the potential barrier occurs because a forward bias (a positive voltage on p-type with respect to n-type) raises the electrostatic potential on the metal side relative to the n-type. For a reverse bias the opposite occurs; the electrostatic potential of the p-type is depressed relative to the n-type, and the potential barrier at the junction becomes larger (V_0+V_r) [32].

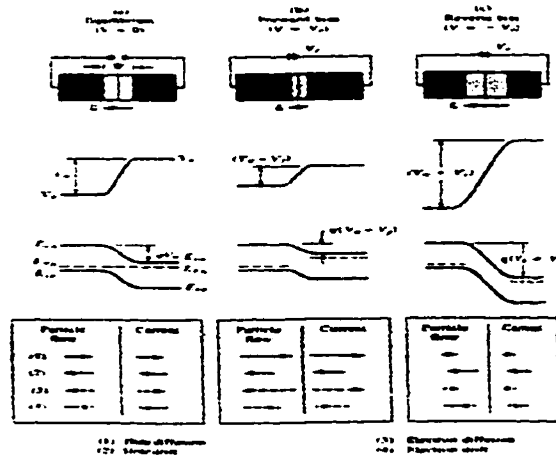

Fig.A2.1 Effects of bias at a p-n junction; transition region width and electric field, electrostatic potential, energy band diagrams, and particle flow and current directions within W for (a) equilibrium (b) forward bias, and (c) reverse bias. [32]

The *electric field* within the transition region can be deduced from the potential barrier. We notice that the field decreases with forward bias, since the applied electric field opposes the built-in field. With reverse bias the field at the junction is increased by the applied field, which is in the same direction as the equilibrium field. The change in electric field E at the junction calls for a change in the *transition region width W*, since it is still necessary that a proper number of positive and negative charges (in the form of uncompensated donor and acceptor ions) be exposed for a given value of the E field. Thus the width W will decrease under forward bias (smaller E, fewer uncompensated charges) and increase under reverse bias. Eq.A2.1 and Eq.A2.2 can be used to calculate W, x_{p0}, and x_{n0} if V_0 is replaced by the new barrier height V_0-V.

$$W = \left[\frac{2\varepsilon V_0}{q}\left(\frac{N_a + N_d}{N_a N_d}\right)\right]^{1/2} = \left[\frac{2\varepsilon V_0}{q}\left(\frac{1}{N_a} + \frac{1}{N_d}\right)\right]^{1/2} \qquad \text{Eq. A2.1}$$

For $V_{bi} = V_0 = \frac{kT}{q}\ln\frac{N_a N_d}{n_i^2}$ Eq. A2.1 can be written as follows

$$W = \left[\frac{2\varepsilon kT}{q^2}\left(\ln\frac{N_a N_d}{n_i^2}\right)\left(\frac{1}{N_a} + \frac{1}{N_d}\right)\right]^{1/2} \qquad \text{Eq. A2.2}$$

The penetration of the transition region into n and p materials can be calculated by using the following equations:

$$x_{p0} = \frac{WN_d}{N_a + N_d} = \left\{\frac{2\varepsilon V_0}{q}\left[\frac{N_d}{N_a(N_a + N_d)}\right]\right\}^{1/2} \qquad \text{Eq. A2.3}$$

$$x_{n0} = \frac{WN_a}{N_a + N_d} = \left\{ \frac{2\varepsilon V_0}{q} \left[\frac{N_a}{N_d(N_a + N_d)} \right] \right\}^{1/2} \qquad \text{Eq. A2.4}$$

The separation of the energy bands is a direct function of the electrostatic potential barrier $(V_n - V_p)$ at the junction. The height of the electron energy barrier is simply the electronic charge q times the height of the electrostatic potential. Thus the bands are separated less $\left[q(V_0 - V_f)\right]$ under the forward bias than at equilibrium, and more $\left[q(V_0 + V_r)\right]$ under reverse bias. Therefore, the shifting of the energy bands under bias implies a separation of the Fermi level on either side of the junction. Under forward bias, the Fermi level on the n side E_{Fn} is above E_{Fp} by the energy qV_f; for the reverse bias, E_{Fp} is qV_r joules higher than E_{Fn}. In energy units of electron volt, the Fermi level in the two neutral regions are separated by an energy (eV) numerically equal to the applied voltage (V).

A2.2 The metal-Semiconductor Junction

The band diagrams for a metal and a semiconductor, not in contact yet, are shown in Fig.A2.2, for the case where $\Phi_{Al} < \Phi_s$. The work function Φ_m, characteristic of a metal (Al), can be defined in terms of the energy required to move an electron from the Fermi level of the metal to outside the metal. The silicon work function, Φ_s, varies depending on the doping of the semiconductor. Fig.A2.3 shows the work-function potential difference $\Phi_{ms} = \Phi_m - \Phi_s$ for Al on Si as the doping is varied. One notice that Φ_{ms} is always negative for this case; and most negative for heavily-doped p-type Si (i.e. for E_F close to the valence band). Fig.A2.3 shows the variation of the metal semiconductor work-function difference Φ_{ms}, with substrate doping concentration, for Si/Al.

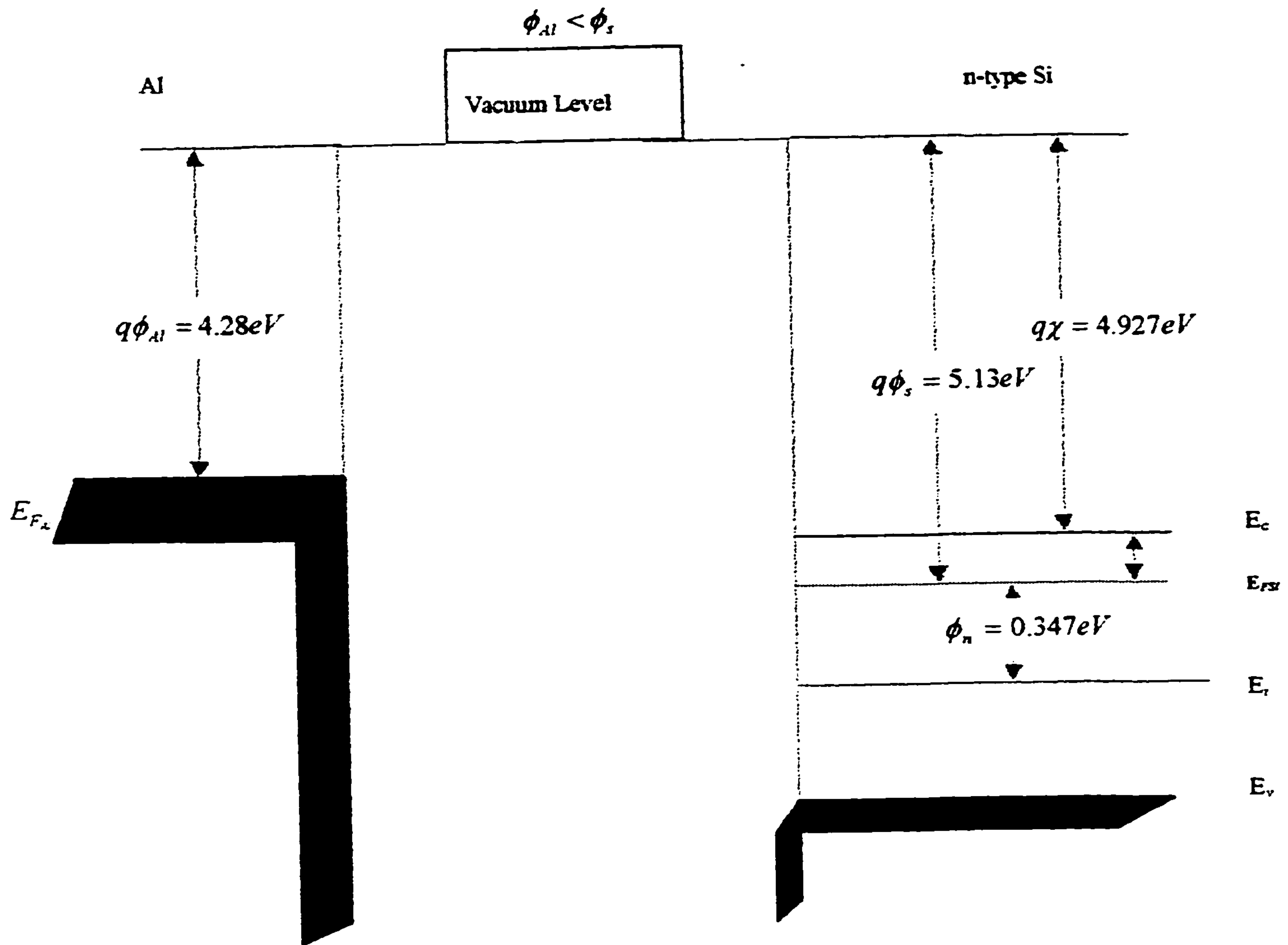

Fig.A2.2 The energy-band for metal-semiconductor junction before contact. For $\Phi_m < \Phi_s$.

The parameters Φ_m and Φ_s are the metal work function of Al (i.e. $\Phi_{Al} = 4.28$V), and n-type Si work function (i.e. $\Phi_s = 5.13$V, where $N_d = 10^{16}$ cm^{-3}), respectively, and $q\chi$ is known as the *electron affinity* that measured from the vacuum level to the semiconductor conduction band edge. The equilibrium potential difference V_0 can be

increased or decreased by the application of either forward- or reversed-bias voltage as in p-n junction. Fig.A2.4 shows thermal equilibrium barrier after contact, to achieve thermal equilibrium in this junction, electron will flow from the metal into the lower energy states on the semiconductor, which makes the surface of the semiconductor more n-type; accumulation of majority carrier near the surface.

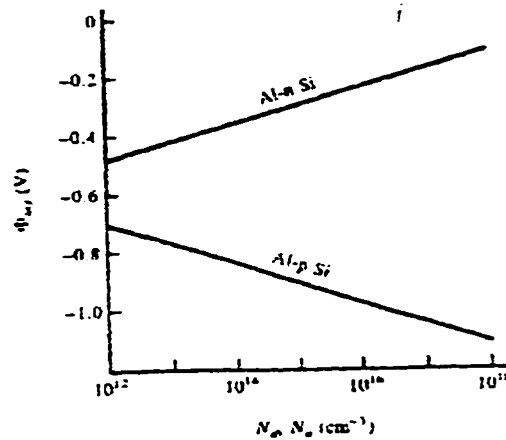

Fig.A2.3 Variation of the metal-semiconductor work function potential difference Φ_{ms} with substrate doping concentration for Al-Si. [32]

The parameter Φ_{Bn} is the barrier height of the semiconductor contact, **the potential barrier seen by electrons in the metal trying to move into the semiconductor**. This barrier is known as the Schottky barrier and is given ideally by:

$$\Phi_{Bn} = (\Phi_m - \chi) \qquad \text{Eq. A2.5}$$

In the semiconductor side, V_{bi} is the *built-in* potential barrier. This barrier, is similar to the case of the p-n junction, **is the barrier seen by electrons in the semiconductor conduction band trying to move into the metal**. The *built-in* potential barrier is given by:

$$V_{bi} = \Phi_{Bn} - \Phi_n \qquad \text{Eq. A2.6}$$

Where $\Phi_n = E_F - E_i = \frac{kT}{q} \ln \frac{N_d}{n_i}$

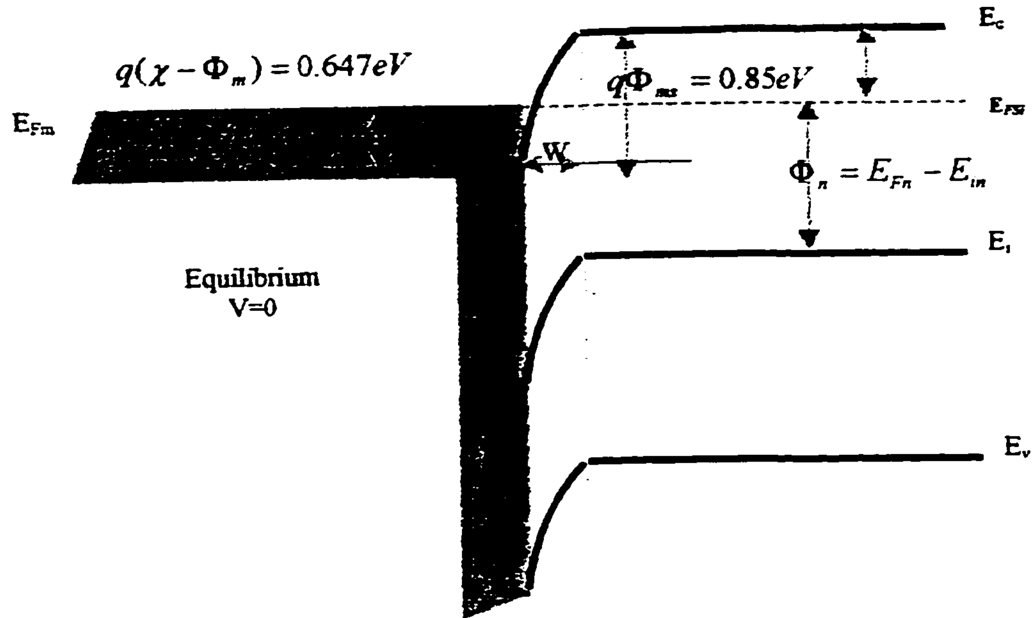

Fig.A2.4 The energy-band diagram of metal-semiconductor after contact for $\Phi_m < \Phi_s$ (Equilibrium State).

For T=300 k $\quad V_t = \frac{kT}{q} = 0.0259V$, $n_i = 1.5 \times 10^{10} cm^{-3}$

Which makes V_{bi} a slight function of the semiconductor doping, as was the case in a p-n junction. If a negative voltage is applied to the n-type with respect to the metal (i.e. cathodic bias), the metal-semiconductor barrier $V_0 = q\Phi_{ms}$ is increased by qV_f, while Φ_{Bn} remains constant. In this situation, electrons can more easily flow from the metal to semiconductor. This bias condition is the forward bias, as shown in Fig.A2.5. If a positive voltage is applied to the semiconductor with respect to the metal (anodic bias), V_r

reduces the semiconductor-metal barrier height $(\Phi_{ms} - V_r)$. This bias condition is the reverse bias as shown in Fig.A2.6. Fig.A2.7 that shows symbolically the main parameters used in these explanations.

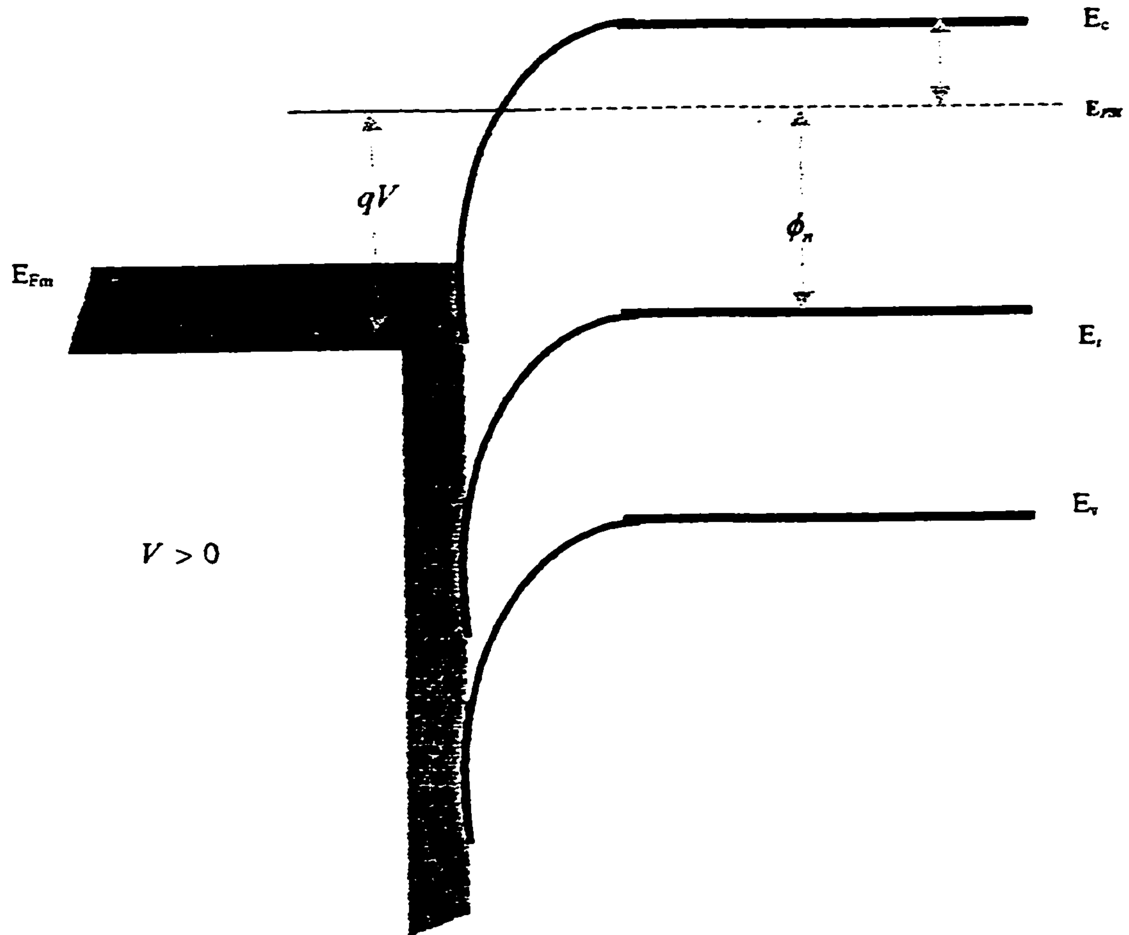

Fig.A2.5The energy-band for metal-n-semiconductor junction with a negative applied voltage to the n-type (cathodic bias). for $\Phi_m < \Phi_s$

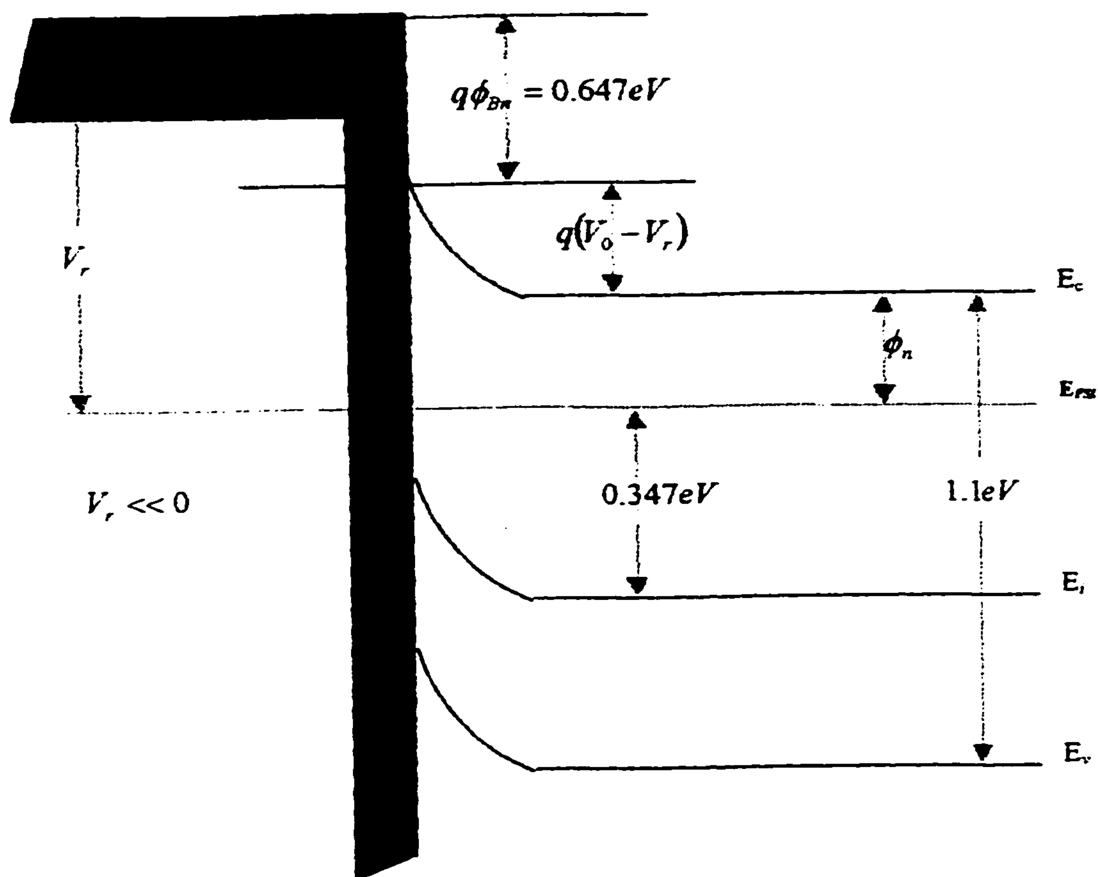

Fig.A2.6 The energy-band for metal-n-semiconductor junction with a positive applied voltage to the semiconductor (anodic bias) . for $\Phi_m < \Phi_s$.

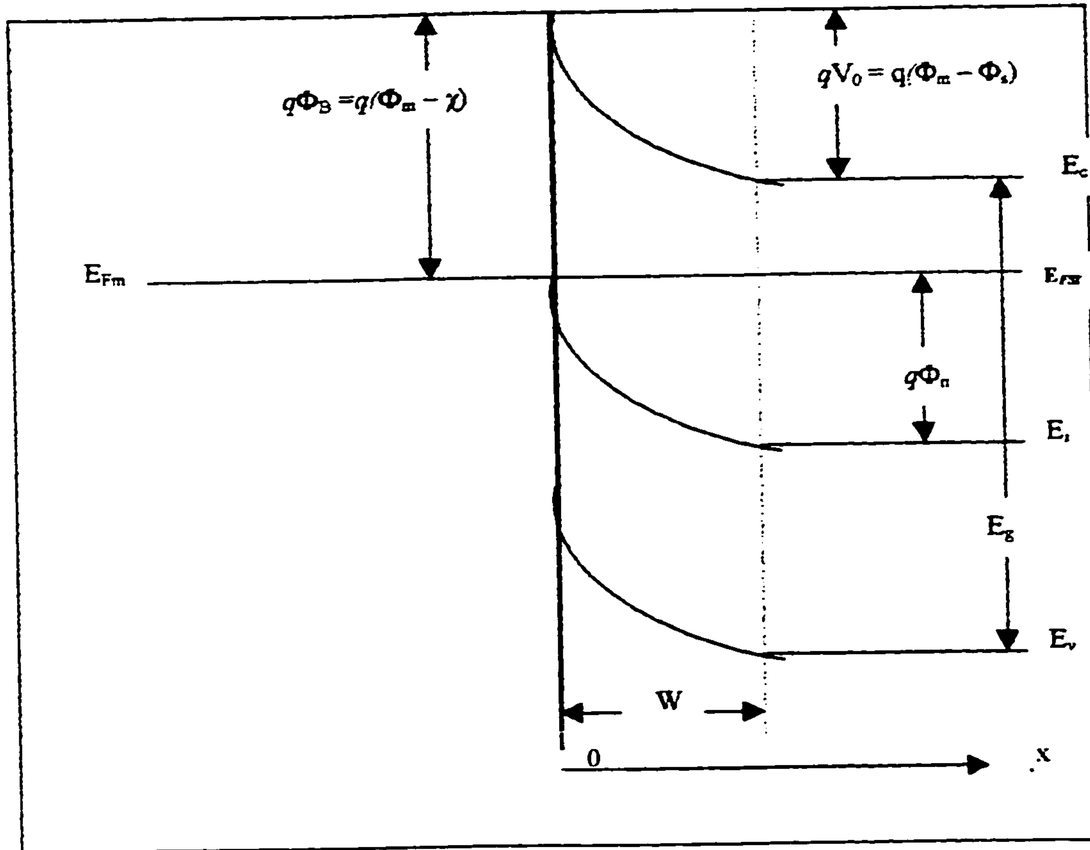

Fig.A2.7 The energy-band diagram shows the main parameters.

A2.3 The Alloyed Metal-Semiconductor Junction

Above is described an idealized metal-semiconductor junction. In reality, a junction between Al and n-type silicon is alloyed such that a thin p-type region is formed at the surface immediately adjacent to the Al. Aluminum is alloyed into n-type Si Sample $N_d=10^{16}$ cm^{-3}, forming p-n junction, assume that the acceptor concentration in the alloyed regrown region is $N_a = 1.5\times10^{18} cm^{-3}$, $\Phi_m < \Phi_s$, $\Phi_m = 4.28V$

$$(\Phi_s - \Phi_m) = V_{bi} = V_0 = \frac{kT}{q} \ln \frac{N_a N_d}{ni^2} = 0.85v$$

$$(\Phi_s - \Phi_m) = V_0 = 0.85 \rightarrow \Phi_{Si} = \Phi_m + V_0 = 4.28 + 0.85 = 5.13v$$

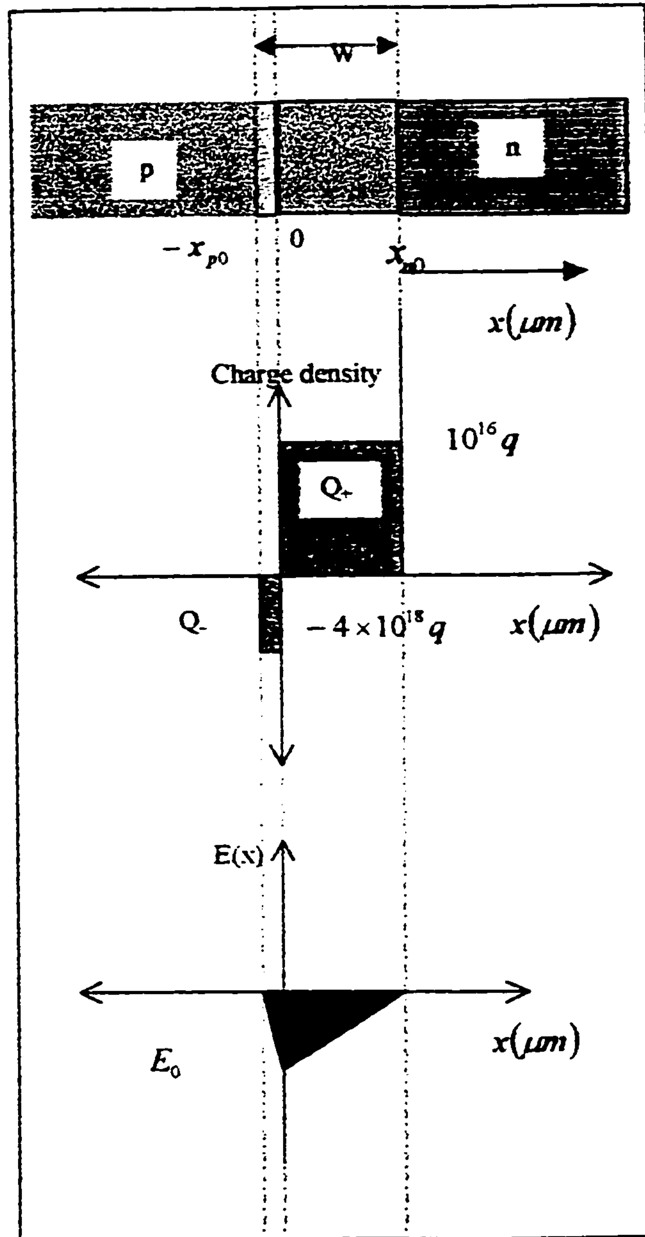

Fig.A2.8 Space charge and electric field distribution within the transition region of a p-n junction with N_a>N_d.

From Eq. A2.1 $$W = \left[\frac{2\varepsilon V_0}{q}\left(\frac{N_a + N_d}{N_a N_d}\right)\right]^{1/2} = \left[\frac{2\varepsilon V_0}{q}\left(\frac{1}{N_a} + \frac{1}{N_d}\right)\right]^{1/2} = 0.334\mu m$$

From Eq. A2.4 $$x_{n0} = \frac{WN_a}{N_a + N_d} = \left\{\frac{2\varepsilon V_0}{q}\left[\frac{N_a}{N_d(N_a + N_d)}\right]\right\}^{1/2} \approx 0.333\mu m$$

Note that, therefore

$$W \approx x_{n0} \cong \sqrt{\frac{2\varepsilon_s (V_{bi} - V)}{qN_d}} = \sqrt{\frac{2 \times 11.9 \times 8.85 \times 10^{-14} \times 0.85}{(1.6 \times 10^{-19} \times 10^{16})}} = 0.334\mu m$$

$$x_{p0} = \frac{WN_d}{N_a + N_d} = \left\{\frac{2\varepsilon V_0}{q}\left[\frac{N_d}{N_a(N_a + N_d)}\right]\right\}^{1/2} = 8.3\,\mathring{A}$$

which is very small as expected, Fig.A2.8.

The electric field $E(x)$

$$\frac{dE}{dx} = \frac{1}{\varepsilon}(-qN_a) \ldots\ldots\ldots 0 < x < x_{n0}$$

$$\frac{dE}{dx} = \frac{1}{\varepsilon}(-qN_d) \ldots\ldots\ldots x_{p0} < x < 0$$

The maximum value of the electric field is

$$E_0 = -\frac{q}{\varepsilon}N_d x_{n0} = -\frac{q}{\varepsilon}N_a x_{p0} = -5.1 \times 10^4 V/cm$$

The charge density at the surface $Q_+ = |Q_-|$

$$Q_+ = -q.Ax_{n0}.N_d$$

$$Q_- = -q.Ax_{p0}.N_a$$

$$E_{Fs} - E_i = \phi_n = \frac{kT}{q}\ln\frac{N_d}{n_i} = 0.0259\ln\frac{10^{16}}{1.5 \times 10^{10}} = 0.347V$$

For the Si the band gap $E_c - E_V = 1.1eV$ so $E_g/2 = E_c - E_i = 0.55eV$, thus

$$E_c - E_F = 0.203eV$$

The electron affinity $q\chi$, from diagram one observed that

$$\chi = \phi_s - (E_F - E_c) = 5.13 - .203 = 4.927V$$

$$q\chi = 4.927eV$$

The barrier height of the semiconductor contact Φ_{Bn}

$$\Phi_{Bn} = (\chi - \phi_m) = 4.927 - 4.28 = 0.647V$$

A2.4 The Al/SiO$_2$/Si Configuration (The MOS Capacitor)

A metal-oxide-semiconductor structure actually, is the heart of the MOSFET. Fig.A2.9 shows the schematic of metal-oxide-semiconductor, one has to pay attention to the metal (i.e. Al is the metal in this work), the semiconductor, and oxide work functions (i.e. $\Phi_m, \Phi_s, \Phi_{ox}$). The energy bands in the semiconductor near oxide-semiconductor interface bend as a voltage is applied across this structure which so far resemble the MOS capacitor structure. The position of the conduction and valence bands relative to the Fermi level at the oxide-semiconductor interface is a function of the MOS capacitor voltage, so that the characteristics of the semiconductor surface is reversible; from p-type to n-type.

Some important definitions are made in the energy band diagram of Fig.A2.10. The work function characteristic of the metal (*Al*) can be defined in terms of the energy required to move an electron from the Fermi level to outside the metal. In this structure;

metal-oxide-semiconductor, it is more convenient to use a *modified work function* $q\Phi'_m$ metal-oxide interface and the metal-semiconductor work function difference is defined as

$$V_{ox0} + \Phi_{s0} = -\Phi_{ms} = -\left[\Phi'_m - \left(\chi' + \frac{E_g}{2q} - \Phi_{fn}\right)\right] \qquad \text{Eq. A2.7}$$

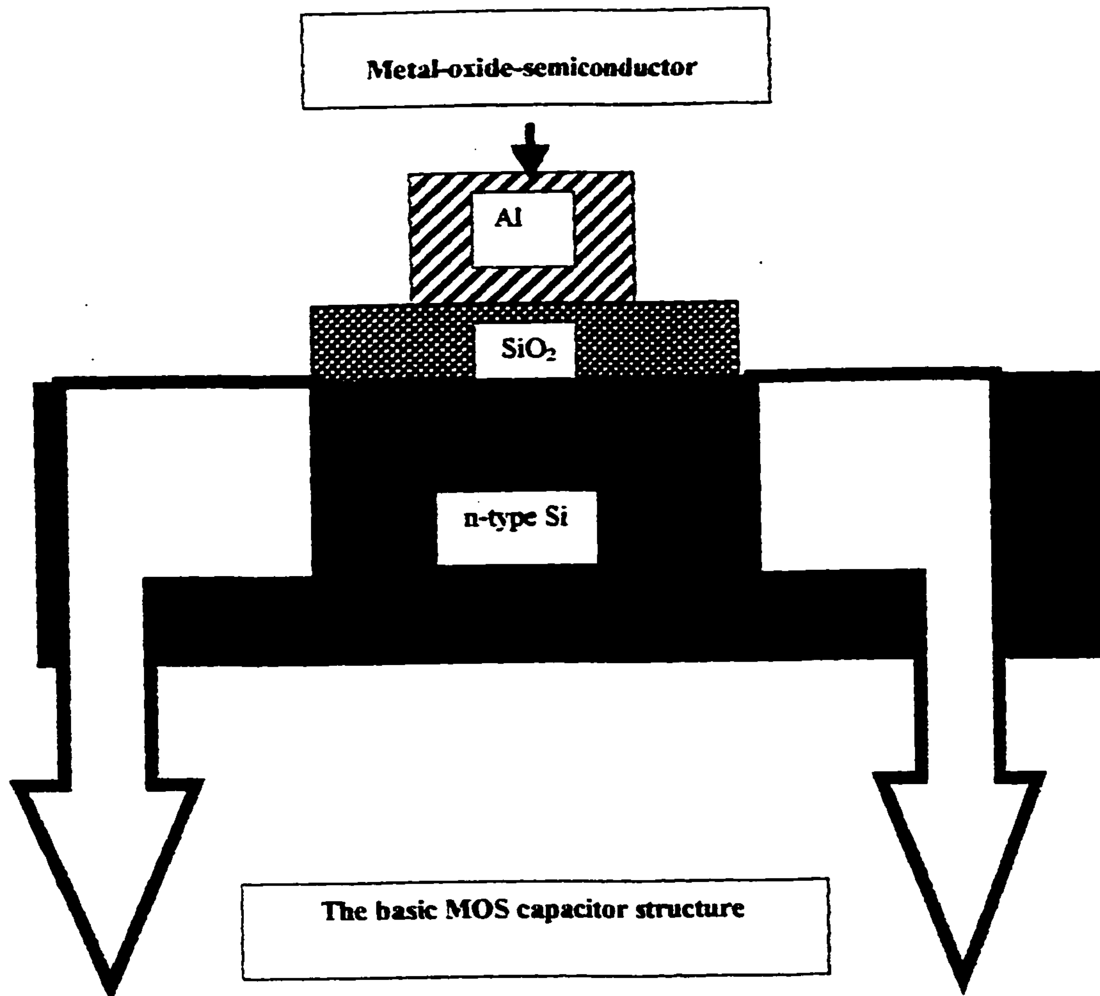

Fig.A2.9 The schematic of the metal-oxide-semiconductor configuration.

The Aluminum-semiconductor work function difference Φ_{ms} can be determined for the work functions of aluminum-silicon dioxide junction, $\Phi'_m = 3.20v$, and a silicon-

silicon dioxide junction, $\chi' = 3.25v$, the band-gap for the silicon, $E_g = 1.1\ eV$, and the n-type doping $N_d = 10^{16}\ cm^{-3}$, the aluminum $N_a = 4 \times 10^{18}\ cm^{-3}$ at $T = 300K$,

$$\Phi_{fn} = V_t \ln\left(\frac{N_d}{n_i}\right) = 0.0259 \ln\left(\frac{10^{16}}{1.5 \times 10^{10}}\right) = 0.347 Volt$$

Then the work function difference for zero applied voltage (OCP) is

$$V_{ox0} + \Phi_{s0} = -\Phi_{ms} = -\left[\Phi'_m - \left(\chi' + \frac{E_g}{2q} - \Phi_{fn}\right)\right]$$

$$\Phi_{ms} = \Phi'_m - \left(\chi' + \frac{E_g}{2q} - \phi_{fn}\right) = 3.20 - (3.25 + .55 - .347) = -0.253 volt$$

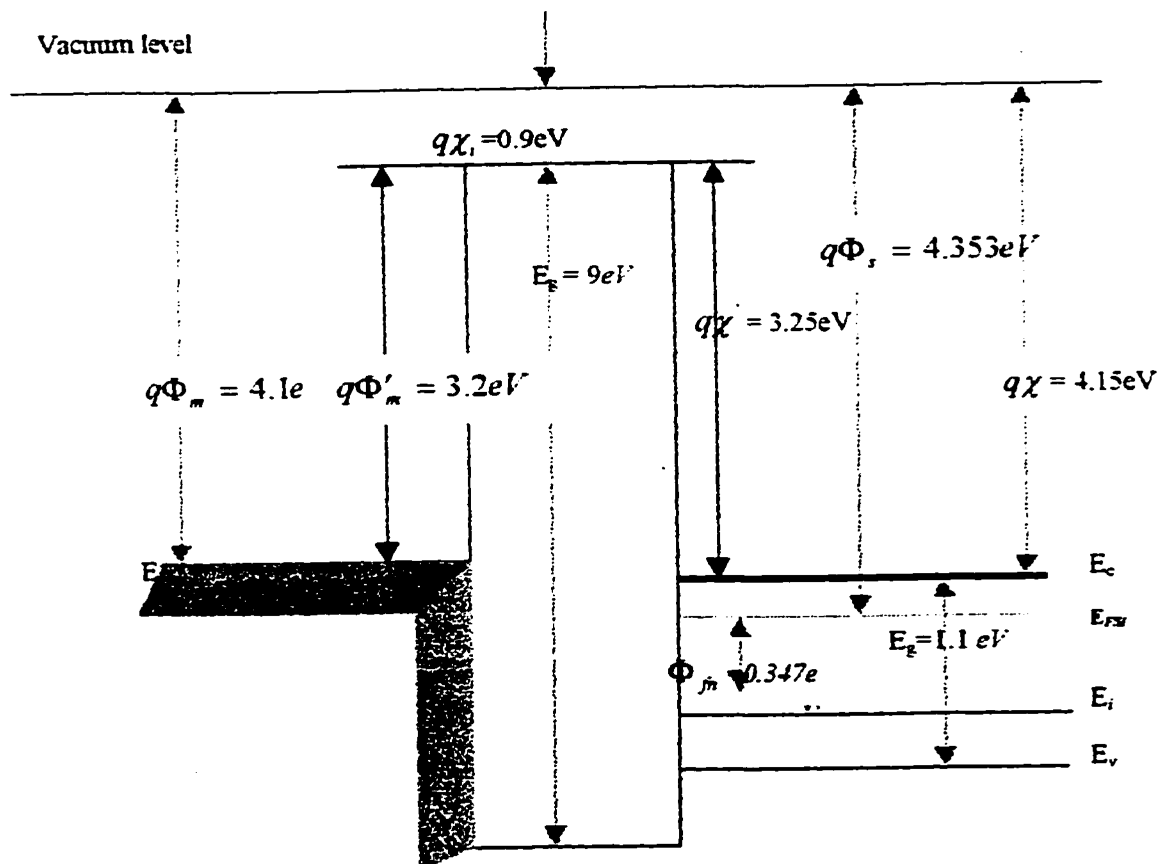

Fig.A2.10 Energy levels in metal-oxide-semiconductor structure prior to contact.

If a voltage is applied, the potential drop across the oxide and the surface potential will change, so the applied voltage V_a can be written as follows,

$$V_a = \Delta V_{ox} + \Delta\Phi_s = V_{ox} + \Phi_s + \Phi_{ms}$$

Where, $V_{ox} = \frac{-Q'_{ss}}{C_{ox}}$, and $C_{ox} = \frac{\varepsilon_{ox}}{t_{ox}} = \frac{(3.9)(8.85\times10^{-14})}{200\times10^{-8}} = 17.3\times10^{-8} F/cm^2$

Q'_{ss} is the equivalent trapped charge per unit area, assume that $Q'_{ss} = 10^{11}$ electronic charges per cm^2 $Q'_{ss} = (10^{11})(1.6\times10^{-19}) = 1.6\times10^{-8} coul/cm^2$.

In the flat band condition, the surface potential is zero, or $\Phi_s = 0$, then

$$V_a = V_{FB} = \Phi_{ms} - \frac{Q'_{ss}}{C_{ox}} = -0.253 - \frac{1.6\times10^{-8}}{17.3\times10^{-8}} = -0.345 volts.$$

So, the applied voltage required to achieve the flat-band condition for this n-type substrate is negative if the amount of fixed oxide charge increases, the flat-band voltage becomes even more negative.

The energy $q\Phi'_m$ is measured from the metal Fermi level to the conduction band of the oxide. Similarly, $q\Phi'_s$ is the modified work function at the semiconductor-oxide interface. another quantity that will be useful in later discussion is $q\Phi_{fn}$ that measures the position of the Fermi level up the intrinsic level E_i for the semiconductor. This quantity indicates how strongly n-type the semiconductor is [32]. The concentration of electrons in the conduction band is

$$N_d = n_0 = n_i e^{(E_F - E_i)/kT} \qquad \text{Eq.A2.8}$$

$$n_i^2 = p_0 n_0 \qquad \text{Eq.A2.9}$$

This structure of Fig.A2.10 is essentially a capacitor in which one plate is a semiconductor and the other one is aluminum (i.e. MOS capacitor). Fig.A2.11 shows the energy-band diagram of the entire metal-oxide-semiconductor structure with zero voltage applied (i.e. *OCP*). The Fermi level is a constant through the entire system at thermal equilibrium [24].If a negative voltage is applied to n-type Si, Fig.A2.12, we effectively deposit a positive charge on the *Al*. In response, we expect an equal net negative charge to accumulate at the surface of n-type Si. In this case n-type substrate this occurs by *electron accumulation* at the semiconductor-oxide interface (cathodic bias). Since $q\Phi_s'$ and $q\Phi_m'$ do not change with applied voltage, moving E_{Fm} down in energy relative to E_{Fs} causes a tilt in the oxide conduction band. We expect such a tilt since an electric field causes a gradient in E_i (and similarly in E_c and E_v)

$$E(x) = \frac{1}{q}\frac{dE_i}{dx} \qquad \text{Eq. A2.10}$$

The energy bands of the semiconductor bend near the surface to accommodate the accumulation of electrons. Since $N_d = n_0 = n_i e^{(E_F - E_i)/kT}$ it is clear that an increase in electron concentration implies an increase in E_F -E_i at the semiconductor surface. Since there is no current passes through this structure (i.e. resemble to MOS structure), there can be no variation in the Fermi level within the semiconductor. therefore, if E_F -E_i is to increase, it must be occur by E_i moving down in energy near the surface.

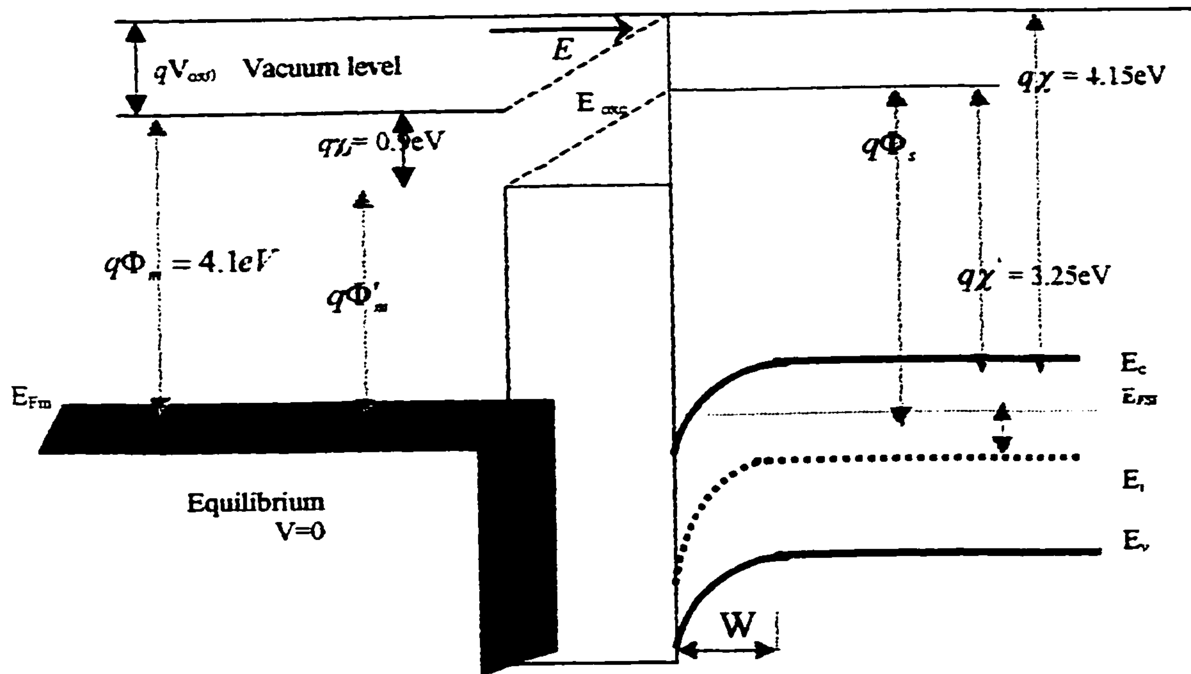

Fig.A2.11 Energy levels of metal-oxide-semiconductor structure in thermal equilibrium after contact.

The result is a bending of the semiconductor bands near the interface. We notice in Fig.A2.12 that Fermi level near the interface lies closer to the conduction band, indicating a large electron concentration than that arising from the doping of the n-type semiconductor. If a positive voltage applied to n-type *Si* as shown in Fig.A2.13. This raises the potential of the metal, lowering the metal Fermi level by qV relative to its equilibrium position. As a result, the oxide conduction band is again tilted.

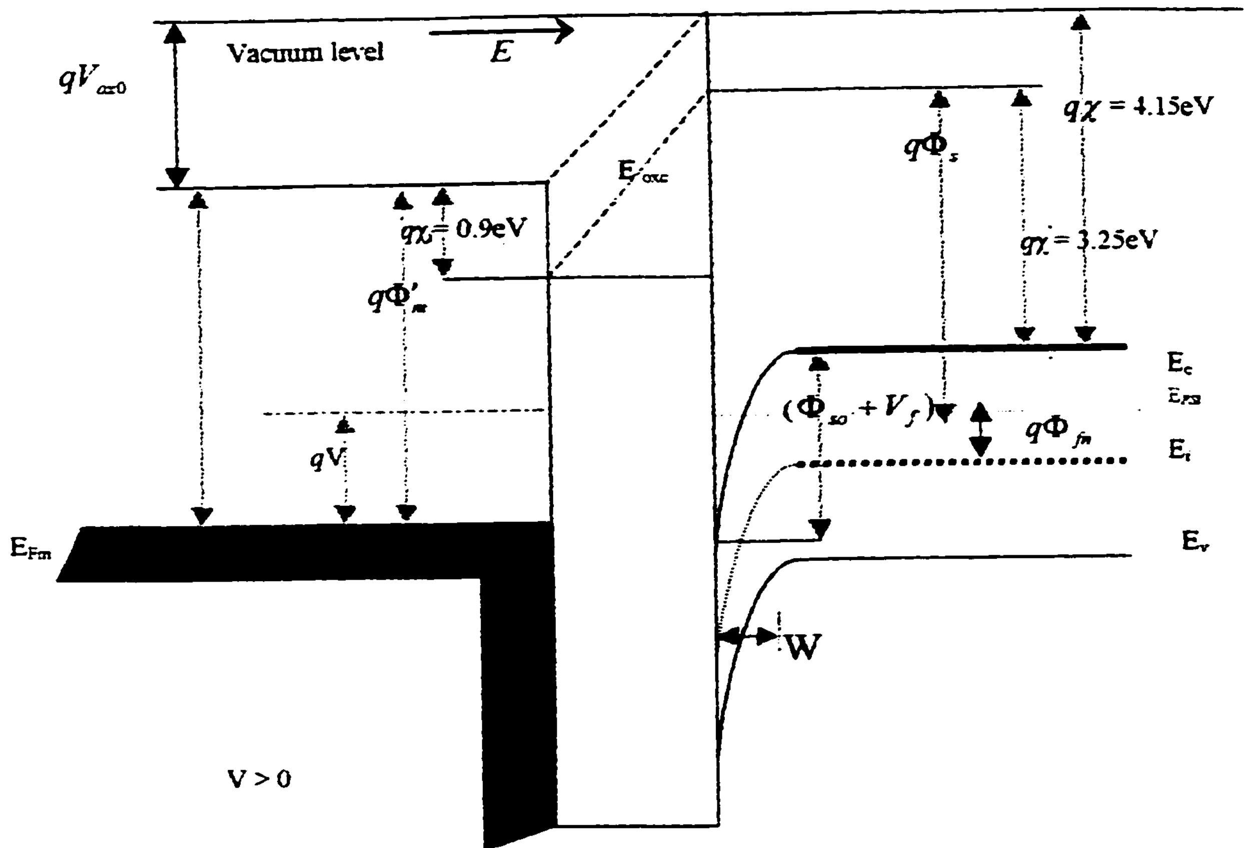

Fig.A2.12 The Energy-band diagram of the metal-oxide-semiconductor structure with n-type substrate for a negative voltage applied to n-type (cathodic bias).

We notice that the slope of this band, obtained simply by moving the metal side up relative to the semiconductor side, is in the proper direction for the applied field, according to Eq.A2.10

$$E(x) = \frac{1}{q}\frac{dE_i}{dx}$$

The positive voltage deposits negative charge on the metal and calls for a corresponding net positive charge at the surface of the semiconductor. such a positive charge in n-type material arises from *depletion* of electrons from the region near the

surface, leaving behind uncompensated ionized donors. In the depleted region the electron concentration decreases, moving E_i closer to E_F and bending the band up near the semiconductor surface.

If we continue to increase the positive voltage to n-type, the bands at the semiconductor surface bend up more strongly. In fact, a sufficiently large positive voltage on n-type can bend E_i *over* E_F as shown in Fig.A2.14.

This is a particularly interesting case, since $E_i >> E_F$ implies a large "hole" concentration in the valence band. In Fig.A2.10 we defined Φ_{s0} at any point x, measured relative to the equilibrium position of E_i. The energy $q\Phi_{s0}$ tells us the extent of band bending at x, and $q\Phi_{s0}$ represents the band bending at the surface.

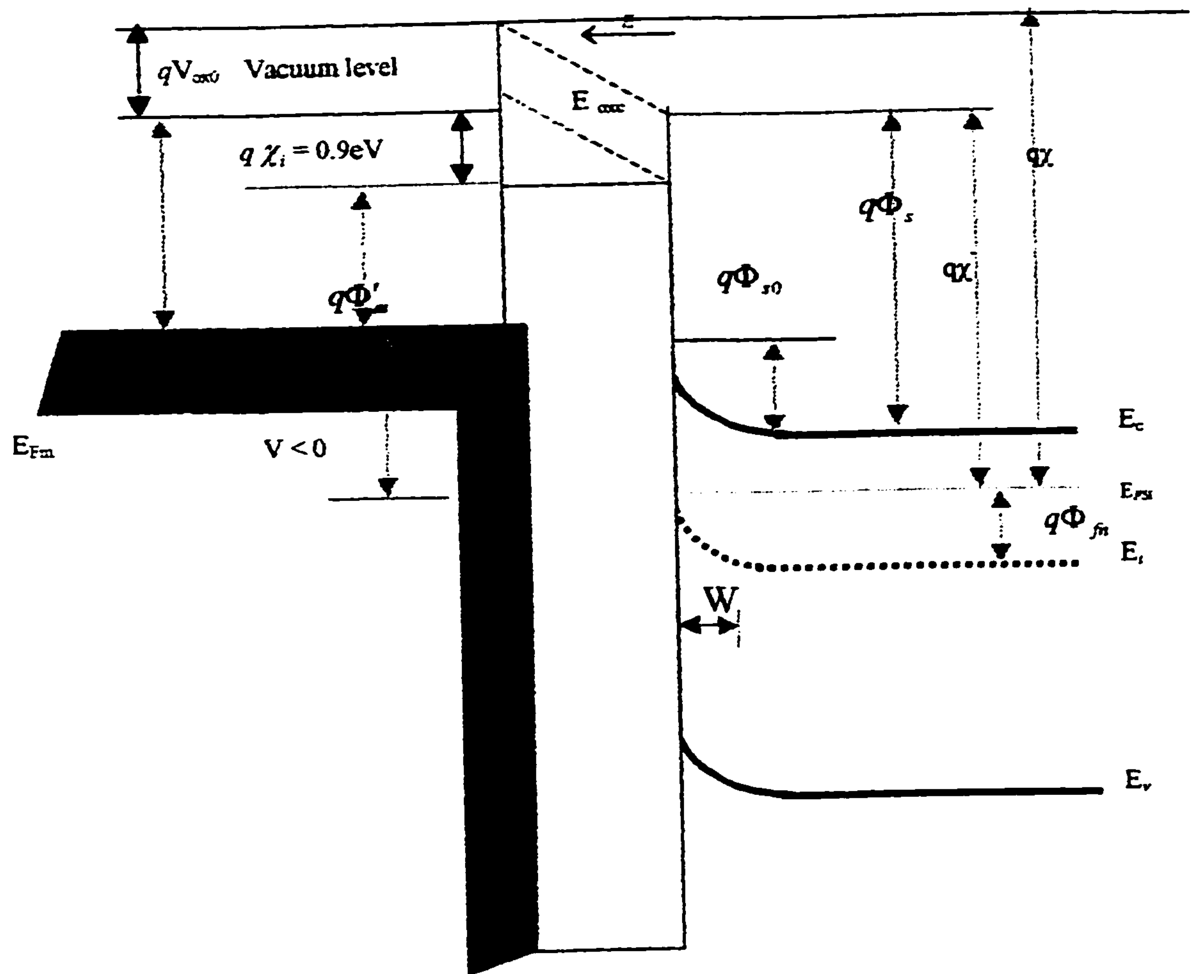

Fig.A2.13 The Energy-band diagram of the metal-oxide-semiconductor structure with n-type substrate for a positive voltage applied to n-type (anodic bias)

We notice that $q\Phi_{s0} = 0$ is the *flat band* condition for this ideal MOS case as shown in Fig.A2.15. When $q\Phi_{s0} > 0$, the bands bend down at the surface, and we have electron accumulation as shown in Fig.A2.12. Similarly, when $q\Phi_{s0} < 0$, we have depletion Fig.A2.13. Finally, when $q\Phi_{s0} << 0$ and larger than $q\Phi_{fn}$ the bands at the surface are bent up such that $E_i(x=0)$ lies above E_F, and inversion layer is obtained as shown in Fig.A2.14.

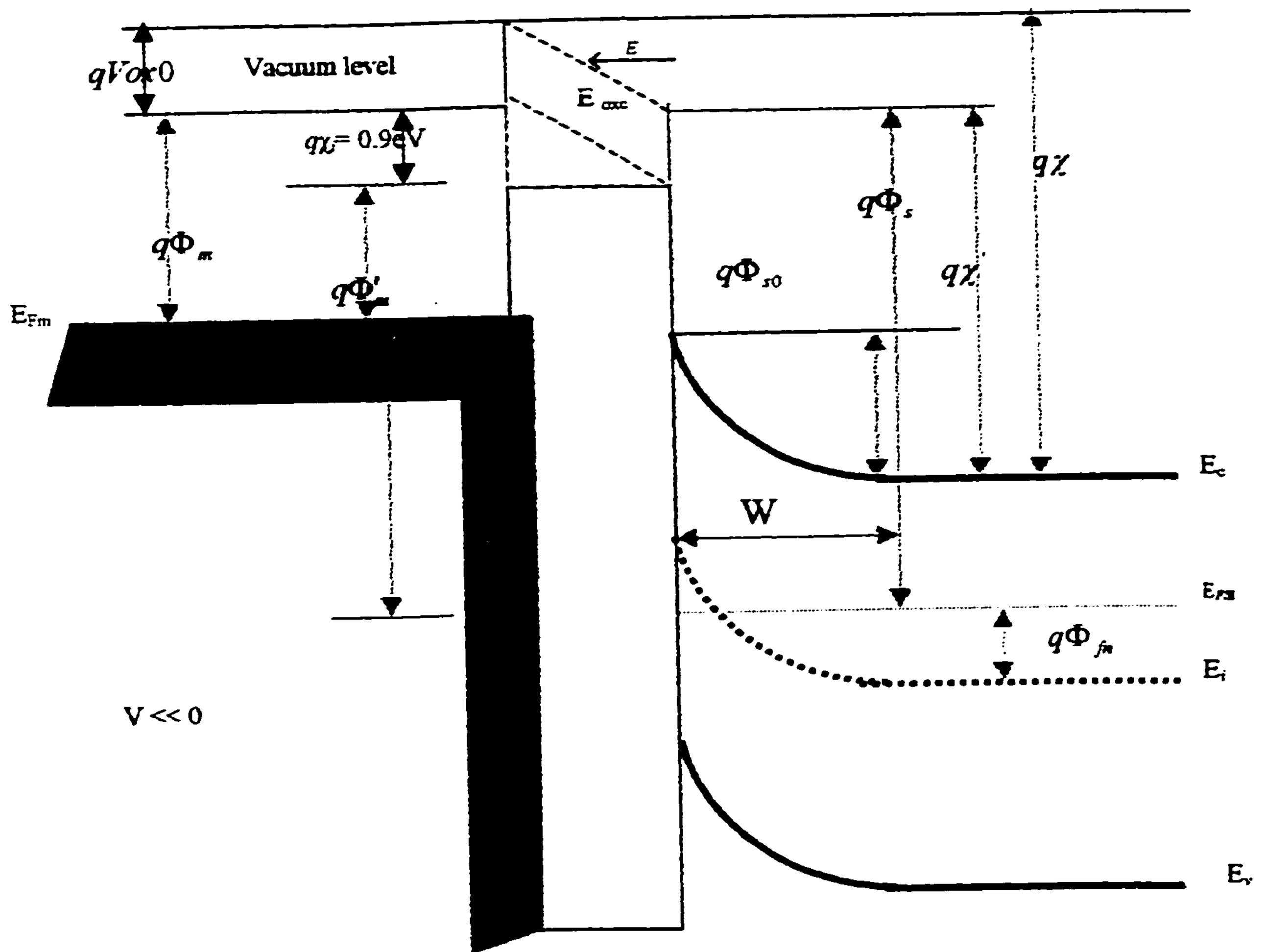

Fig.A2.14 The Energy-band diagram of the metal-oxide-semiconductor structure with n-type substrate for a "large" positive voltage applied to n-type (anodic bias).

The space charge width can be written in a form similar to that of a one-sided p-n junction

$$x_d = \left\{ \frac{2\varepsilon_s \Phi_{s0}}{eN_d} \right\}^{1/2} \qquad \text{Eq.A2.11}$$

at equilibrium

$$q\Phi_{s0} = -0.253v \qquad W = x_d = \left\{ \frac{2(11.7)(8.85\times10^{-14})(0.253)}{(1.6\times10^{-19})(10^{16})} \right\}^{1/2} = 0.181\mu m$$

and the maximum space charge width, x_{dT} at the inversion transition point can be calculated from Eq.A2.11 by setting $q\Phi_{s0} = \Phi_{fn}$

$$x_{dT} = \left\{ \frac{4\varepsilon_s \Phi_{fn}}{qN_d} \right\}^{1/2} \qquad \text{Eq.A2.12}$$

$$x_{dT} = \left\{ \frac{4(11.7)(8.85\times10^{-14})(0.347)}{(1.6\times10^{-19})(10^{16})} \right\}^{1/2} = 0.30\mu m .$$

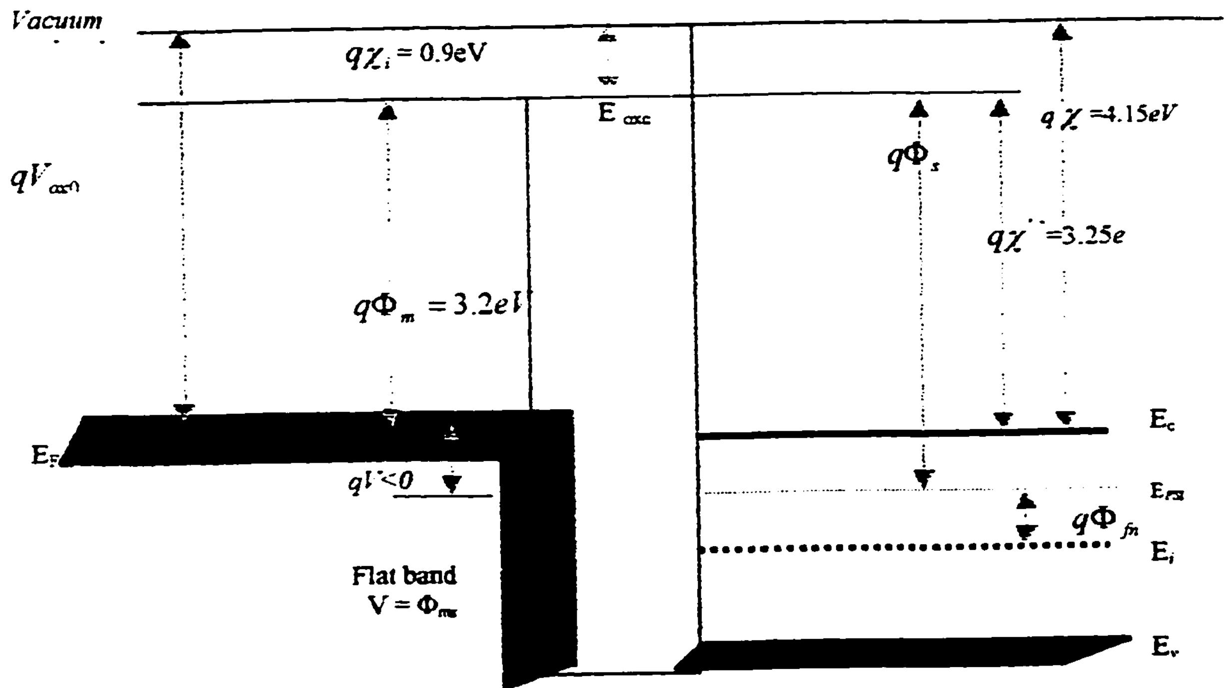

Fig.A2.15 Energy-band diagram of the metal-oxide-semiconductor structure at Flat band.

A2.5 Band Analysis in Equilibrium Electrochemical Context.

The energy band diagram at the electrode-solution interface associated with different applied voltages provides insight into the etch-stop mechanism. Fig.A2.4 and Fig.A2.11 show the n-type band diagram for Al/Si and Al/SiO_2/Si structures after contact, and before they have got inside the solution, respectively. When the structures dunk in the solution, at this point the Fermi level of the Al/Si and Al/SiO_2/Si (F_{ms} and F'_{ms}, respectively) align with the redox level in the solution, as depicted in Fig.A2.16 and Fig.A2.17, respectively. On the side of the electrolyte the main reactants are hydroxide ions and water molecules [36].Palik *et al* suggested [35,36,37] as well Seidel *et al* proposed [37] that the redox couple H_2O/OH^-, plays a key role in the reaction. At zero *pH* this couple is defined as the *normal hydrogen electrode (NHE)*. In semiconductor electrochemistry, a value of $E_{ref} = -4.5eV$ for *NHE*, as derived by Lohmann [55] is mostly used. A strong pH dependence has been found for most semiconductors. Especially in case of oxide semiconductors, the pH dependence has been measured quantitatively. Such experiments have yielded a shift of 0.059eV/pH as shown by various authors [27,55]. In other word, the potential; $E_{ref} = -4.5eV$ shifts towards more positive values by 0.059eV/pH [27]. Therefore, for *p*H around 11.6, used in this experiment (i.e. 5wt.% TMAH with dissolved Si 16.5g/l) an electrode potential of approximately $0.6844eV$ *vs.* NHE, amounting to $\Phi_{sol} = E_{SS} = -3.8156eV$ with respect to vacuum and as usual $\Phi_m < \Phi_s$, based on Fig.A2.3, where E_{ss} is the Al/Si structure/electrolyte barrier energy (i.e. $E_{ss} = E_{sol} - E_c$), and the *redox potential* (E_{redox}) represents the energy level associated

with the species in solution, and is analogous to a Fermi level inside the solution [26,27]. The energy bands of the silicon bends downward for both n-type and p-type, due to the injection of electrons from the solution into the silicon as it was illustrated in Eq.A2.13 and Eq.A2.14. The degree of the band bending is greater for the p-type than for the n-type silicon, due to the greater initial difference between Fermi levels of the electrolyte and the electrode [37]. The band diagram of Al/Si structure has different behavior inside the solution Fig.A2.16 shows this band diagrams clearly.

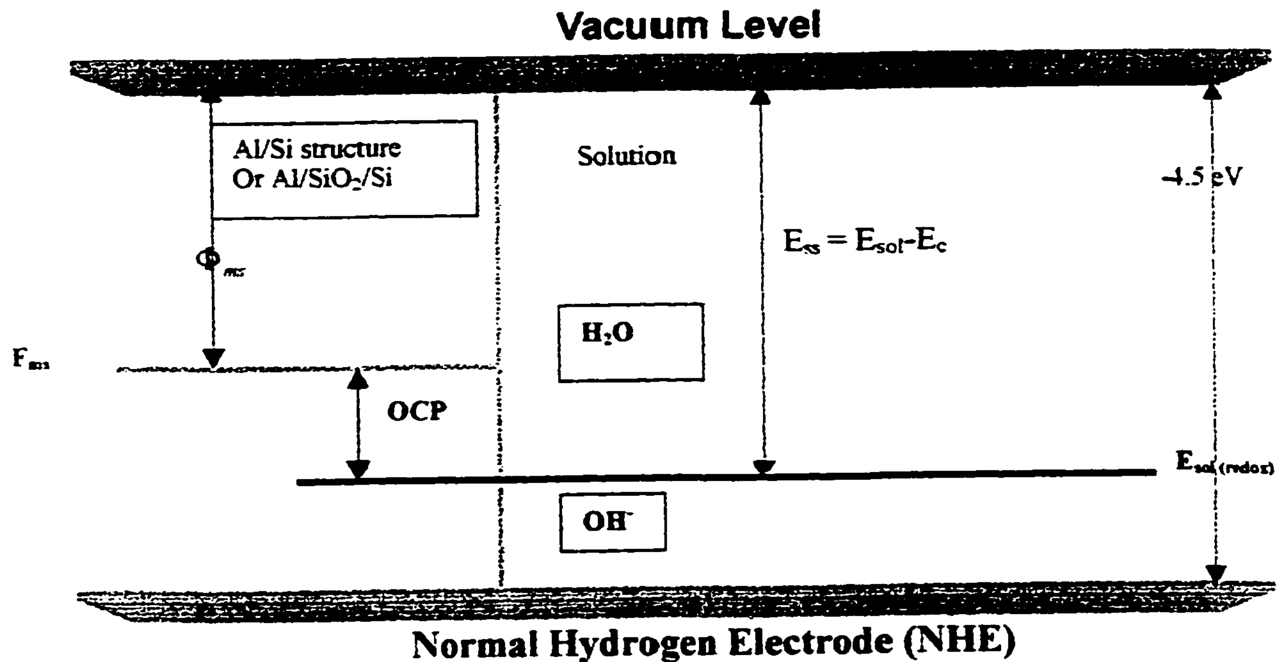

Fig.A2.16 The Combination the band Diagram of an Al/Si structure with the solution, the Fermi level of Al/Si (F_{ms}) separated with OCP vale from the redox level of the solution (E_{sol}).

If the potential of the silicon is raised relative to the solution (made more anodic). The "hole" concentration at the surface goes up, which corresponding to the situation at the Passivation Potential (PP), the associated energy band diagram is shown in Fig.A2.6 and Fig.A2.13, 14 for Al/Si and Al/SiO_2/Si structures, respectively. If a negative voltage is applied to the silicon relative to the solution (*cathodic bias*) a strong accumulation of electrons occurs in the conduction band. Then, electrons can flow from the Si electrode to solution via the OH^-/H_2O couple, the associated energy band diagram is shown in Fig.A2.5 and Fig.A2.12 for Al/Si and Al/SiO_2/Si structures, respectively. In the silicon crystal the electronic energy levels can be described in the usual way by the valence and the conduction band with gap of $1.1eV$. The position of the Fermi level depends on the dopant concentration, being above midgap for n-type and below midgap for p-type silicon. The electron affinity of silicon χ, which equivalent to the distance of the lower edge of the conduction band to the vacuum level, is 4.05 eV [16,17,32].

Palik and *et al* [31]proposed that on the side of the electrolyte the main reactants are hydroxide ions and water molecules {OH^-/H_2O}, therefore, the applied potential divides between the Si space-charge layer and the liquid Helmholtz layer. Helmholtz layer extremely important double layer in both semiconductor and metal electrochemistry, is consider to be formed between two planar sheets of charge. One is due to ions in solution attracted by the charge surface. The other is due to charge at the surface of the solid.[21]. The redox couple OH^-/H_2O, plays a key role in the reaction [31].

After immersion of the wafer into the electrolyte, the Fermi levels on both sides of the solid/liquid interface will be brought to the same level by a transfer of electrons from the electrolyte into the silicon crystal (i.e. OCP situation) as it was indicated in

Eqs.A2.13,14. This will lead to a downward bending of the conduction and valence bands which similar for n-type in both structures as indicated in Figs.A2.4,12 for Al/Si and Al/SiO_2/Si structures, respectively. The doping level in the semiconductor determines the extension of the resulting surface space charge layer [49].

The etching reaction *transfers electrons* from the OH^- into the Si surface bond (or the conduction band at the surface) and then to the etch products (no net current flow *"OCP"*). This sequence of charge transfer must be maintained in order for etching to continue. If the charge transfer sequence is broken, one expects the etching to stop. This may be accomplished in n-type silicon through a *cathodic bias* [4,31] when strong accumulation of electrons occurs in the conduction band. Then, electrons can flow from the Si electrode to solution via the OH^-/H_2O couple. Water, which would normally participate in etching, is electrolyzed to produce H_2 and current carrying OH^- through the reduction reaction Eq. A2.17. Also, OH^- ions cannot easily discharge electrons into the accumulated conduction band, owing to the relative positions of the redox Fermi level and the conduction-band edge at the surface. Both mechanism would decrease the etch rate. If an *anodic potential* is applied to n-type Si that raises the OH^-/H_2O level with respect to the conduction band, causing electron current to flow into the depleted conduction band of Si Eq.A2.16, presumably with some etching continuing. Eventually, the few thermal holes can fall into the filled redox state, causing some oxide to grow, stopping the etching, and drastically reducing the nearly saturated current at passivation. The etching and the etch stop based on an energy level approach, these ideas are illustrated in Fig.A2.4,5,6 and Fig.11,12,14 for Al/Si and Al/SiO_2/Si structures,

respectively, in terms of the Si conduction and bands, the redox couple level of OH^-/H_2O and the Fermi levels.

They are two voltage regions of importance to us, and they are separated by the passivation potential (PP). Just cathodic of the PP, the sample etches; while just anodic an oxide grows. For oxide-free surfaces, the OCP is always at more negative voltages than the PP. Another parameter which is very important in electrochemical reactions at semiconductor electrodes is the flatband potential (V_{FB}), the flatband potential of the n-type sample occurs at a voltage slightly cathodic of the PP. The flatband potentials have been determined for Si in 2*M* KOH [*1 molecule =1g/mol*], V_{FB}=-1.0 V (i.e. OCP= -1.2 V) for n-type [4,31]. From these numbers, Palik *et al* observed that flatband occurs between the OCP and the passivation potential (PP). Therefore, the n-type sample is in electron accumulation during etching and in depletion at oxide producing potential [4]. The flatband also determined for Al/Si and Al/SiO_2/Si structures in TMAH, V_{FB}=-0.85V and V_{FB}=-0.345, respectively (i.e. OCP =-1.6v) and this agreed with Palik's *et al* observations.

A2.6 The Chemical Reactions and Nernst Equation

Tetra-methyl ammonium hydroxide (TMAH); having the molecular formula $\{(CH_3)_4NOH\}$,was used a silicon etchant in this investigation, because it is less toxic alternative to other anisotropic etchant (i.e. KOH, EDP), safe to work with, stable for the range of temperature usually used. As an organic material it does not cause any metal ion contamination and it has high oxide, nitride and aluminum selectivity.

A2.6.1 Chemical reactions consideration

Potentiometric measurements are based on thermodynamics relationships and more particularly the Nernst equation, which relates to the concentration of the electroactive species. Several schemes of chemical reactions have been proposed by several authors [4] and experimental of Palik *et al* has revealed that OH^--groups play a key role in the chemical reaction [16,20].

At equilibrium; (OCP), based on Palik's *et al* suggestion [31], Seidel *et al* proposed that the reaction for silicon etching in aqueous alkaline solutions can be broken down into two separate steps [16,20]:

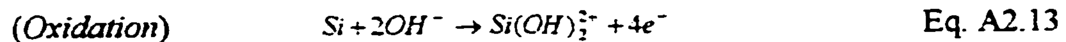

(*Oxidation*) $Si + 2OH^- \rightarrow Si(OH)_2^{2+} + 4e^-$ Eq. A2.13

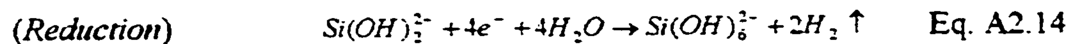

(*Reduction*) $Si(OH)_2^{2+} + 4e^- + 4H_2O \rightarrow Si(OH)_6^{2-} + 2H_2 \uparrow$ Eq. A2.14

In the first step, as shown in Eq.A2.13, electrons are injected into the conduction band of the Silicon as was shown in Fig.A2.6, 3.13. These are used in the reduction step Eq.A2.14. Hydrogen forms as a byproduct.

If a positive potential is applied to the silicon relative to the solution (made more anodic), the holes concentration at the surface goes up as was shown in Fig.A2.8,16, and this corresponding for the situation at the passivation potential (*PP*). The bias causes water molecules to electrolyze, and the resulting hydroxyl ions are attracted to the silicon surface, They then hydrolyze silicon atoms at the surface, which can be as shown in Eq.A2.15:

$$Si^{2+} + 2(OH^-) \rightarrow Si(OH)_2 \qquad \text{Eq.A2.15}$$

This silicon hydroxide slows the attack of the silicon surface by water molecules. Hydrogen gas is liberated from the $Si(OH)_2$, as shown in Eq.A2.16, which causes the formation of silicon dioxide, in the electrochemical etch stop, this oxide is referred to as an anodic oxide:

$$Si(OH)_2 \rightarrow SiO_2 + 2H_2 \uparrow \qquad \text{Eq.A2.16}$$

If a negative voltage applied to semiconductor relative to the solution (cathodic bias) a strong accumulation of electrons occurs in the conduction band as was shown in Fig.A2.7,14. Then, electrons can flow from the Si electrode to solution via the OH^-/H_2O couple. Water, which would normally participate in etching, is electrolyzed to produce H_2 and current carrying OH^- through the reduction reaction:

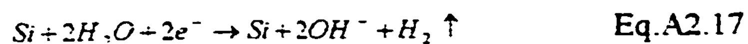

$$Si + 2H_2O + 2e^- \rightarrow Si + 2OH^- + H_2 \uparrow \qquad \text{Eq.A2.17}$$

Also, OH^- ions cannot easily discharge electrons into the accumulated conduction band, owing to the relative positions of the redox Fermi level and the conduction-band edge at the surface. Both mechanism would decrease the etch rate.

A2.6.2 Principles and Fundamental Relations

By considering the electrodes individually, the two electrode processes are easily combined to obtain the entire cell process, there are reduction processes with the oxidized species reduced by n electrons to give a reduce species:

$$ox + ne^- \rightarrow red$$

The general Nernst equation expression relates the half-cell potential to the effective concentrations of the redox couple is:

$$E_{cell} = E^{o} - \frac{RT}{nF}\ln\frac{[red]}{[ox]} = E^{o} + \frac{RT}{nF}\ln\frac{[ox]}{[red]}$$

$$E_{cell} = E^{o}_{red} - E^{o}_{ox} - \left\{\frac{2.303RT}{4f}\log K^{2}_{eq}K^{2}_{w} + \frac{(2.303)RT}{f}pH\right\} \qquad \text{Eq. A2.18}$$

Some conversion factors:

$1. f = 96500C/mole^{-} = 96500J/V$
$2. T(k^{o}) = T(C^{o}) + 273.15$
$3. \ln x = 2.303\log x$
$4. R = 8.3144 Jmol^{-1}K^{-1}$

Eq.A2.18 shows that E_{cell} depends on and works as a function of *p*H and T, as a matter of fact that, the *p*H is function of temperature more details will be later on.

According to what is mentioned above, the assumption of E_{ss} to be constant won't work any more, as an example in 25wt.% TMAH, for T= 42.9 °C , pH =14.38, E_{ss}= -3.65158eV with respect to NHE, and for T= 59.4 °C, pH =13.92, E_{ss}= -3.67872eV with respect to NHE, and for T = 80.1°C, pH =13.28, E_{ss}= -3.71648eV with respect to NHE, the difference between the E_{ss}'s schematically is shown in Fig.A2.17.

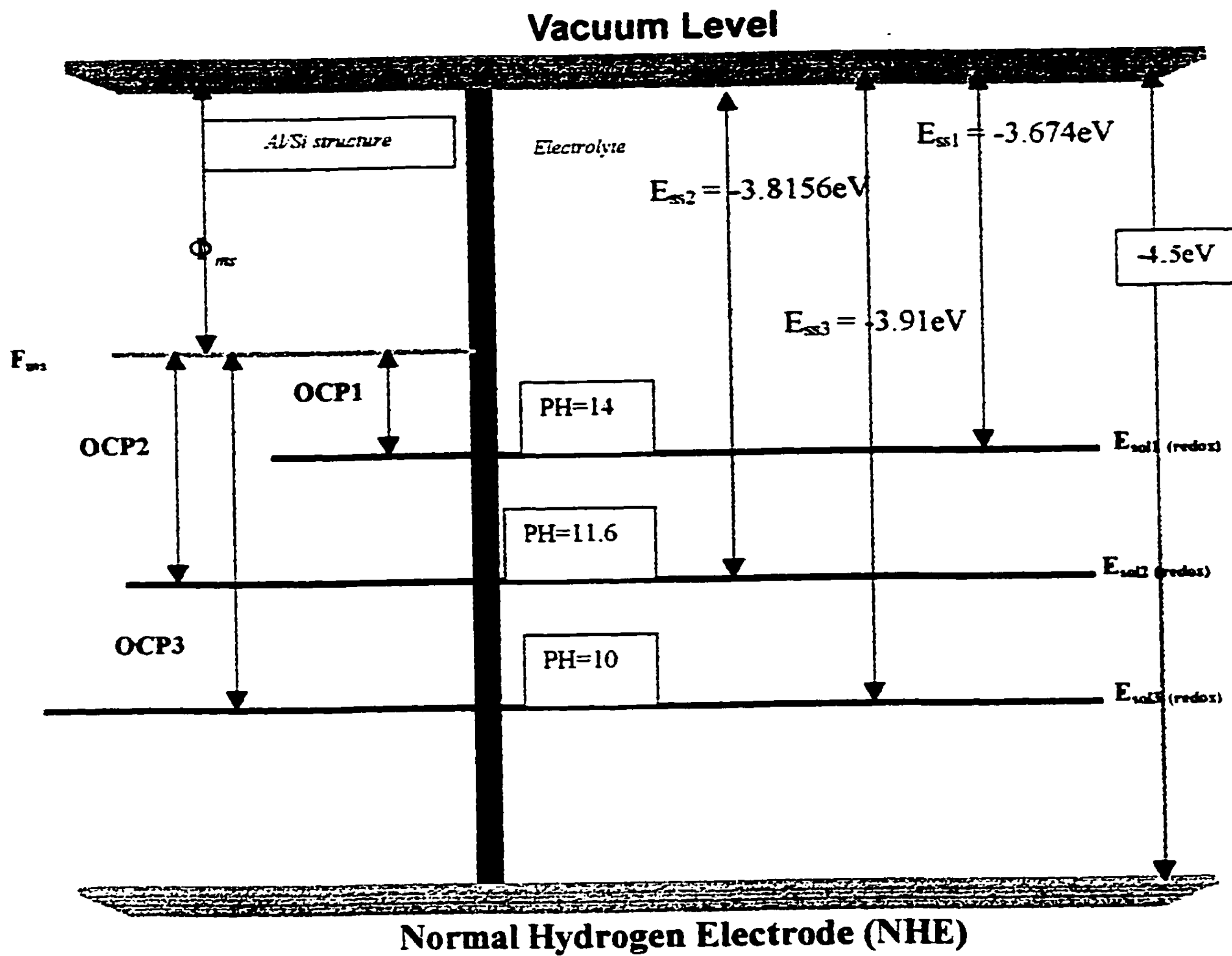

Fig.A2.17 The effect of the pH and T on the OCP and E_{ss}

A2.7 Nemirovsky Discussion: (Non-Equilibrium Electrochemistry)

The energy band diagram of silicon in contact with TMAH solution 25 wt.% was studied recently by Nemirovsky *al et* [9]. They have constructed the energy band

diagram for n-and p-type Si <100>, assuming that E_{ss} is constant and independent of the doping type and level. Fig.A2.18 shows the band diagrams of these models.

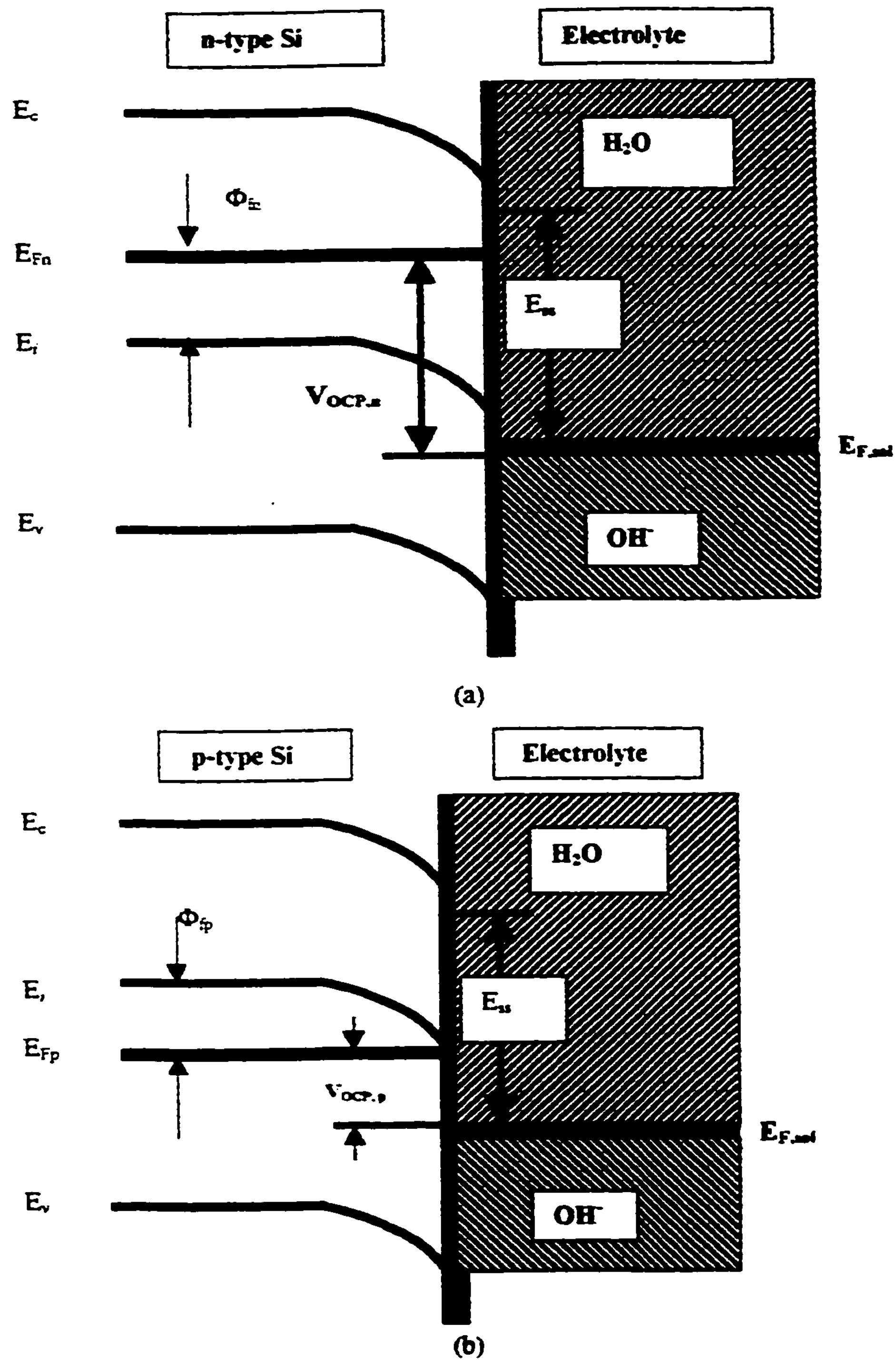

Fig.A2.18 The energy band diagrams that proposed by Nemirovsky (a) n-type Si (b) p-type Si. [9]

It s very useful to get a physical insight of the electrochemical etch process and its dependence upon doping level, type, temperature, illumination and the optimal design of electrochemical etch stop. This study was based on measured current-voltage characteristics, the capacitance-voltage characteristics and on the determination of the flat-band voltage from the measured total band bending at OCP, of both types of silicon (n-and p-type). They presented a new approach for the construction of the energy band of silicon in contact with anisotropic alkaline etch solutions. It emphasizes the non-equilibrium operation of the electrochemical cell even at OCP because two electrode reactions rather than a single electrode reaction occur at the OCP, i.e. the reduction reaction of the water and the oxidation of silicon. Which means that the Fermi level at OCP are not aligned at it was assumed by the previous researches [4,19,20]. The new model and the methodology that was presented by Nemirovsky *al et.*, is applicable to all the anisotropic alkaline etch solutions such as KOH and EDP.

A2.8 How The Energy Band Diagram Interact With OCP, pH and T?

The energy band diagram of the silicon is a useful tool for understanding the etching mechanism (i.e. OCP), and the effect of the experimental parameters (i.e. pH and T). After immersion the wafer into the electrolyte, the Fermi level on both sides of the silicon /electrolyte interface will not be brought to the same level, due to the non-equilibrium nature this system [9], even at the OCP. In contrast to the previous studied [20], the Fermi levels of the silicon and the electrolyte are not aligned at OCP. By definition, the potential value of the OCP is used to determine the separation between the two Fermi levels, and it is given by the following equations, for both types of silicon [9]:

$$V_{OCP_N} = E_{SS} + \phi_{SO_n} - \frac{E_g}{2} + \phi_{fn} \qquad \text{Eq.A2.19}$$

$$V_{OCP_P} = E_{SS} + \phi_{SO_p} - \frac{E_g}{2} + \phi_{fp} \qquad \text{Eq.A2.20}$$

Where, E_{SS} is the separated energy between the Fermi level of the electrolyte and the conduction band of the silicon (i.e. $E_{ss} = E_{sol} - E_c$), and which strongly dependant on pH as we will see later. $\phi_{so_n}, and \phi_{so_p}$ that represents the band bending at the surface, ϕ_{fn} and $\phi_{fp} = \frac{kT}{q} \ln \frac{N_{D,A}}{n_i}$ that measure the position of the Fermi level up or down the intrinsic level E_i for n-type and p-type silicon, respectively, by the fact that $n_i = \sqrt{N_c N_v e^{-E_g/2kT}}$ has a strong temperature dependence, therefore E_F can also vary with temperature, E_g is the Si band gap which also varies somewhat with temperature (i.e. E_g varies from about 1.11eV at 300 K to about 1.16 eV at 0 K). Base on these equations, one can notify that the OCP affects by a lot of parameters (i.e. *p*H, Temperature and dopant concentration...), and this effect will change certainly the construction of the energy band diagram of silicon in contact with TMAH solutions.

On the side of the electrolyte the main reactants are hydroxide ions and water molecules, the redox couple H_2O/OH^-, plays a key role in the reaction [20,30,31]. At zero *p*H this couple is defined as the normal hydrogen electrode (NHE) with a potential of -4.5 eV with respect to vacuum [54], this potential shifts towards more positive value by 59m eV/*p*H. For 25 wt.% TMAH at 21.1 °C *p*H range around 15.57, used in our experiments, an electrode potential is expected of approximately 0.92 eV *vs.* NHE, amounting to −3.58

eV with respect to the vacuum. So the variation of pH means altering the solution buffer capacity; buffer anions can alter the structure of the interface, such

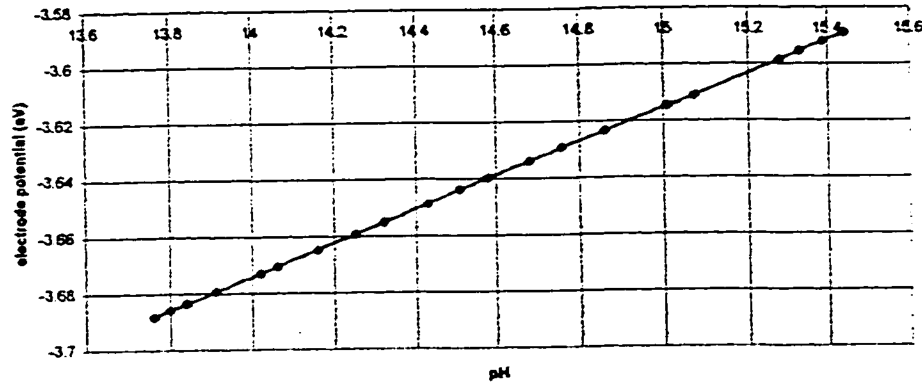

Fig.A2.19 The electrolyte potential with respect to vacuum *vs.* the variation of pH.(25 wt.% TMAH, p-type Si)

criteria must be taken carefully into consideration when proposing and discriminating between mechanisms. Fig.A2.19 illustrates the electrolyte potential with respect to vacuum *vs.* the variation of pH.

A2.9 Conclusions

The construction of the energy band diagram of pure silicon (i.e. n-type and p-type) was discussed, and the OCP definition also was given (i.e. Eq.A2.19 and Eq.A2.20, respectively), and the effect the experimental parameters including pH, temperature, and doping concentrations have elaborated in details. The Si/Al and Si/SiO_2/Al construction have the same behavior, except one parameter will change. For the pure silicon a work function of the silicon was used $\Phi_{Si} = 4.05eV$ [20,49], where the work function of Si/Al given by $\Phi_{ms} = V_{bi} = V_0 = \frac{kT}{q}\ln\frac{N_a N_d}{n_i^2}$ and the metal -semiconductor work function difference of the Si/SiO_2/Al is given by $q\Phi_{ms} = \left[\Phi'_m - \left(\chi' + \frac{E_g}{2e} - \Phi_{fn}\right)\right]$ [50]. Since the

work function does not change with applied potential, moving the Fermi level down or up (i.e. n-type and p-type respectively). Consequently, the V_{OCP} in Eq.A2.19 and Eq.A2.20 for n-type and p-type respectively, will change because of the total band bending at OCP (i.e. ϕ_{s0_n} and ϕ_{s0_p}) will change, too.

This Appendix includes a compendium of well-known ideas and others' research. The integrated summary of these facts is a useful contribution toward the understanding of the electrochemical aspects of anisotropic etching, and serves as a foundation for the design of experiments in Appendix 3 and Chapter 3, and interpretation of experimental data in Chapter 4. Based on the analyses in this chapter, it is sensible to assume that the electrochemical behavior will vary with sample geometry, and will vary depending on which structures are immersed in the solution.

APPENDIX 3

PILOT TESTS:

LINEAR-SWEEP-VOLTAMMETRY (LSV) TESTS

A3.1 INTRODUCTION

These experiments aim to explore the behavior of several sample configurations of Al/SiO_2/Si in TMAH etchant. Electrochemical linear sweep voltammetry (LSV) measurements are done, and the curves are examined to find the open-circuit potential (OCP) and passivation potential (PP).

A3.2 SAMPLE CONFIGURATIONS

Several sample configurations were used; table A3.1 will illustrate in details these configurations:

Table A3. 1 Sample Configurations

Code	Sample ID	The Front Description	The Back Description	The etchant
FsiBsi	N2	Open Si	open Si	5wt% TMAH dissolved Si
FsiAsiBsi	N4	Al in contact with Si	open Si	5wt% TMAH dissolved Si
FsiBsi	P7	Si	open Si	5wt% TMAH dissolved Si
FsiAsiBsi	P9	Al in contact with Si	open Si	5wt% TMAH dissolved Si
FsiBsi	NE0	Open Si	Open Si	25wt% TMAH
FsiBsi	NE1	Open Si	Open Si	5wt% TMAH
FsiBsi	NE2	Open Si	Open Si	5wt% TMAH dissolved Si
FoxAsiBsi	S2	Al in contact with SiO_2&Si	open Si	5wt% TMAH dissolved Si
FoxAoxBsi	S5	Al in contact with SiO_2	open Si	5wt% TMAH dissolved Si
FoxAoxBox	S9	Al in contact with SiO_2	covered with SiO_2	5wt% TMAH dissolved Si
FoxAsiBox	S10	Al in contact with SiO_2&Si	Covered with SiO_2	5wt% TMAH dissolved Si

A3.3 SAMPLE PREPARATION PROCEDURES.

1. The starting silicon wafer with 4" diameter n-type and p-type {100}-oriented, thickness 500-550 μm, and phosphorous-doped (ρ=10-30 Ω.cm) and boron-doped (ρ=20-40 Ω.cm), respectively, were used.
2. Cut the samples into pieces roughly 2in by 2in. (See Fig. A3.1(a)).
3. Clean using the following steps:
   - 1:1 H_2SO_4:H_2O_2 ratio, 5 minutes on hot plate, boiling. Then rinse in DI water.
   - 1:1:5 HCl:H_2O_2:H_2O ratio, 5 minutes on hot plate, boiling. Then rinse in DI water.
   - 1:1:5 NH_4OH:H_2O_2:H_2O ratio, in room temperature for 5 minutes.
   - 1:50 dilute HF:H_2O, ratio, dip for 30-60 seconds. Then rinse in DI water.
   - Dry the sample by blowing N_2.
4. Thermal oxidation to create material for etch mask, on both top and bottom of the pieces: 7.5 hrs in wet O_2 at T=1100 °C, to grow approximately 2 μm.(see Fig. A3.1(b)).

$$t_{ox} = \frac{x_o^2}{B} + \frac{x_o}{B/A},$$

$$B \equiv Parabolic_rate_constant = 0.6 \mu m^2 / hr @ T = 1100^o C, wetoxidation$$

$$B / A \equiv Linear_rate_constant = 2.441 \mu m / hr @ 1100^o C, wetoxidation$$

5. Spin photoresist on backside (backside first, that will be more protected to the front side and not harm at all), at 5000 RPM for 20-30 sec at room temperature.
6. Bake at 95 °C for 10 minutes.
7. Spin positive photoresist (Microposit, 1350J, Shipley, USA) on front side at 5000 RPM for 20-30 sec at room temperature. (See Fig. A3.1(c)).
8. Expose photoresist on front side through first mask.

- for FsiBsi, no Al in contact with silicon, use mask pattern Fig. A3.2(a1).
- for FsiAsiBsi, Al in contact with silicon, use mask pattern Fig. A3.2(b1).
- for FoxAsiBsi, Al in contact with silicon, use mask pattern Fig. A3.2(b1).
- for FoxAoxBox, Al in contact with silicon, use mask pattern Fig. A3.2(b1).

9. Expose photoresist on backside through second mask.
   - For FsiBsi, no Al in contact with silicon, use mask pattern Fig. A3.2(a2).
   - For FsiAsiBsi, Al in contact with silicon, use mask pattern Fig. A3.2(a2).
   - For FoxAsiBsi, Al in contact with silicon, use mask pattern Fig. A3.2(a2).
   - For FoxAoxBox, Al in contact with silicon, use mask pattern Fig. A3.2(a2).

10. Develop (Microposit 352, Shipley, MA. USA).

11. Postbake at 115 °C for 20 mins.

12. Etch un-covered SiO_2 in buffered HF (i.e. BHF), a mixture of 1 part 49% aqueous HF and 7 parts NH_4F, to selectively etch the SiO_2, and not the Si or the photoresist. In this step, the wafer is dipped until the un-covered areas are hydrophobic (both front and backsides are etched simultaneously). (See Fig. A3.1(d)).

13. Strip photoresist in acetone, 10-25 sec.

14. Spin positive photoresist on front side at 5000 RPM for 20-30 sec at room temperature, in preparation for Al liftoff step.

15. Expose photoresist on front side through third mask.
   - for FsiBsi, no Al in contact with silicon, use mask pattern Fig. A3.2(a3).
   - for FsiAsiBsi, Al in contact with silicon, use mask pattern Fig. A3.2(b3).
   - for FoxAsiBsi, Al in contact with silicon, use mask pattern Fig. A3.2(b3).
   - for FoxAoxBox, Al in contact with silicon, use mask pattern Fig. A3.2(b3).

16. Develop.

17. Postbake at 115 °C for 20 mins. (See Fig. A3.1(e)).

18. Place into Al evaporator (Edwards, Auto 306), and deposit Al on the front side. This deposits Al over the top of the photoresist, and contacts the Si or SiO_2 where there is no photoresist.

19. Remove from Al evaporator, and remove photoresist and the unwanted Al by immersing in hot acetone for awhile (i.e. to be sure that the wafer became clean). (See Fig. A3.1(f)).

20. Place the samples once more into Al evaporator, and deposit Al on the backside for ohmic contact.

21. Remove from Al evaporator, and remove photoresist and the unwanted Al by immersing in hot acetone for awhile (i.e. to be sure that the wafer became clean). (See Fig. A3.1(f)).

22. Apply phosphorous gel for n-type sample and boronsilicate gel for p-type, then insert the samples in the furnace for 2.5 hr at 1100 °C.

23. Apply silver paste (i.e. H20E, part A, and H20E part B hardener) to the backside Al contact area. Care was taken to ensure that the backside Al was completely covered with.

24. Apply epoxy patch (Hysol Engineering Adhesives) to connect Pt wire to the backside contact Care was taken to ensure that the backside Al was completely covered with.

25. Ready for electrochemical LSV experiments.

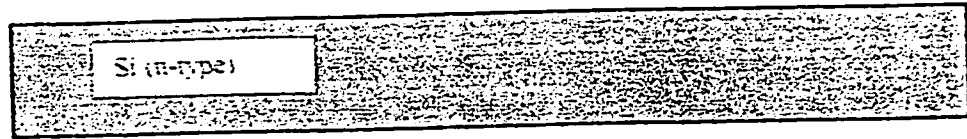

(a)

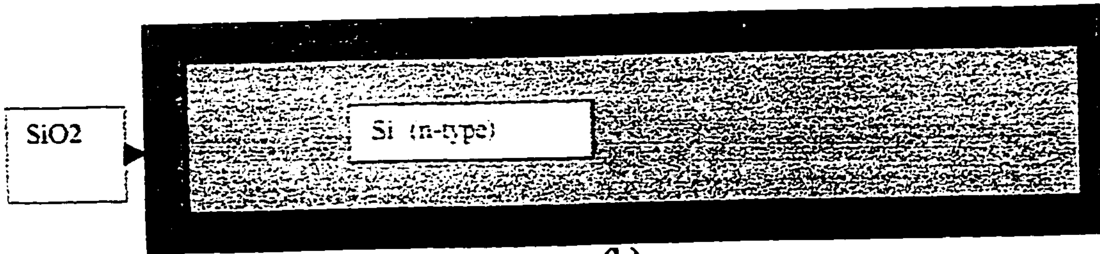

(b)

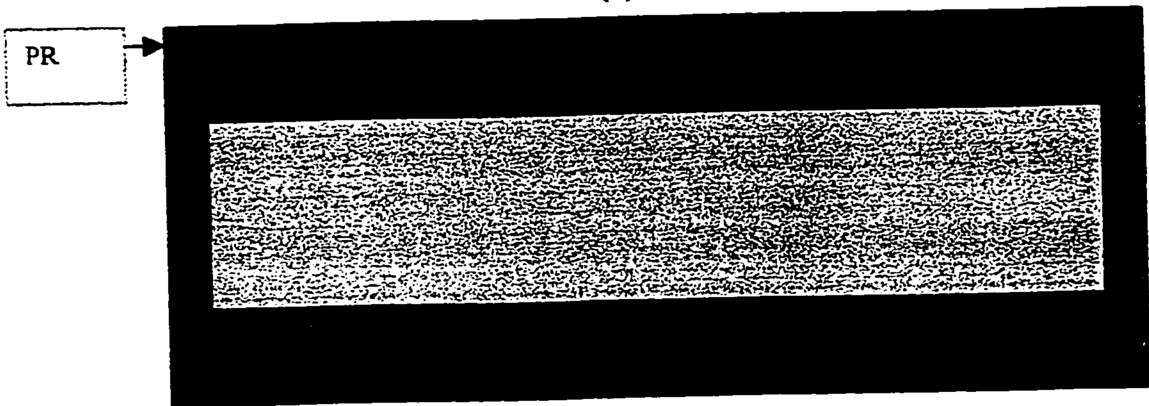

(c)

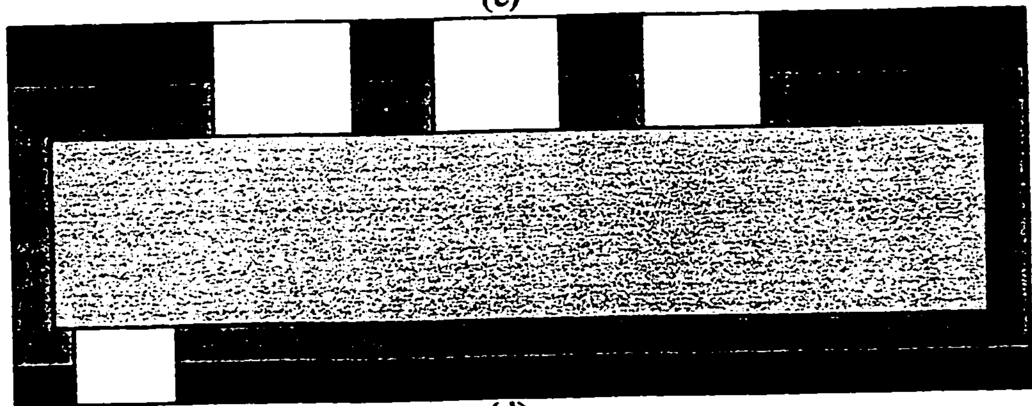

(d)

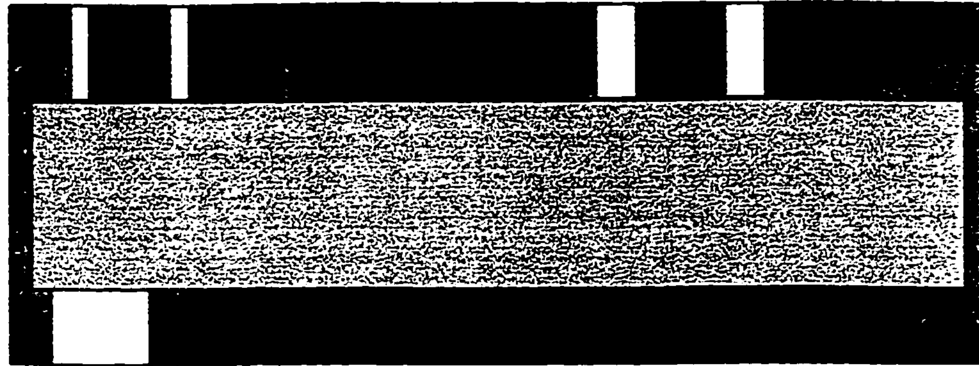

(e)

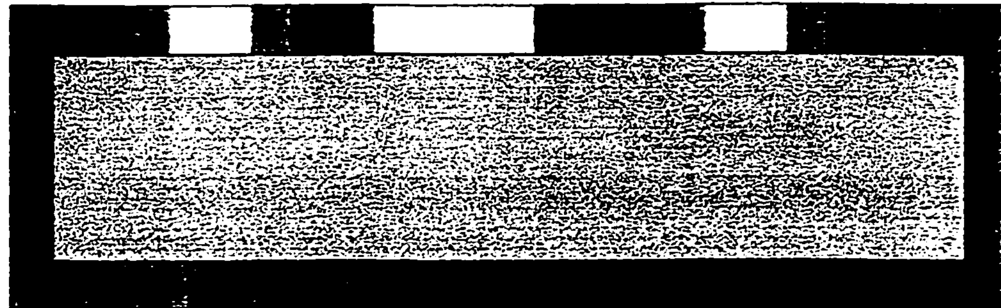

(f)

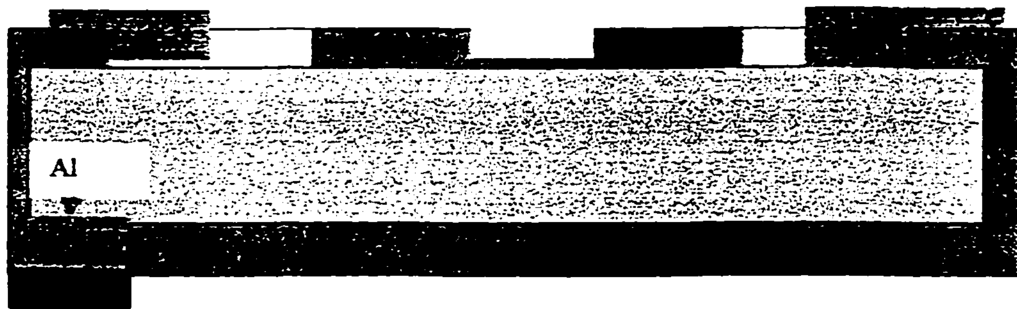

Pt

(g)

Fig.A3.1 Process steps, for the samples that Aluminum deposit over silicon and the samples that aluminum deposit over silicon and silicon oxide.

(a1)

(b1)

(a2)

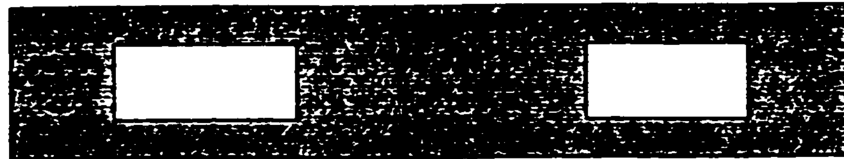

(a3)

(b3)

Fig.A3.2 The mask diagrams: (a1) for the front side of the structures code FsiBsi, (b1) for the front side structures code FoxAoxBsi and FoxAsiBox (a2) for backside of the structures to define Al contact area (a3) for the front side structures code FoxAsiBsi and FoxAsiBox where the Al in contact with SiO_2&Si, and (b3) for the front side structures code FoxAoxBsi and FoxAoxBox where the Al in contact with SiO_2.

A3.4 EXPERIMENTAL PROCEDURE.

The experimental samples were prepared in 11 different sample configurations as outlined in sections A3.2 and A3.3. For all the experiments, commercially available tetra-methyl ammonium hydroxide (TMAH) $\{(CH_3)_4NOH\}$ at 25wt% was used (purchased from Moses Lake Industries INC., USA) Lower concentrations were obtained by diluting the TMAH with DI water.

When it was intended to passivate Al by the method of dissolving silicon in the etchant [44], low concentration (5wt%) TMAH was used, because the amount of dissolved silicon needed to passivate the aluminum increases roughly proportionally with the TMAH concentration, according to Fig A3.3. Also, the etch rate of silicon is at a maximum near 5wt% TMAH [56]. In 5wt% TMAH, 16.5g/l of powdered silicon (polycrystalline silicon powder, Pro. No. 267414, Sigma-Aldrich, ON. Canada) was dissolved gradually into the solution at 45 °C, prior to the LSV experiments. This technique has been reported to passivate Al during etching of silicon, by producing silicates in the solution [44], and by lowering the pH of the solution [3].

All of these experiments were carried out in a glass vessel with a reflux condenser under typical laboratory illumination. The solutions were not stirred during the experiments, and the temperature was held at 80 °C with ± 1°C accuracy, by a thermometer. The working electrode and the reference electrode were connected to the potentiostat (model SR930 DSP lock-in Amplifier, manufacturer SRS, USA. The entire system controlled by

a software call echem; cyclic voltammetry program, IEEE HP 488 manufacturer in USA. As shown in Fig. A3.4.

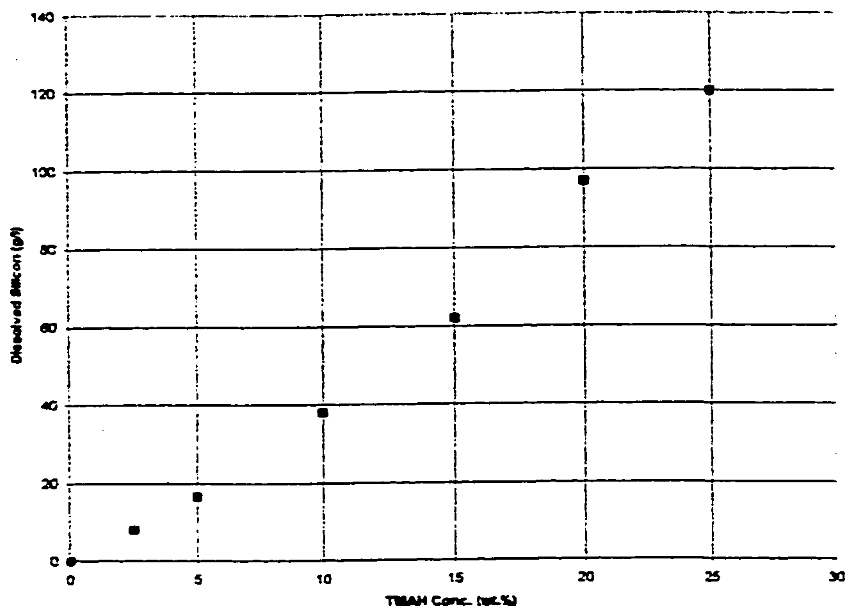

Fig.A3.3 The amount of dissolved silicon required to passivate exposed aluminum for various TMAH concentrations.[56]

Immediately prior to immersion in the TMAH for a LSV experiment, each sample was dipped into dilute (1:50) HF solution at room temperature, to remove native oxide, and rinsed in DI water. The pH value was monitored continuously by a standard pH electrode with temperature compensation. After immersion in the TMAH, the electrodes were connected, and the LSV experiment initiated.

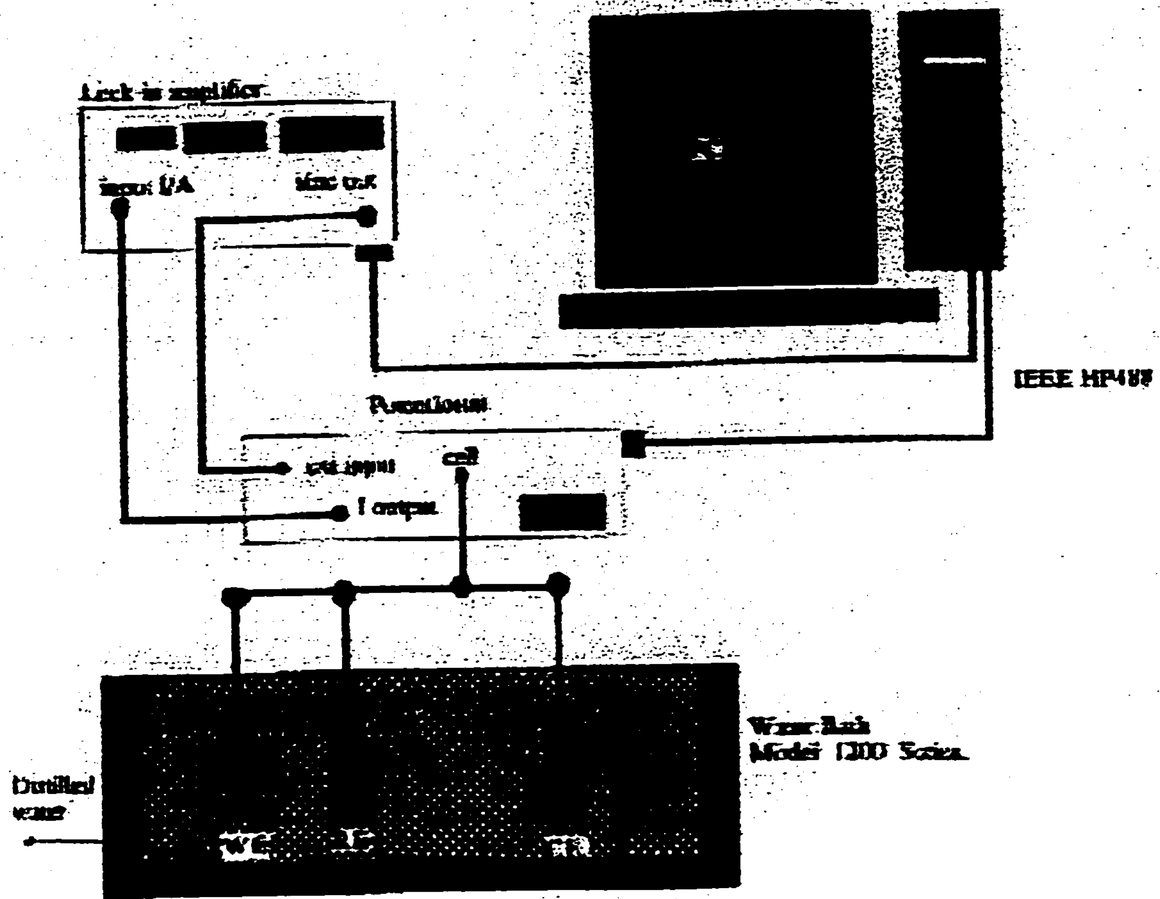

Fig.A3.4 The experimental setup for the electrochemical technique.

A3.5 LINEAR SWEEP VOLTAMMETRY (LSV) MEASUREMENT TECHNIQUE.

A potentiostat was used to control the electrode potentials, working-electrode (WE), counter-electrode (CE), and reference-electrode (RE), as schematically shown in Fig. A3.5.

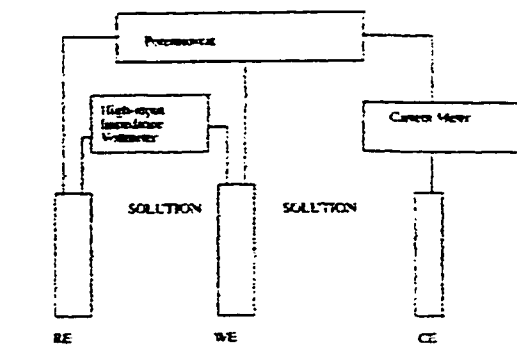

Fig.A3.5 Circuit diagram for potentiostatic measurements.[51]

The potentiostat drives currents into the CE, such that the potential between the RE and the working electrode is brought to the desired value. The CE is made of an electrochemically inert material, Pt. In these experiments the RE is Ag/AgCl, selected because it maintains relatively stable interfacial potentials over varying current densities[44,45]. The RE draws no current, since it is connected to the high-impedance input of the op-amp shown in Fig.A3.6. This electrode is situated as close as possible to the WE, in order to minimize potential drops in the solution. Note that in this circuit, there are two relevant electrical "ground" points: the potentiostat system ground, which is connected to the WE, and the solution reference potential, the RE. The general set-up for these measurements is shown in Fig. A3.4.

The principles and operation of the potentiostat are explained further in Appendix 1. The LSV measurements were done using potentiostat model SR830 DSP lock-in amplifier, manufacturer SRS, USA. The potential between the WE and RE is swept from negative to positive, with scan rate of 5mV/s, to generate *I-V* curves. A typical plot of current density vs. applied potential is shown in Fig.A3.7. Such a graph indicate three particularly important potentials [4], the open-circuit potential (OCP), the passivation

potential (PP), and the oxide-formation potential (OFP). The open-circuit potential (OCP), is the potential on the WE when there is no net current flow. This is not a thermal equilibrium, but is a steady-state [9] of electrochemical processes between the WE and electrolyte, such that $I = 0$ mA.

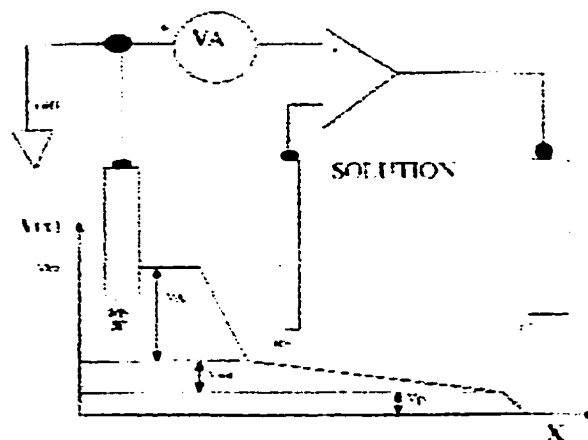

Fig.A3.6 Potential drops in the circuit with the potentiostat no longer matter, as the reference electrode draws no current.[44]

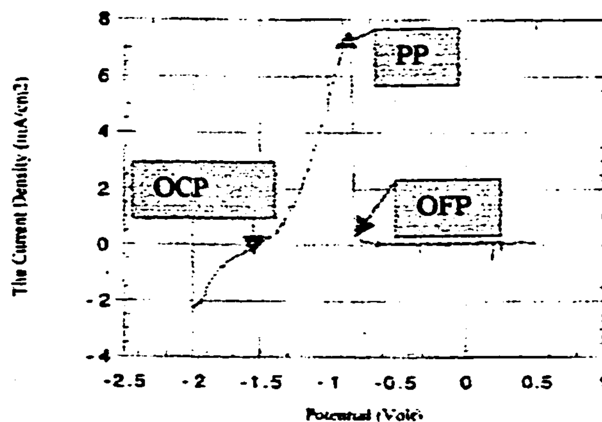

Fig.A3.7 *I-V* characteristics of n-type Si in TMAH 5 wt.% at 80 ^{o}C. the potential is relative to Ag/AgCl reference electrode. The exact magnitude of the current profile depends on the working electrode area.

At this potential, the etch rate is usually at or near its maximum value [4], and decreases at more anodic or cathodic potentials. At the passivation potential (PP), the electrode current begins to drop, and the etch process is more and more inhibited for potentials more positive (more anodic). At the oxide formation potential, the etching is stopped.

A3.6 RESULTS.

Fig.A3.8 compares LSV curves for different mixtures of TMAH, n-type samples with very similar structure and patterning, structure FSiBSi, were used in LSV experiments with the following TMAH mixtures:

- 25wt% TMAH pH = 13.4 at temperature 80 °C
- 5wt% TMAH pH = 12.4 at temperature 80 °C
- 5wt% TMAH with 16.5g/l dissolved silicon pH = 11.7 at temperature 80 °C.

Fig.A3.8 Current-voltage characteristics of (100) n-type silicon for different concentrations of TMAH (25 wt.% TMAH, 5 wt.% TMAH, and 5 wt.% TMAH with dissolved silicon) at 80 °C.

The PP is seen to be more negative when the pH is low. Table A3.2 will illustrate and summarize the cases, structures, type, pH, area and some other experimental results, and it will show the number of the figures for each case. The scan rate was (SR) 5 mV/s and the sweep applied potential was from –2 volt to + 0.5 volt, through all of the experiments.

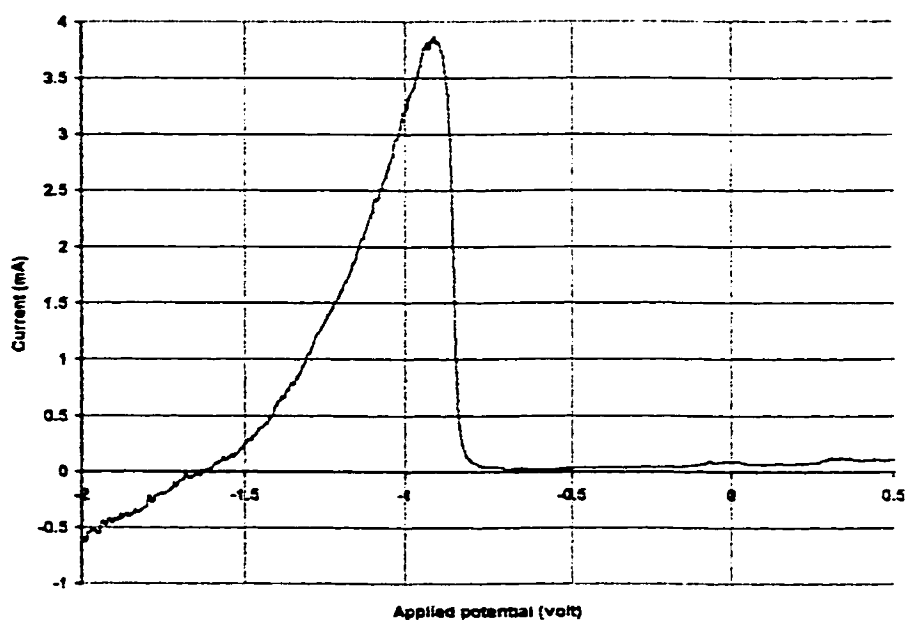

Fig.A3.9 *I-V* characteristics Linear Sweep Voltammetry profile, using 25 wt.% TMAH, n-type Si{100}, pH = 13.4 at a temperature of 80 °C, (its code FsiBsi).

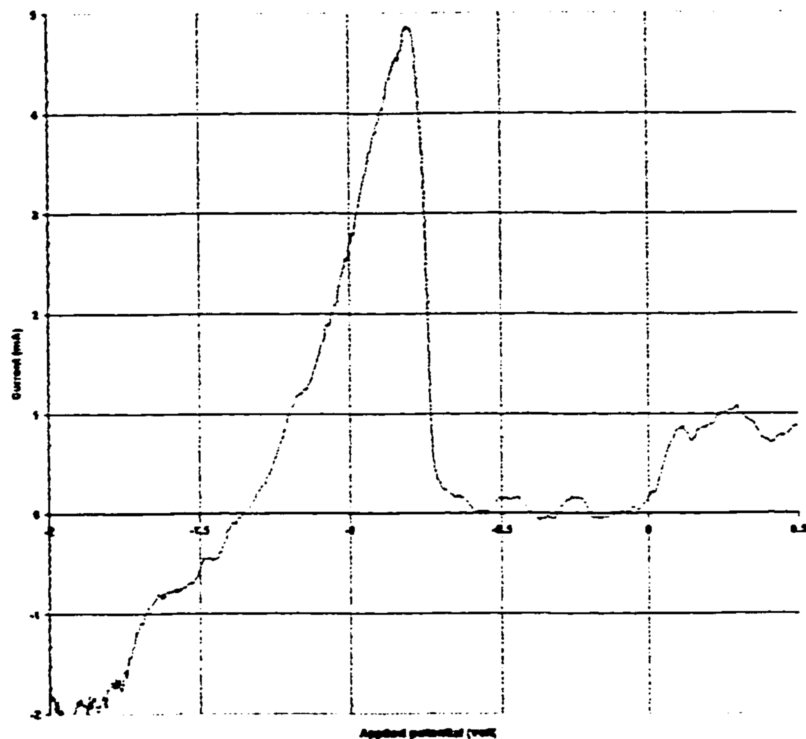

Fig.A3. 10 *I-V* characteristics Linear Sweep Voltammetry profile, using 5 wt.% TMAH, n-type Si{100}, pH = 12.4 at a temperature of 80 °C. (code FsiBsi).

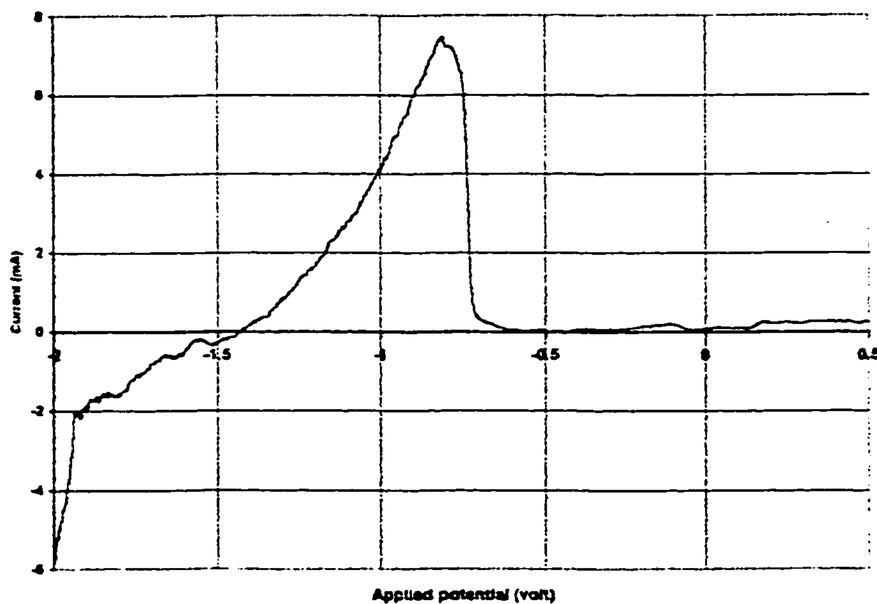

. Fig.A3. 11 *I-V* characteristics Linear Sweep Voltammetry profile, using 5 wt.% TMAH with dissolved Si, n-type Si{100}, pH = 11.7 at a temperature of 80 °C. (code FsiBsi).

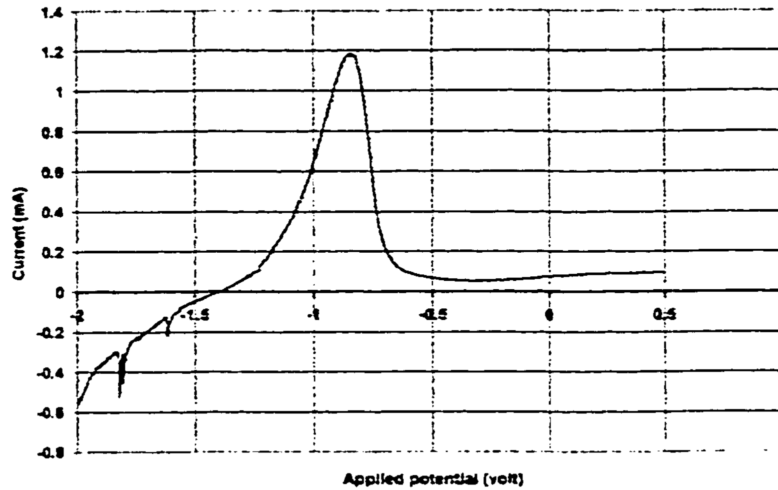

Fig.A3.12 Current-voltage characteristics of n-type Si{100}, (front side) aluminum deposited on Si and SiO_2, (backside) open Si, in 5wt.% TMAH with dissolved silicon, at temperature 80 °C. (code FoxAsiBsi).

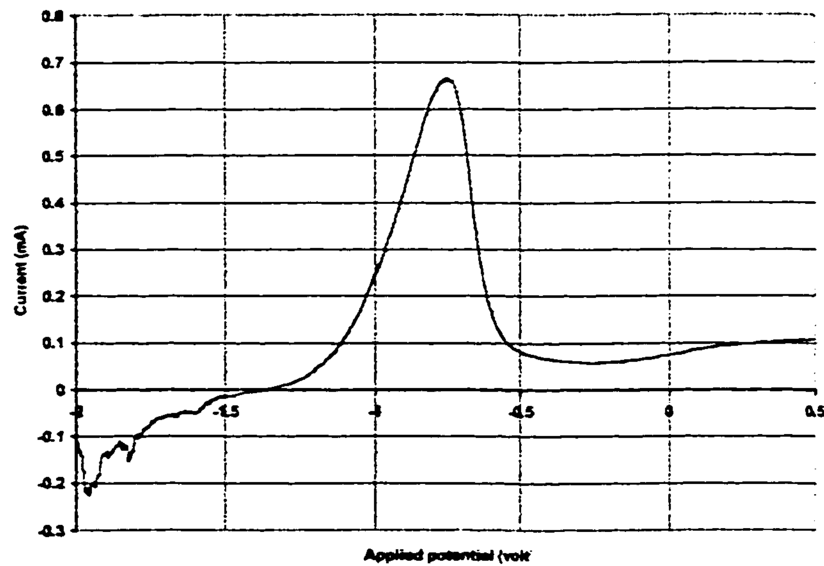

Fig.A3.13 Current-voltage characteristics of n-type Si{100}, (front side) aluminum deposited on SiO_2, (backside) open Si, in 5wt% TMAH with dissolved silicon, at temperature 80 °C. (code FoxAoxBsi).

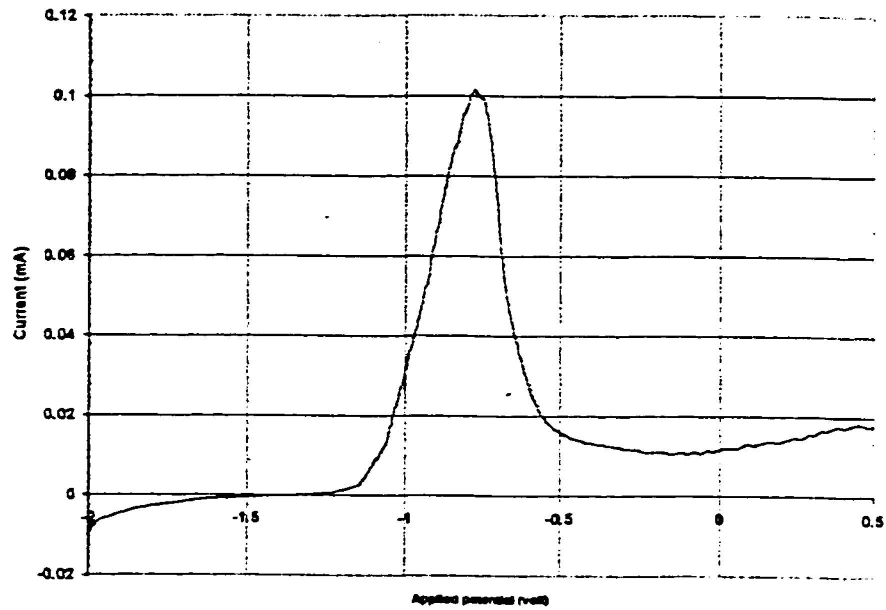

Fig.A3.14 Current-voltage characteristics of n-type Si{100}, (front side)aluminum deposited on SiO_2, (backside) is covered with SiO_2, in 5wt% TMAH with dissolved silicon, at temperature 80 °C. (code FoxAoxBox).

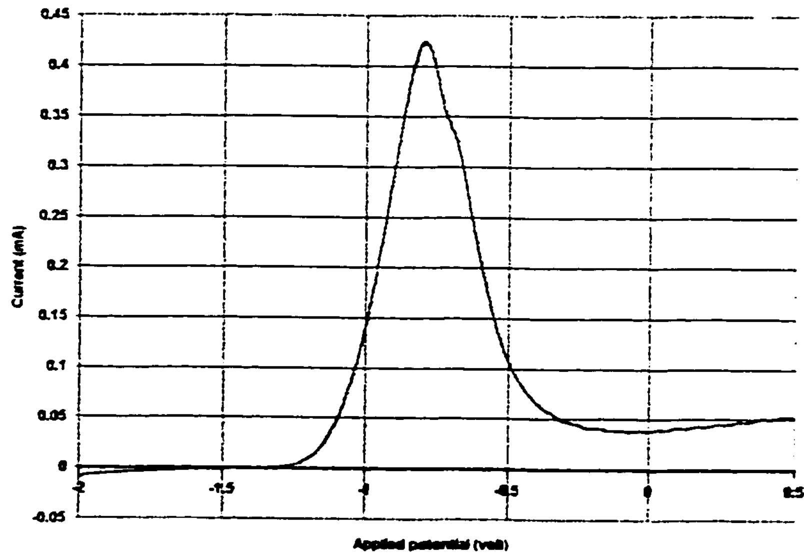

Fig.A3.15Current-voltage characteristics of n-type Si{100}, (front side) aluminum deposited on Si and SiO_2 (backside) is covered with SiO_2, in 5wt.% TMAH with dissolved silicon at 80 °C. (code FoxAsiBox)

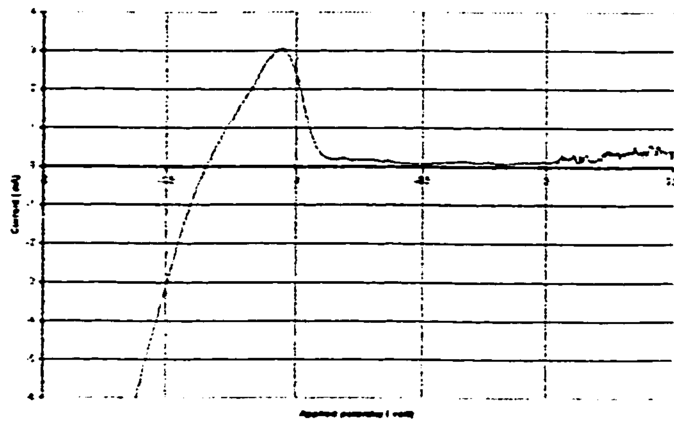

Fig.A3.16 Current-voltage characteristics of n-type Si{100} (front side) open Si, (backside) open Si, in 5wt.% TMAH with dissolved silicon at 80 °C. (code FsiBsi).

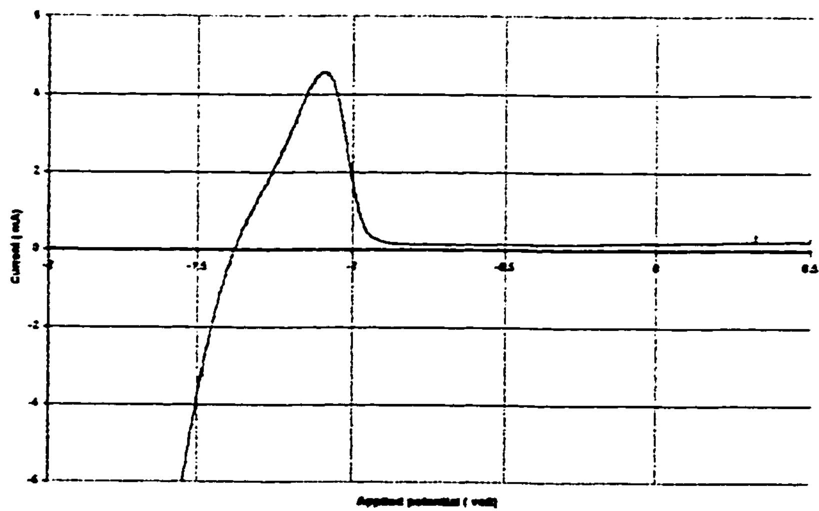

Fig.A3.17 Current-voltage characteristics of n-type Si{100}, (front side) aluminum deposited on Si, (backside) is open Si, in 5wt.% TMAH with dissolved silicon at 80 °C. (code FsiAsiBsi).

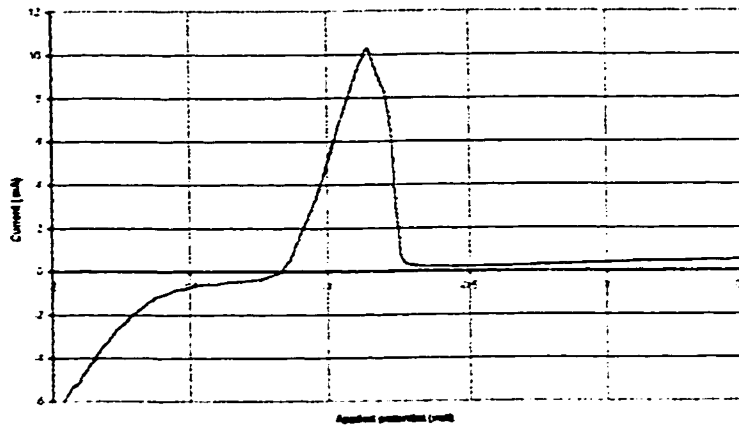

Fig.A3.18 Current-voltage characteristics of p-type Si{100}, (front side) open Si, (backside) open Si, in 5 wt.% TMAH with dissolved silicon at 80 °C. (code FsiBsi).

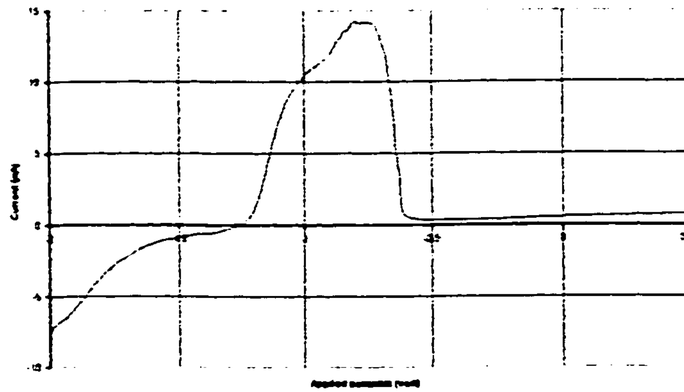

Fig.A3.19 Current-voltage characteristics of p-type Si {100}, (front side) aluminum deposited on Si, (backside) is open Si, in 5wt.% TMAH with dissolved silicon at 80 °C. (code FsiAsiBsi).

Table A3.2 Summary of the structure descriptions and their experimental results.

Code	ID& type	FS	BS	The etchant	FS Area Cm^2	BS Area cm^2	pH	T °C	OCP (v)	PP (v)	OFP (V)	I_{max} mA	Figure No.
FsiBSi	N2 n-type	Open Si	Open Si	5wt% TMAH dissolved Si	2.42	1.5	11.7	80	-1.352	-0.988	-0.78	1.51	A3.16
FsiBSi	N4 n-type	Al in contact with Si	Open Si	5wt% TMAH dissolved Si	3.0	2.1	11.7	80	-1.376	-1.09	-.944	4.56	A3.17
FsiBSi	P7 p-type	Si	Open Si	5wt% TMAH dissolved Si	4.32	3.0	11.7	80	-1.32	-0.972	-0.824	2.73	A3.18
FsiBSi	P9 p-type	Al in contact with Si	Open Si	5wt% TMAH dissolved Si	6.0	6.5	11.7	80	-1.434	-0.876	-0.724	8.33	A3.19
FsiBSi	NE0 n-type	Open Si	Open Si	25wt% TMAH	3.5	2.1	13.4	80	-1.398	-0.97	-0.47	10.6	A3.9
FsiBSi	NE1 n-type	Open Si	Open Si	5wt% TMAH	5.5	4.6	12.4	80	-1.34	-1.256	-1.07	3.86	A3.10
FsiBSi	NE2 n-type	Open Si	Open Si	5wt% TMAH dissolved Si	7.0	7.0	11.7	80	-1.422	-0.888	-0.76	8.93	A3.11
FoxBSi	S2 n-type	Al in contact with SiO_2&Si	open Si	5wt% TMAH dissolved Si	1.017	2.5	11.7	80	-1.400	-0.848	-0.604	1.186	A3.12
FoxBSi	S5 n-type	Al in contact with SiO_2	open Si	5wt% TMAH dissolved Si	1	2.066	11.7	80	-1.362	-0.754	-0.552	0.665	A3.13
FoxBSi	S9 n-type	Al in contact with SiO_2	covered with SiO_2	5wt% TMAH dissolved Si	2.250 E-03	0	11.7	80	-1.322	-0.770	-0.504	0.1011	A3.14
FoxBox	S10 n-type	Al in contact with SiO_2&Si	covered with SiO_2	5wt% TMAH dissolved Si	5.906 E-03	0	11.7	80	-1.352	-0.798	-0.376	0.425	A3.15

A3.7 SUMMARY.

Several sample geometries were fabricated, with backside either open-Si or covered with SiO_2, and front side Al either touching the silicon or silicon oxide or both of them. Linear Sweep Voltammetry (LSV) experiments were conducted on the different sample geometries and typical curves were found, including OCP, PP, and OFP. The PP was found to roughly decrease with pH of the solution. No other systematic variations of these parameters were discerned. The OCP and PP values found in these measurements were not consistent with galvanic cell and those found in the literature. It was suspected that the reason for the unpredictable results may be due to ohmic contacts being damaged during immersion in the solution (i.e. TMAH).

Table A3.3 Summary of the LSV results

LSV Experimental Results **T =80 °C. RE= Ag/AgCl**			
Etchant	<100>Si type	OCP (volt)	PP (volt)
5wt% TMAH/Si	N2 n-type	-1.352	-0.988
5wt% TMAH/Si	N4 n-type	-1.376	-1.09
5wt% TMAH/Si	P7 p-type	-1.32	-0.972
5wt% TMAH/Si	P9 p-type	-1.434	-0.876
25wt% TMAH	NE0 n-type	-1.398	-0.97
5wt% TMAH	NE1 n-type	-1.34	-1.256
5wt% TMAH/Si	NE2 n-type	-1.422	-0.888
5wt% TMAH/Si	S2 n-type	-1.400	-0.848
5wt% TMAH/Si	S5 n-type	-1.362	-0.754
5wt% TMAH/Si	S9 n-type	-1.322	-0.770
5wt% TMAH/Si	S10 n-type	-1.352	-0.798